論文 / 著書情報
Article / Book Information

題目(和文)	プラスミドDNAデリバリーを指向したpH変換型ポリ双性イオン導入ナノシステムの開発
Title(English)	Development of Stepwise pH Responsive Polyzwitterion Introduced Nanocarrier for Plasmid DNA Delivery
著者(和文)	SHENXin
Author(English)	Xin Shen
出典(和文)	学位:博士(学術), 学位授与機関:東京工業大学, 報告番号:甲第12605号, 授与年月日:2023年9月22日, 学位の種別:課程博士, 審査員:西山 伸宏,三浦 裕,中村 浩之,小畠 英理,丸山 厚,曽根 正人
Citation(English)	Degree:Doctor (Academic), Conferring organization: Tokyo Institute of Technology, Report number:甲第12605号, Conferred date:2023/9/22, Degree Type:Course doctor, Examiner:,,,,,
学位種別(和文)	博士論文
Type(English)	Doctoral Thesis

Development of Stepwise pH-Responsive Polyzwitterion-Introduced Nanocarrier for Plasmid DNA Delivery

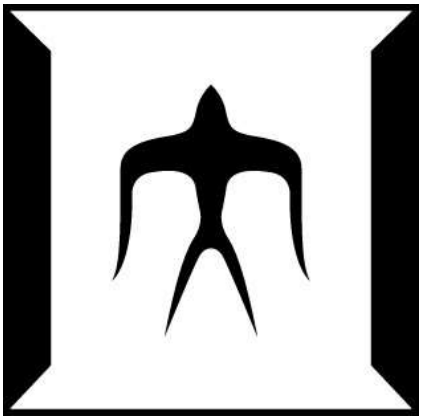

Tokyo Institute of Technology
Department of life science and technology

Doctoral Dissertation

SHEN XIN

Supervisor: Professor Nobuhiro Nishiyama
Associated Professor Yutaka Miura

June 2023

Catalogue

Abbreviation

Abbreviation	Full name
ATP	Adenosine triphosphate
A/J	A/JJmsSlc
BLG-NCA	γ-benzyl-L-glutamate N-carboxy anhydride
C/A	The ratio of cationic charges to anionic charges
CCK	Cell Counting Kit-8
DBCO	Dibenzocyclooctyne
DBCO-NHS	Dibenzocyclooctyne-N-hydroxysuccinimidyl ester
DCl	Deuterium chloride
DCM	Diethyl ether, dichloromethane
DET	Diethylenetriamine
DMEM	Dulbecco Modified Eagle Medium
DMF	*N*, *N*-Dimethylformamide
DNA	Deoxyribonucleic acid
DMSO	Dimethyl sulfoxide
DMSO-*d6*	Deuterated dimethyl sulfoxide
D-PBS(−)	Dulbecco's phosphate buffered saline
EMEM	Eagle's Minimum Essential Medium
EPR	Enhanced permeability and retention
HEPES	4-(2-hydroxyethyl)-1-piperazineethanesulfonic acid
IC_{50}	Half maximal inhibitory concentration
LDH	Lactate dehydrogenase
LNP	Lipid nanoparticle
MES	2-(*N*-morpholino)ethanesulfonic acid
MeOH	Methanol

mRNA	Messenger ribonucleic acid
N_3-PEG	Methoxypolyethylene glycol azide
NP	Nanoparticles
pK_a	Acid dissociation constant
PAMAM	Polyamidoamine
PECAM-1	Anti-platelet endothelial cell adhesion molecule-1
PEI	Polyethyleneimine
PEG	Poly(ethylene glycol)
PGDC	PGlu(DET-Car)-coated polyplex micelle
PGlu(DET-Car)	Poly(N-{N'-[N''-(2-carboxyethyl)-2-aminoethyl]-2-aminoethyl}glutamide)
PLL	Polylysine
PM	Polyplex micelle
pK_a	Acid dissociation constant
RI	Refractive index
RES	Reticuloendothelial system
RNAi	RNA interference
SEC	Size exclusion chromatography
sFlt-1	Soluble fms-like tyrosine kinase-1
THF	Tetrahydrofuran
TEA	Triethylamine
TMS	Tetramethyl silane
VEGF	Vascular endothelial growth factor

Chapter 1 General Introduction

1.1 Background of gene therapy

Tumors are widely acknowledged as a multifaceted group of diseases that manifest as the unrestrained proliferation of distinct aberrant cellular populations attributable to genomic mutations, ultimately culminating in the formation of metastatic foci in remote anatomical locales. As cancer has become one of the deadliest diseases in the world [1, 2], finding efficient and non-toxic treatments is of great interest. Traditional therapeutic approaches such as surgery, chemotherapy, and irradiation often cause treatment failure, resulting in recurrence, metastasis, and even death [3, 4]. In contrast, gene therapy is a promising treatment that can achieve long-lasting or curative effects by inhibiting, adding, replacing, or editing genes in tumor cells to improve therapeutic outcomes [5].

1.1.1 Gene therapy

Genes are the basic unit of heredity and contain the genetic information of living organisms by transcribing from deoxyribonucleic acid (DNA) to messenger ribonucleic acid (mRNA) and then translating to protein to maintain basic life activities [6]. In disease conditions, mutations in genes, result in either decreased or anomalous protein expression. Gene therapies are generally aimed at replacing missing, mutated, or defective genes, correcting endogenous mutations, or altering cell function to correct the protein expression [7]. After decades of intensive research, many clinical products have been approved with more in the pipeline for the treatment of several diseases, including cancer [8-11], and it is poised to make a significant impact on medicine in the coming years (**Table 1-1**). The emerging field of gene therapy entails several approaches aiming at modulating gene activity, encompassing various techniques. The production of abnormal or deficient proteins in the body can be facilitated by direct transport of the gene such as plasmid DNA or mRNA. RNA interference (RNAi) technology can silence gene expression at the mRNA level. The CRISPR/Cas9 system embodies a versatile gene-editing technology capable of executing precise alterations

to genomic DNA, including excisions, insertions, and modifications of genetic elements.

Table 1-1. Approved gene therapy products in cancer therapy within 20 years.

Year	Trade name	Manufacture	Therapeutic indication	Ref.
2003	Gendicine	Shenzhen SiBiono GeneTech	Head and neck squamous cell carcinoma (HNSCC)	[12]
2005	Oncorine	Shanghai Sunway Biotech	Nasopharyngeal carcinoma	[13]
2010	Rexin-G	Epeius Biotechnologies	Metastatic solid tumors	[14]
2015	Imlygic	Amgen	Melanoma	[15]
2017	Kymriah	Novartis	Relapsed B cell acute lymphoblastic leukemia	[16]
2017	Yescarta	Kite Pharma (Gilead)	Relapsed or Refractory large B cell lymphoma	[17]
2021	Breyanzi	Celgene (Bristol Myers Squibb)	Relapsed or refractory diffuse large B cell lymphoma; follicular lymphoma	[18]
2021	Abecma	bluebird bio	Multiple myeloma	[19]
2021	Delytact (G47Δ)	Daiichi Sankyo	Malignant Glioma	[20]
2022	Carvykti	Legend Biotech	Relapsed or refractory multiple myeloma	[21]

1.1.2 Barriers in gene delivery for cancer therapy

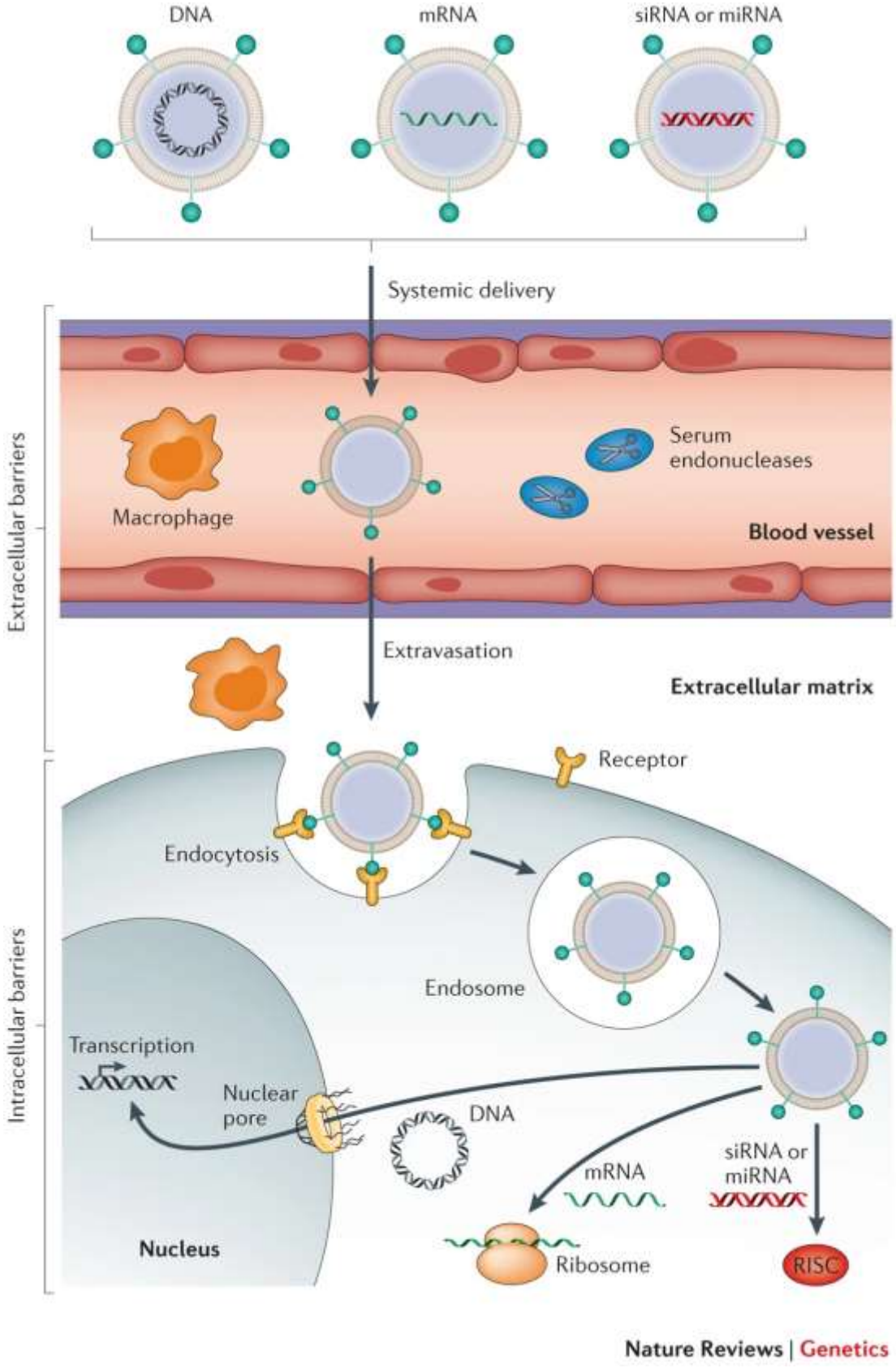

Figure 1-1. Barriers to successful *in vivo* delivery of nucleic acids using non-viral vectors [24]. Effective delivery of nucleic acid drugs requires overcoming multiple barriers, including serum endonuclease degradation, immune detection, renal clearance, and nonspecific interactions. In addition, they require extravasation from the bloodstream and targeting of specific tissues, effective cellular uptake, and endosomal escape, which can be facilitated through the use of specific ligands and carrier components.

To achieve successful antitumor-based gene therapy, it is important to overcome biological barriers and ensure that nucleic acid drugs reach the targeted tumor site. This can be a challenging task after systematic administration, given the various obstacles that these gene vehicles need to overcome during their journey [22, 23]. For instance, as depicted in **Figure 1-1**, in order to prevent the breakdown of nucleus acids by serum endonucleases and avoid immune detection, nucleic acids need to be condensed. In addition, they must avoid renal clearance and prevent nonspecific interactions with other substances in the bloodstream. To reach the tumor tissue, the nucleus acid drugs need to extravasate from the bloodstream and mediate the cell internalization. However, nucleic acids face significant challenges in permeating cellular membranes due to their negative charge, high molecular weight, and hydrophilic nature. Moreover, once inside the cells, they must escape from the endo/lysosome to exert their activities. For instance, siRNA and miRNA mimics must be loaded into the RNA-induced silencing complex (RISC), while mRNA needs to be bound to the translation machinery. Additionally, DNA is transported into the cell nucleus to exert its therapeutic activity. Thus, gene therapy for tumors requires attention to these various biological and physiological hurdles to achieve successful treatment outcomes [24].

(1) Tumor extracellular microenvironment

Acidosis represents a salient hallmark of neoplastic microenvironments, pervading the tumor tissue with profound effects on its biology and therapeutic response. The acidic

extracellular milieu of the tumor microenvironment, typified by a pH range of 6.1-7.0 [25, 26], is closely intertwined with the aberrant metabolic phenotype of neoplastic cells, often referred to as the Warburg effect [27]. The Warburg hypothesis posited that neoplastic cells preferentially adopt anaerobic glycolysis over oxidative phosphorylation as their primary metabolic pathway, even in the presence of oxygen, owing to the compromised functionality of their mitochondria. This metabolic reprogramming confers an inherent proclivity for the generation of pyruvate-derived lactate *via* intensified anaerobic glycolysis, with the monocarboxylate transporter system facilitating the efflux of lactate into the extracellular compartment (**Figure 1-2**). The net result of this phenomenon is the imposition of an acidic microenvironment within the tumor microenvironment [28].

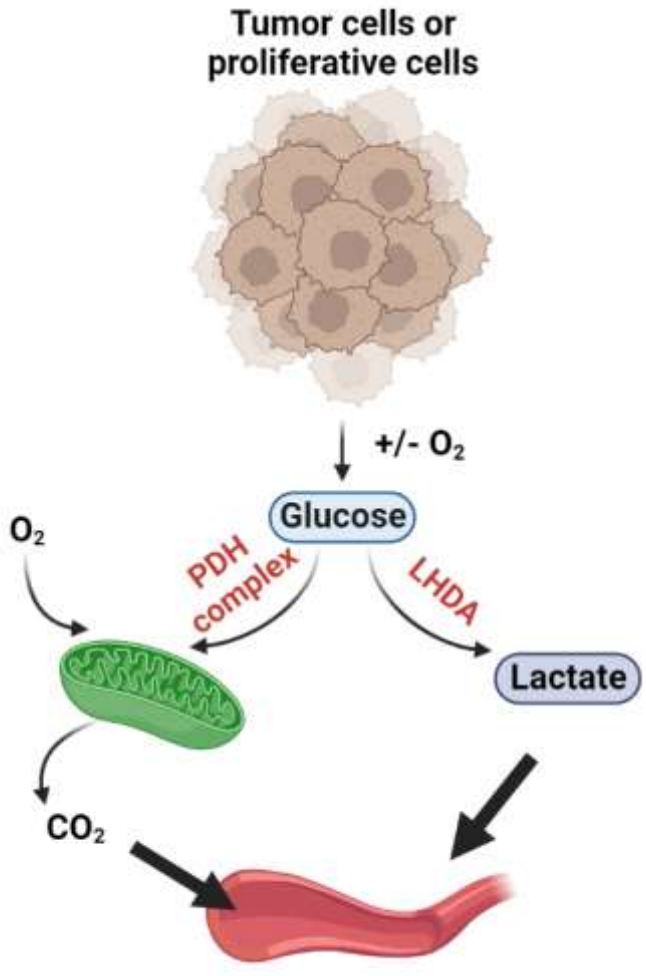

Figure 1-2. Mechanism of Warburg effect in tumor or proliferating tissue. In cancer cells, glycolysis is facilitated by the upregulation of certain enzymes such as hexokinase and pyruvate kinase, which promote glucose uptake and pyruvate conversion, respectively. It also shows that the Warburg Effect can lead to the accumulation of metabolic intermediates such as lactate, which can be exported from cancer cells and contribute to the acidic microenvironment commonly observed in tumors.

(2) Tumor intracellular microenvironment

The successful intracellular delivery of nucleic acids encompasses a multi-step process, involving various stages from administration to distribution and cellular uptake. After internalization into the tumor cell, multiple intracellular obstacles must be surmounted to enable transcription and translation of exogenous genes. The primary hurdle in this process is presented by the endosomal compartment, which impedes intracellular trafficking of gene carriers. The mildly acidic early endosomes with a pH of 6.5, which ultimately lead to late endosomes (pH ~ 5.5) and lysosomes that exhibit lower pH levels (pH ~ 4.5) and potential enzymatic degradation [29]. The regulation of the acidic microenvironment within the endosome is governed by the functionality of ATP-dependent proton pumps, specifically the V-type H^+ ATPase and H^+/Cl^- exchangers [30]. In the majority of cases, confinement of internalized gene carriers within endocytic compartments leads to the degradation of both the carrier and its accompanying DNA in endosomal or lysosomal compartments. Endosomal escape represents a pivotal aspect to be taken into account during the design phase of non-viral gene carriers. A comprehensive comprehension of the underlying mechanisms facilitates the intelligent formulation of molecules that integrate ionizable groups possessing an optimal pK_a. This strategic incorporation enables proficient interaction with the endosomal membrane, leading to effective destabilization.

1.2 Development of polymer-based gene delivery system for gene therapy

1.2.1 Polymeric delivery systems for gene therapy

In the pursuit of efficient gene therapy through systemic administrations, various gene delivery carriers have been developed [31-33]. Among them, nonviral gene carriers are extensively examined such as polymeric nanoparticles [34, 35], owing to their low host immunogenicity, low cost for large-scale manufacturing, and tunable surface modifications [36-38].

To facilitate complexation of the nucleic acid payload by electrostatic interaction with positively charged excipients into nanoparticles of a size suitable for internalization by cells and to guide intracellular trafficking of exogenous nucleic acids, various types of polymers have been explored, as listed in **Figure 1-3**. These polymers often consist of repeating single monomers with positively charged groups to complexes with negatively charged nucleic acids, thus condensing the nucleic acids into smaller-sized nanoparticles to protect them against nuclease attack and degradation. The earliest development, dating back to 1965, is diethylaminoethyl (DEAE) dextran for the use of transfection of poliovirus RNA and SV40 viral DNA [39, 40]. In addition, cationic polymers with amino acid backbones such as polylysine (PLL), poly-L-ornithine (PLO), and poly-L-arginine (PLR) also had the potential to be used for the transfer of nucleic acids into cells [41-43]. Polymers with inherent endosomal escape ability to improve transfection efficiency are a milestone in the development of polymer-based gene delivery, and the most important representatives are polyethyleneimine (PEI) and polyamidoamine (PAMAM) dendrimer [44, 45].

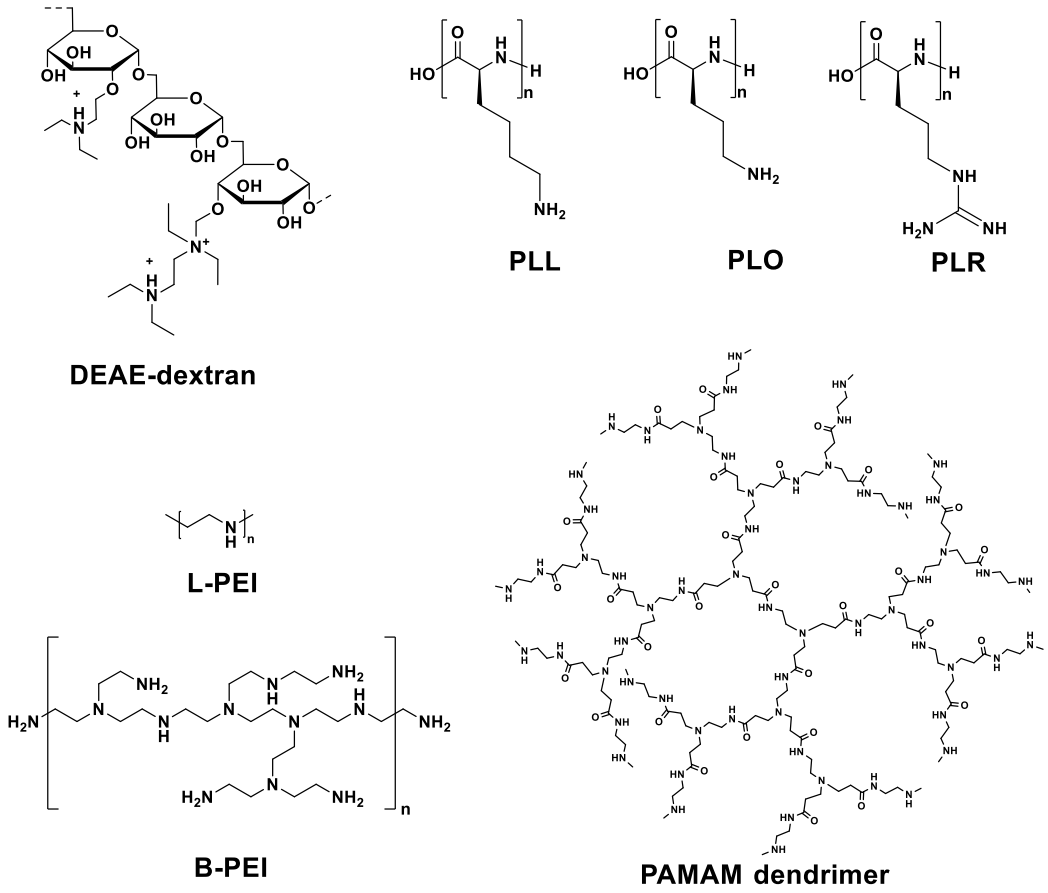

Figure 1-3. Chemical structure of the polymers for gene delivery. {DEAE-dextran, diethylaminoethyl-dextran; PLL, poly-L-lysine; PLO, poly-L-ornithine; PLR, poly-L-arginine. Polyethylenimine in linear (L-PEI) or branched (B-PEI); poly(amidoamine) PAMAM dendrimer}.

Among them, PEI is the most commonly employed agent for DNA/RNA transfection. It is available in two main forms, namely linear PEI (L-PEI) and branched PEI (B-PEI) [46]. A key characteristic of these molecules is their high cationic charge density, resulting from the presence of a protonable amino nitrogen atom every third atom. This attribute is particularly relevant since it plays a crucial role in the transfection process by facilitating the formation of complexes with negatively charged nucleic acids, leading to efficient gene delivery. Importantly, PEI exhibits a notable buffer capacity at low pH values of lysosomes due to its numerous nitrogen atoms. In 1997, Behr postulated the “proton-sponge” hypothesis, which suggests that the unprotonated

amines of PEI can absorb protons that are pumped into the lysosome [47]. This mechanism leads to an increased influx of Cl^- ions, and water, which in combination with osmotic swelling and repulsion between protonated amine groups, causes the swelling of PEI and the eventual rupture of the lysosomal membrane. Consequently, the contents of the lysosome are released into the cytoplasm. This hypothesis provides a possible explanation for the remarkable efficiency of PEI in facilitating the delivery of nucleic acids into cells. Therefore, PEI is extensively employed for gene transfection and is currently considered the benchmark standard in all transfection experiments [48-50].

However, cationic polymer gene vectors are known to possess some inherent drawbacks, including their non-degradability and toxicity, which is dependent on their molecular weight. PEI toxicity can result in apoptosis and necrosis, which may be attributed to the generation of defects in the cell surface, mitochondria, or nuclear membranes [51]. Moreover, PEI can inhibit mitochondrial ATP synthesis, which further contributes to its cytotoxic effects [52]. The innate immune system is also activated by cationic polymers such as PEI, PAMAM, and PLL, leading to *in vivo* complement activation. Hence, a thorough evaluation of the toxicological effects of these non-viral vectors is essential before their use in clinical settings.

1.2.2 Polyplex micelle in gene delivery system

To address the limitations associated with cationic polymeric gene delivery systems, a polyplex micelle delivery system was developed with the neutral hydrophilic shell polymer such as poly(ethylene glycol) (PEG) coated on the polyplexes, which can effectively shield their surface charge from the external environment and improve colloidal stability, ultimately reducing undesirable interactions and enhancing their circulation kinetics [53-55]. Moreover, the polyplex micelles (PMs) exhibit a distinctive core-shell arrangement, wherein nucleus acids undergo condensation through complexation with a cationic segment, leading to its packaging within a core

compartment. The advantageous structural attributes of PMs facilitate significant colloidal stability when present in a biological milieu, thereby bestowing therapeutic effects upon systematic administration.

As mentioned above, PEG has been extensively investigated as a shielding agent and is widely employed in gene delivery systems [56-58]. It is a polyether compound composed of repeating ethoxy units resulting from the ring-opening polymerization of ethylene oxide. The hydrophilic characteristics of PEG chains grafted onto nanoparticles (NPs) generate a hydrated cloud that can effectively shield the surface of NPs from phenomenon such as aggregation, opsonization, and phagocytosis. This phenomenon referred to as the "stealth" property, significantly prolongs the circulation time of NPs [59]. PEGylated NPs with long-circulating properties have the potential to target tumors following systemic administration, owing to the enhanced permeability and retention (EPR) effect. Kissel and his co-workers revealed that upon administration of a high dose of PEGylated PEI, a more favorable organ deposition pattern was observed along with a significant reduction in acute *in vivo* toxicity [60]. Saltzman et al. found that PEGylation of poly(amine-co-ester) polyplexes can significantly improve the stability of the gene carriers to *in vivo* delivery of mRNA to the lung [61]. These publications highlighted the continued interest in using PEG as a tool to improve the efficacy and safety of gene delivery systems.

The application of PEGylation in gene delivery has yielded numerous favorable outcomes, while also highlighting certain possible downsides associated with its extensive use. One of these potential drawbacks is the presence of PEG-imparted charge shielding and steric hindrance to the polyplex surface, thereby hindering interactions with anionic molecules on the cell surface and reducing subsequent cellular uptake [62-64]. Consequently, the low cellular uptake and intracellular trafficking of gene carriers were observed. Moreover, the immunogenicity of PEG has garnered increased attention from researchers due to the observation of rapid clearance of PEGylated therapeutics upon repeated administrations, commonly referred to as the accelerated blood clearance

(ABC) phenomenon [65-67]. This phenomenon was initially discovered in PEGylated liposomes and was attributed to the occurrence of anti-PEG immunoglobulin M (IgM) in the spleen. The conundrum associated with the application of PEG in gene delivery systems has been coined as the “PEG dilemma”. Therefore, it is vital to create an alternative carrier system which can simultaneously exhibit the above requirements for gene carriers before and after cellular uptakes.

Recently, polyzwitterions, possessing equivalent positive and negative charges, have emerged as a compelling alternative shielding material to PEG due to their remarkable ultra-hydrophilicity and anti-fouling characteristics [68, 69]. Zwitterions exhibited enhanced hydration *via* ionic solvation when compared to PEG, exhibiting antifouling performance for prolonged blood circulation. They demonstrated resistance to cell adhesion and were capable of evading immune responses, leading to reduced non-specific interactions with biological fluids such as serum or blood platelets [70]. Furthermore, the ability of polyzwitterions undergoing charge conversion in response to acidic conditions, such as those found in tumors and endosomes [71], provides a mechanism for transitioning from a stealthy to a sticky state, thereby facilitating the interaction with negatively charged phospholipids in cellular membranes. These traits made polyzwitterion a promising candidate for biomedical applications. In recent publications, Chen *et al.* reported a novel pH-responsive zwitterionic polymer, PEI-poly(L-lysine)-poly(L-glutamic acid) (PELG), coating positively charged PEI/DNA complexes for gene delivery [72]. The resultant polyplexes demonstrated an intriguing ability to regain a positive charge in the acidic tumor microenvironments, leading to enhanced cellular uptake and elevated transfection efficiency. This study highlights the potential of pH-sensitive zwitterionic polymers as a promising platform for gene therapy applications.

In our previous work, we developed a polyzwitterion, poly(*N*-{*N*’-[*N*’’-(2-carboxyethyl)-2-aminoethyl]-2-aminoethyl}glutamide) [PGlu(DET-Car)], which has the pH-responsive net charge changeable ability [73]. The ethylenediamine moiety in

PGlu(DET-Car) displayed two distinct acid dissociation constant (pK_a) values around 8.9 and 6.5. Thus, the net charge of PGlu(DET-Car) is neutral in blood and healthy tissue (pH 7.4). In contrast, double protonation of the ethylenediamine moiety ($NH_2^+CH_2CH_2NH_3^+$) at the acidic milieu of the tumor extracellular environment turns its net charge positive, enabling enhanced interactions with anionic tumor tissue constituents for enhanced tumor cellular uptake (**Figure 1-4**). Indeed, the surface covering of nanocarriers with PGlu(DET-Car) fully exploited the advantage of these two characteristic pK_a properties for responding to slight changes in the pH of healthy and tumor tissue, thereby exhibiting enhanced accumulation and deep penetration to hypoxic tumor regions [74]. Moreover, PGlu(DET-Car) modified lipid nanoparticle demonstrated enhanced cellular uptake in cancerous pH, high tumor accumulation, and significant tumor growth inhibition when encapsulated siPLK-1 [75].

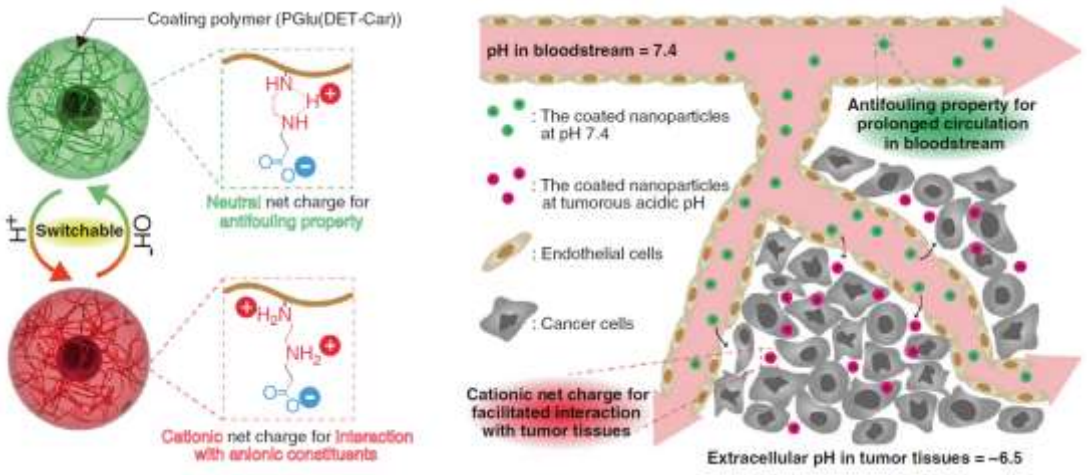

Figure 1-4. Illustration of PGlu(DET-Car)-based tumor delivery of the coated nanomaterials [76].

1.3 Philosophy of this research

In the present study, we constructed PGlu(DET-Car) conjugated branched-PEI [PGlu(DET-Car)-bPEI)] to formulate a polyplex micelle (PM) based on polyion

complexation between pDNA and PGlu(DET-Car)-bPEI (**Figure 1-5**). PGlu(DET-Car) segment served as the outer shell of the PMs, exhibiting pH-responsive performance. Owing to the substantial protonation of the ethylenediamine groups in PGlu(DET-Car), the PM has the charge-conversion property that could switch its surface charge from neutral to positive as pH decrease. Following this electrostatic self-assembly, pDNA is packaged into a core compartment, and the PGlu(DET-Car) chains surround the core as a protective shell compartment. This distinctive core-shell architecture of PMs empowers pDNA protection against nucleases and proteins upon systemic administration. We systematically studied the charge switchability of PGlu(DET-Car) to slight pH changes for promoting cell-interactive properties and facilitating endo/lysosomal escape capability of PGlu(DET-Car) as a versatile shell material using the PM platform in a murine neuroblastoma cell line (Neuro-2A) and human hepatoma cell line (Huh-7 cell) line. We further extended our investigations on the utility of PGlu(DET-Car) surface-covered PM for establishing *in vivo* stealth properties, tumor-interactive abilities, and gene transfection efficacies upon tail-vein intravenous injection in A/JJmsSlc (A/J) mice bearing Neuro-2A tumor model. Ultimately, PGlu(DET-Car) surface-shielded PM loading a therapeutic pDNA encoding sFlt-1 gene for antiangiogenesis therapy was challenged to systemic treatment of Neuro-2A, one of the most refractory solid tumors. Our data demonstrated that PGlu(DET-Car)-covered PM exhibited excellent stealth properties such as extended blood retention and low liver and spleen accumulation, tumor-interactive features for enabling enhanced tumor accumulation compared to counterpart PEG-shielded PM. These results highlighted the universality of the polyzwitterion-based design for constructing nano-carriers for future gene therapy.

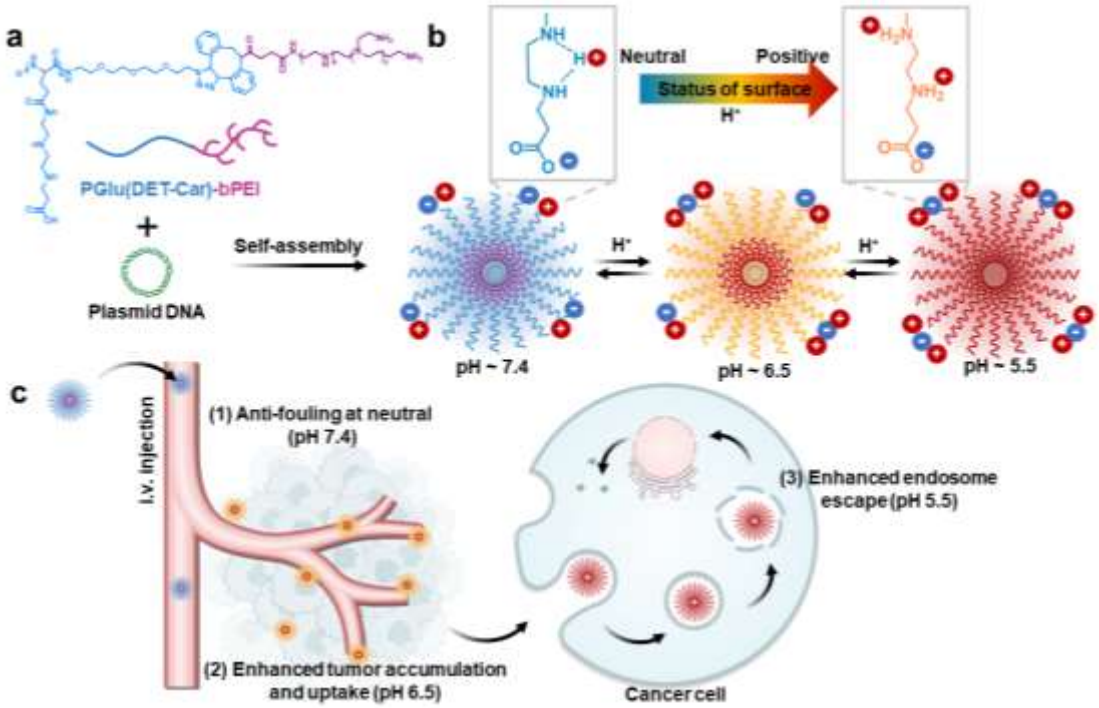

Figure1-5. Stepwise pH-triggered charge conversion of PGlu(DET-Car)-coated polyplex micelle (PGDC PM) for the effective gene delivery. (a) Chemical structure of PGlu(DET-Car)-bPEI conjugates and formation of the PGDC PM. (b) Protonation behavior and surface charge conversion of PGDC PM in the acid environment. (c) Illustration of the gene delivery strategy by PGDC PM after the i.v. injection. (1) During the blood circulation, the net neutral charge of the PGDC shell at physiological pH 7.4 provides anti-biofouling capabilities. (2) PGDC shell in the tumor extracellular milieu (pH 6.5) shifts its charge from neutral to mediumly cationic, inducing strong interactions with tumor tissue constituents and promoting cellular internalization of PGDC PM. (3) The cationic charge of the PGDC shell is further augmented in the endo-/lysosomal compartment (pH 5.5), facilitating the endosomal membrane disruption for the efficient gene transfection.

1.4 Outline of the dissertation

Chapter 2 encompassed the synthesis of the polyzwitterion-modified polymers and entailed an investigation into the protonation behavior of PGlu(DET-Car). Subsequently, **Chapter 3** detailed the preparation and characterization of polyplex micelles (PMs)

utilizing the aforementioned synthesized polymers. Moving forward, **Chapter 4** focused on evaluating the *in vitro* gene delivery efficiency of PGDC PMs against murine neuroblastoma and human hepatoma cell lines, with the aim of establishing their potential as a versatile platform to facilitate cellular uptake and subsequent endosomal escape of nucleic acid-based therapeutics. **Chapter 5** involved a comprehensive study of the *in vivo* biodistribution profile and gene transfection efficiency of the PMs, and further employed them for anti-angiogenic gene therapy in an *in vivo* cancer model. Finally, **Chapter 6** provided a comprehensive conclusion and outlined future avenues of investigation to address the remaining challenges and enhance the current system.

1.5 References

[1] R. L. Siegel, K. D. Miller, N. S. Wagle, A. Jemal, Cancer statistics, 2023. CA Cancer J. Clin.73 (1) (2023) 17-48. https://doi.org/10.3322/caac.21763.

[2] E. E. Calle, R. Kaaks, Overweight, obesity, and cancer: epidemiological evidence and proposed mechanisms. Nat. Rev. Cancer 4 (8) (2004) 579-591. https://doi.org/10.1038/nrc1408.

[3] J. Ferlay, M. Colombet, I. Soerjomataram, C. Mathers, D.M. Parkin, M. Piñeros, A. Znaor, F. Bray, Estimating the global cancer incidence and mortality in 2018: GLOBOCAN sources and methods. Int. J. Cancer 144 (8) (2019) 1941-1953. https://doi.org/10.1002/ijc.31937.

[4] E. Pérez-Herrero, A. Fernández-Medarde, Advanced targeted therapies in cancer: Drug nanocarriers, the future of chemotherapy. Eur J Pharm Biopharm. 93 (2015) 52-79. https://doi.org/10.1016/j.ejpb.2015.03.018.

[5] C.E. Dunbar, K.A. High, J.K. Joung, D.B. Kohn, K. Ozawa, M. Sadelain, Gene therapy comes of age, Science 359 (6372) (2018) eaan4672. https://doi.org/10.1126/science.aan4672.

[6] H. Pearson, Genetics: what is a gene? Nature. 441 (7092) (2006) 398-401.

https://doi.org/10.1038/441398a.

[7] A. Mullard, Gene therapies advance towards finish line. Nat. Rev. Drug Discov. 10 (10) (2011) 719-720. https://doi.org/10.1038/nrd3572.

[8] O. Khorkova, C. Wahlestedt, Oligonucleotide therapies for disorders of the nervous system. Nat. Biotechnol. 35 (3) (2017) 249-263. https://doi.org/10.1038/nbt.3784.

[9] A. Fischer, S. Hacein-Bey-Abina, M. Cavazzana-Calvo, 20 years of gene therapy for SCID. Nat. Immunol. 11 (6) (2010) 457-460. https://doi.org/10.1038/ni0610-457.

[10] M. Tachibana, P. Amato, M. Sparman, J. Woodward, D.M. Sanchis, H. Ma, N.M. Gutierrez, R. Tippner-Hedges, E. Kang, H.S. Lee, C. Ramsey, K. Masterson, D. Battaglia, D. Lee, D. Wu, J. Jensen, P. Patton, S. Gokhale, R. Stouffer, S. Mitalipov Towards germline gene therapy of inherited mitochondrial diseases. Nature 493 (7434) (2013) 627-631. https://doi.org/10.1038/nature11647.

[11] A. Fischer, M. Cavazzana-Calvo, Gene therapy of inherited diseases. Lancet 371 (2008) 2044-2047. https://doi.org/10.1016/S0140-6736(08)60874-0.

[12] W. Guo, H. Song, Development of gene therapeutics for head and neck cancer in China: from bench to bedside. Hum. Gene Ther. 29 (2) (2018) 180-187. https://doi.org/10.1089/hum.2017.230.

[13] M. Liang, Oncorine, the world first oncolytic virus medicine and its update in China. Curr Cancer Drug Targets 18 (2) (2018) 171-176. https://doi.org/10.2174/1568009618666171129221503.

[14] E.M. Gordon, F.L. Hall, Rexin-G, a targeted genetic medicine for cancer. Expert Opin Biol Ther 10 (5) (2010) 819-832. https://doi.org/10.1517/14712598.2010.481666.

[15] A. Poh, First oncolytic viral therapy for melanoma. Cancer Discov. 6 (1) (2016) 6. https://doi.org/10.1158/2159-8290.

[16] S.J. Si Lim, S.A. Grupp, A.M. DiNofia, Tisagenlecleucel for treatment of children and young adults with relapsed/refractory B-cell acute lymphoblastic leukemia.

Pediatr Blood Cancer 68 (9) (2021) e29123. https://doi.org/10.1002/pbc.29123.

[17] Z. Halford, M.K. Anderson, L.L. Bennett, Axicabtagene ciloleucel: clinical data for the use of CAR T-cell therapy in relapsed and refractorylarge B-cell lymphoma. Ann. Pharmacother. 55 (3) (2021) 390-405. https://doi.org/10.1177/1060028020944233.

[18] J.R. Westin, M.J. Kersten, G. Salles, J.S. Abramson, S.J. Schuster, F.L. Locke, C. Andreadis, Efficacy and safety of CD19-directed CAR-T cell therapies in patients with relapsed/refractory aggressive B-cell lymphomas: observations from the JULIET, ZUMA-1, and TRANSCEND trials. Am. J. Hematol. 96 (10) (2021) 1295-1312. https://doi.org/10.1002/ajh.26301.

[19] FDA, FDA Approves Idecabtagene Vicleucel for Multiple Myeloma. Available from: https://www.fda.gov/drugs/resources-information-approved-drugs/fda-approves-idecabtagene-vicleucel-multiple-myeloma.

[20] Press Release Daiichi Sankyo Launches DELYTACT ® Oncolytic Virus G47Δ in Japan. Available from: https://www.daiichisankyo.com.

[21] FDA, CARVYKTI. Available from: https://www.fda.gov/vaccines-blood-biologics/carvykti.

[22] S. Hager, F.J. Fittler, E. Wagner, M. Bros, Nucleic acid-based approaches for tumor therapy. Cells, 9 (9) (2020) 2061. https://doi.org/10.3390/cells9092061.

[23] J.A. Kulkarni, D. Witzigmann, S.B. Thomson, S. Chen, B.R. Leavitt, P.R. Cullis, R. van der Meel, The current landscape of nucleic acid therapeutics, Nat. Nanotechnol. 16 (6) (2021) 630-643. https://doi.org/10.1038/s41565-021-00898-0.

[24] H. Yin, R.L. Kanasty, A.A. Eltoukhy, A.J. Vegas, J.R. Dorkin, D.G. Anderson, Non-viral vectors for gene-based therapy. Nat. Rev. Genet. 15 (8) (2014) 541-55. https://doi.org/10.1038/nrg3763.

[25] E. Boedtkjer, S.F. Pedersen, The acidic tumor microenvironment as a driver of cancer, Annu. Rev. Physiol. 10 (2020) 103-126. https://doi.org/10.1146/annurev-physiol-021119-034627.

[26] Y. Kato, S. Ozawa, C. Miyamoto, Y. Maehata, A. Suzuki, T. Maeda, Y. Baba, Acidic extracellular microenvironment and cancer. Cancer Cell Int. 13(1) (2013) 89. https://doi.org/10.1186/1475-2867-13-89.

[27] M.V. Liberti, J.W. Locasale, The warburg effect: how does it benefit cancer cells? Trends Biochem. Sci. 41 (3) (2016) 211-218. https://doi.org/10.1016/j.tibs.2015.12.001.

[28] S. Bose, C. Zhang, A. Le, Glucose metabolism in cancer: the warburg effect and beyond. Adv Exp Med Biol. 1311 (2021) 3-15. https:// doi.org/10.1007/978-3-030-65768-0_1.

[29] Y.B. Hu, E.B. Dammer, R.J. Ren, G.Wang, The endosomal-lysosomal system: from acidification and cargo sorting to neurodegeneration. Transl. Neurodegener. (2015) 18. https://doi.org/10.1186/s40035-015-0041-1.

[30] M. Ko, A. Quiñones-Hinojosa, R. Rao, Emerging links between endosomal pH and cancer. Cancer Metastasis Rev. 39 (2) (2020) 519-534. https://doi.org/10.1007/s10555-020-09870-1.

[31] O.S. Fenton, K.N. Olafson, P.S. Pillai, M.J. Mitchell, R. Langer, Advances in biomaterials for drug delivery, Adv. Mater. 30 (29) (2018) 1705328. https://doi.org/10.1002/adma.201705328.

[32] S.A. Dilliard, D.J. Siegwart, Passive, active and endogenous organ-targeted lipid and polymer nanoparticles for delivery of genetic drugs, Nat. Rev. Mater. (2023) 1-19. https://doi.org/10.1038/s41578-022-00529-7.

[33] H. Yin, R.L. Kanasty, A.A. Eltoukhy, A.J. Vegas, J.R Dorkin., D.G. Anderson, Non-viral vectors for gene-based therapy, Nat. Rev. Genet. 15 (8) (2014) 541-555. https://doi.org/10.1038/nrg3763.

[34] T.G. Park, J.H. Jeong, S.W. Kim, Current status of polymeric gene delivery systems. Adv. Drug Deliv. Rev. 58 (4) (2006) 467-486. https://doi.org/10.1016/j.addr.2006.03.007.

[35] T.J. Thomas, H.A. Tajmir-Riahi, C.K.S. Pillai, Biodegradable polymers for gene

delivery. Molecules 24 (20) (2019) 3744. https://doi.org/10.3390/molecules24203744.

[36] P. Zhang, E. Wagner, History of Polymeric Gene Delivery Systems. Top Curr. Chem. 375 (2) (2017) 26. https://doi.org/10.1007/s41061-017-0112-0.

[37] J.K. Vasir, V. Labhasetwar, Polymeric nanoparticles for gene delivery. Expert Opin. Drug Deliv. 3 (3) (2006) 325-44. https://doi.org/10.1517/17425247.3.3.325.

[38] G. Lin, H. Zhang, L. Huang, Smart polymeric nanoparticles for cancer gene delivery. Mol. Pharm. 12 (2) (2015) 314-321. https://doi.org/10.1021/mp500656v.

[39] A. Vaheri, J.S. Pagano, Infectious poliovirus RNA: a sensitive method of assay. Virology 27 (3) (1965) 434-436. https://doi.org/10.1016/0042-6822(65)90126-1.

[40] J.H. McCutchan, J.S. Pagano, Enchancement of the infectivity of simian virus 40 deoxyribonucleic acid with diethylaminoethyl-dextran. J. Natl. Cancer Inst. 41 (2) (1968) 351-357.

[41] E. Wagner, M. Ogris, W. Zauner, Polylysine-based transfection systems utilizing receptor-mediated delivery. Adv. Drug Deliv. Rev. 30 (1-3) (1998) 97-113. https://doi.org/10.1016/s0169-409x(97)00110-5.

[42] V.C. Bond, B. Wold, Poly-L-ornithine-mediated transformation of mammalian cells. Mol. Cell Biol. 7 (6) (1987) 2286-2293. https://doi.org/10.1128/mcb.7.6.2286-2293.1987.

[43] P.F. Ferrari, E. Zattera, L. Pastorino, P. Perego, D. Palombo, Dextran/poly-L-arginine multi-layered $CaCO_3$-based nanosystem for vascular drug delivery. Int. J. Biol. Macromol. 177 (2021) 548-558. https://doi.org/10.1016/j.ijbiomac.2021.02.058.

[44] R. Kircheis, L. Wightman, E. Wagner, Design and gene delivery activity of modified polyethylenimines, Adv. Drug Deliv. Rev. 53 (3) (2001) 341-358. https://doi.org/10.1016/s0169-409x(01)00202-2.

[45] F. Abedi-Gaballu, G. Dehghan, M. Ghaffari, R. Yekta, S. Abbaspour-Ravasjani, B. Baradaran, J.E.N.Dolatabadi, M.R. Hamblin, PAMAM dendrimers as efficient

drug and gene delivery nanosystems for cancer therapy. Appl. Mater. Today. 12 (2018) 177-190. https://doi.org/10.1016/j.apmt.2018.05.002.

[46] M. Jäger, S. Schubert, S. Ochrimenko, D. Fischer, U.S. Schubert, Branched and linear poly(ethylene imine)-based conjugates: synthetic modification, characterization, and application. Chem Soc Rev. 41 (2012) 4755-4767. https://doi.org/10.1039/c2cs35146c.

[47] A. Akinc, M. Thomas, A.M. Klibanov, R. Langer, Exploring polyethylenimine-mediated DNA transfection and the proton sponge hypothesis. J. Gene Med. 7 (5) (2005) 657-663. https://doi.org/10.1002/jgm.696.

[48] W.T. Godbey, K.K. Wu, A.G. Mikos, Poly(ethylenimine) and its role in gene delivery. J. Control Release 60 (2-3) (1999) 149-160. https://doi.org/10.1016/s0168-3659(99)00090-5.

[49] X. Wang, D. Niu, C. Hu, P. Li, Polyethyleneimine-based nanocarriers for gene delivery. Curr. Pharm. Des. 21 (42) (2015) 6140-6156. https://doi.org/10.2174/1381612821666151027152907.

[50] K. Park, PEI-DNA complexes with higher transfection efficiency and lower cytotoxicity. J. Control Release 140 (1) (2009) 1. https://doi.org/10.1016/j.jconrel.2009.09.015.

[51] S.M. Moghimi, P. Symonds, J.C. Murray, A.C. Hunter, G. Debska, A. A. Szewczyk, Two-stage poly(ethylenimine)-mediated cytotoxicity: implications for gene transfer/therapy. Mol. Ther. 11 (6) (2005) 990-995. https://doi.org/10.1016/j.ymthe.2005.02.010.

[52] A. Hall, A.K. Larsen, L. Parhamifar, K.D. Meyle, L.P. Wu, S.M. Moghimi, High resolution respirometry analysis of polyethylenimine-mediated mitochondrial energy crisis and cellular stress: mitochondrial proton leak and inhibition of the electron transport system. Biochim. Biophys. Acta. 1827 (10) (2013) 1213-1225. https://doi.org/10.1016/j.bbabio.2013.07.001.

[53] K. Osada, Development of functional polyplex micelles for systemic gene therapy.

Polym J. 46 (2014) 469–475. https://doi.org/10.1038/pj.2014.49.

[54] N. Nishiyama, Y. Bae, K. Miyata, S. Fukushima, K. Kataoka, Smart polymeric micelles for gene and drug delivery. Drug Discov. Today Technol. 2 (1) (2005) 21-26. https://doi.org/10.1016/j.ddtec.2005.05.007.

[55] S. Uchida, K. Kataoka, Design concepts of polyplex micelles for in vivo therapeutic delivery of plasmid DNA and messenger RNA. J. Biomed. Mater. Res. A. 107 (5) (2019) 978-990. https://doi.org/10.1002/jbm.a.36614.

[56] J.S. Suk, Q. Xu, N. Kim, J. Hanes, L.M. Ensign, PEGylation as a strategy for improving nanoparticle-based drug and gene delivery. Adv. Drug Deliv. Rev. 99 (Pt A) (2016) 28-51. https://doi.org/10.1016/j.addr.2015.09.012.

[57] M. Oba, K. Miyata, K. Osada, R.J. Christie, M. Sanjoh, W. Li, S. Fukushima, T. Ishii, M.R. Kano, N. Nishiyama, H. Koyama, K. Kataoka, Polyplex micelles prepared from ω-cholesteryl PEG-polycation block copolymers for systemic gene delivery. Biomaterials 32 (2) (2011) 652-663. https://doi.org/10.1016/j.biomaterials.2010.09.022.

[58] M. Ogris, S. Brunner, S. Schüller, R. Kircheis, E. Wagner, PEGylated DNA/transferrin-PEI complexes: reduced interaction with blood components, extended circulation in blood and potential for systemic gene delivery. Gene Ther. 6 (4) (1999) 595-605. https://doi.org/10.1038/sj.gt.3300900.

[59] R. Gref, M. Lück, P. Quellec, M. Marchand, E. Dellacherie, S. Harnisch, T. Blunk, R.H. Müller, 'Stealth' corona-core nanoparticles surface modified by polyethylene glycol (PEG): influences of the corona (PEG chain length and surface density) and of the core composition on phagocytic uptake and plasma protein adsorption. Colloids Surf. B Biointerfaces. 18 (3-4) (2000) 301-313. https://doi.org/10.1016/s0927-7765(99)00156-3.

[60] T. Merdan, K. Kunath, H. Petersen, U. Bakowsky, K.H. Voigt, J. Kopecek, T. Kissel, PEGylation of poly(ethylene imine) affects stability of complexes with plasmid DNA under in vivo conditions in a dose-dependent manner after intravenous

injection into mice. Bioconjug. Chem. 16 (4) (2005) 785-792. https://doi.org/10.1021/bc049743q.

[61] M.K. Grun, A. Suberi, K. Shin, T. Lee, V. Gomerdinger, Z.M. Moscato, A.S. Piotrowski-Daspit, W.M. Saltzman, PEGylation of poly(amine-co-ester) polyplexes for tunable gene delivery. Biomaterials 272 (2021) 120780. https://doi.org/10.1016/j.biomaterials.2021.120780.

[62] Y. Sadzuka, K. Kishi, S. Hirota, T. Sonobe, Effect of polyethyleneglycol (PEG) chain on cell uptake of PEG-modified liposomes. J. Liposome Res. 13 (2) (2003) 157-172. https://doi.org/10.1081/lpr-120020318.

[63] D. Pozzi, V. Colapicchioni, G. Caracciolo, S. Piovesana, A.L. Capriotti, S. Palchetti, S. De Grossi, A. Riccioli, H. Amenitsch, A. Laganà, Effect of polyethyleneglycol (PEG) chain length on the bio-nano-interactions between PEGylated lipid nanoparticles and biological fluids: from nanostructure to uptake in cancer cells. Nanoscale 6 (5) (2014) 2782-2792. https://doi.org/10.1039/c3nr05559k.

[64] S. Mishra, P. Webster, M.E. Davis, PEGylation significantly affects cellular uptake and intracellular trafficking of non-viral gene delivery particles, Eur. J. Cell Biol. 83 (3) (2004) 97-111. https://doi.org/10.1078/0171-9335-00363.

[65] A.S. Abu Lila, H. Kiwada, T. Ishida, The accelerated blood clearance (ABC) phenomenon: clinical challenge and approaches to manage. J. Control Release 172 (1) (2013) 38-47. https://doi.org/10.1016/j.jconrel.2013.07.026.

[66] M.M. El Sayed, H. Takata, T. Shimizu, Y. Kawaguchi, A.S. Abu Lila, N.E. Elsadek, E. Alaaeldin, Y. Ishima, H. Ando, A. Kamal, H.A. Sarhan, T. Ishida, Hepatosplenic phagocytic cells indirectly contribute to anti-PEG IgM production in the accelerated blood clearance (ABC) phenomenon against PEGylated liposomes: Appearance of an unexplained mechanism in the ABC phenomenon. J. Control Release. 323 (2020) 102-109. https://doi.org/10.1016/j.jconrel.2020.04.011.

[67] B.M. Chen, T.L. Cheng, S.R. Roffler, Polyethylene glycol immunogenicity: theoretical, clinical, and practical aspects of anti-polyethylene glycol antibodies.

ACS Nano 15 (9) (2021) 14022-14048. https://doi.org/10.1021/acsnano.1c05922.

[68] L. Mi, S. Jiang, Integrated antimicrobial and nonfouling zwitterionic polymers. Angew. Chem. Int. Ed. Engl. 53 (7) (2014) 1746-1754. https://doi.org/10.1002/anie.201304060.

[69] S. Jiang, Z. Cao, Ultralow-fouling, functionalizable, and hydrolyzable zwitterionic materials and their derivatives for biological applications. Adv. Mater. 22 (9) (2010) 920-932. https://doi.org/10.1002/adma.200901407.

[70] M. Debayle, E. Balloul, F. Dembele, X. Xu, M. Hanafi, F. Ribot, C. Monzel, M. Coppey, A. Fragola, M. Dahan, T. Pons, N. Lequeux, Zwitterionic polymer ligands: an ideal surface coating to totally suppress protein-nanoparticle corona formation? Biomaterials 19 (2019) 119357. https://doi.org/10.1016/j.biomaterials.2019.119357.

[71] M. Ilčíková, J. Tkáč, P. Kasák, Switchable materials containing polyzwitterion moieties. Polymers 7 (11) (2015) 2344-2370. https://doi.org/10.3390/polym7111518.

[72] J. Wang, S. Yuan, Y. Zhang, W. Wu, Y. Hu, X. Jiang, The effects of poly(zwitterions)s versus poly(ethylene glycol) surface coatings on the biodistribution of protein nanoparticles. Biomater. Sci. 4 (9) (2016) 1351-1160. https://doi.org/10.1039/c6bm00201c.

[73] A.H. Ranneh, H. Takemoto, S. Sakuma, A. Awaad, T. Nomoto, Y. Mochida, M. Matsui, K. Tomoda, M. Naito, N. Nishiyama, An ethylenediamine-based switch to render the polyzwitterion cationic at tumorous pH for effective tumor accumulation of coated nanomaterials, Angew. Chem. Int. Ed. 57 (18) (2018) 5057-5061. https://doi.org/10.1002/anie.201801641.

[74] A. Awaad, H. Takemoto, M. Iizuka, K. Ogi, Y. Mochida, A.H. Ranneh, M. Toyoda, M. Matsui, T. Nomoto, Y. Honda, K. Hayashi, K. Tomoda, T. Ohtake, Y. Miura, N. Nishiyama, Changeable net charge on nanoparticles facilitates intratumor accumulation and penetration, J. Control Release 346 (2022) 392-404.

https://doi.org/10.1016/j.jconrel.2022.04.025.

[75] Y.J. Sung, H. Guo, A. Ghasemizadeh, X. Shen, W. Chintrakulchai, M. Kobayashi, M. Toyoda, K. Ogi, J. Michinishi, T. Ohtake, M. Matsui, Y. Honda, T. Nomoto, H. Takemoto, Y. Miura, N. Nishiyama, Cancerous pH-responsive polycarboxybetaine-coated lipid nanoparticle for smart delivery of siRNA against subcutaneous tumor model in mice, Cancer Sci. 113 (12) (2022) 4339-4349. https://doi.org/10.1111/cas.15554.

[76] H. Takemoto, N. Nishiyama, Construction of nanomaterials based on pH-responsive polymers for effective tumor delivery. Polym. J. 53 (2021) 1353–1360. https://doi.org/10.1038/s41428-021-00542-7.

Chapter 2. Synthesis of Polymers and Their Cytotoxicity

2.1 Introduction

In this research, the PEI was chosen for polyion complexes (polyplexes) formulation through electrostatic self-assembly between anionic nucleus acids and cationic polymers as the standard transfection material [1-3]. Meanwhile, PGlu(DET-Car) was selected as the pH-responsive polyzwitterion segment whereas the ethylenediamine-based carboxy betaine underwent stepwise protonation as pH decreased [4-6]. At physiological conditions (pH 7.4), PGlu(DET-Car) exhibits a neutral net charge, thus it does not involve in the formation with negatively charged nucleic acids. The net charge of the PGlu(DET-Car) turns to cationic in response to an acidic environment allowing the interaction with negatively charged cell membranes for effective cellular uptake and endosomal escape. To make these two segments together, copper-free click chemistry allowing efficient and selective reactions between two types of moieties: azide and strained alkynes *i.e.,* DBCO was introduced in this system [7].

First, azide functionalized PGlu(DET-Car) [(N_3-PGlu(DET-Car)] was obtained as our previous report [5]. The side chains of the N_3-PBLG were modified with tert-butyl 3-{[(2-aminoethyl)-2-aminoethyl]-amino}-propanoate *via* aminolysis, followed by elimination of the tert-butyl groups to yield N_3-PGlu(DET-Car). Also, N_3-PEG was used to investigate as a conventional control as it is widely used as the hydrophilic shielding material with non-ionic property. The molecular weight of PEG was selected based on the average value of the hydrodynamic sizes of the PGlu(DET-Car), using size exclusion chromatography. Then, PEI with DBCO terminus (PEI-DBCO) was prepared by a condensation reaction of the primary amine groups on bPEI (M_w = 25 kDa) and the DBCO-NHS while maintaining the stoichiometry ratio (*i.e.*, 10/1 eq., primary amine basis). Subsequent click conjugation between N_3-PGDC and DBCO-bPEI using the freeze-thaw technique [8]. Likewise, PEG-bPEI was also synthesized as a control polymer. Finally, to evaluate the biocompatibility of the polymers, their cytotoxicity was evaluated in two cell lines, *i.e.*, Huh-7 (human hepatoma cell line) and Neuro2a

(murine neuroblastoma cell line). The cell viability assay was performed by using CCK assay to evaluate the cellular metabolic activity in cells [9]. In addition, a LDH assay was performed to assess the disruption of the cellular membrane after incubation with the polymers, to deepen the understanding of the interaction with the cellular membrane.

2.2 Materials and Methods

2.2.1 Materials

γ-benzyl-L-glutamate N-carboxy anhydride (BLG-NCA) was purchased from Chuo Kaseihin Co., Inc. (Tokyo, Japan). Diethyl ether, dichloromethane (DCM), *N*, *N*-Dimethylformamide (DMF), *n*-hexane, ethyl acetate, methanol (MeOH), diethylenetriamine (DET), 2-hydroxypridine, dimethyl sulfoxide (DMSO), tetrahydrofuran (THF), triethylamine (TEA), and ethanol were purchased from Wako Pure Chemical Industries, Ltd. (Osaka, Japan). 2-hydroxypyridine was obtained from Tokyo Chemical Industry Co., Ltd. (Tokyo, Japan). Deuterated dimethyl sulfoxide (DMSO-*d6*) containing 1 v/v% tetramethyl silane (TMS) was purchased from Cambridge Isotope Laboratories, Inc. (Tewksbury, MA, USA). Dibenzocyclooctyne-N-hydroxysuccinimidyl ester (DBCO-NHS) was purchased from Click Chemistry Tools, Ltd. (Scottsdale, AZ, USA). PEI (25-kDa), 11-azido-3,6,9-trioxaundecan-1-amine, N_3-PEG (20-kDa), deuterium chloride (DCl) Dulbecco's phosphate buffered saline (D-PBS(−)), penicillin/streptomycin, Dulbecco Modified Eagle Medium (DMEM), Eagle's Minimum Essential Medium (EMEM), trypsin-EDTA, were purchased from Sigma Aldrich (St. Louis, MO, USA). Cell Counting Kit-8 (CCK) and Lactate dehydrogenase (LDH) Kit was purchased from Dojindo Molecular Technologies Co., Inc. (Kumamoto, Japan).

2.2.2 Synthesis of azide-terminated poly(γ-benzyl-L-glutamate) (N_3-PBLG)

PBLG with azide functional group was synthesized by ring-opening polymerization of BLG-NCA with 11-azido-3,6,9-trioxaundecan-1-amine as the initiator (**Scheme 2-1**). Briefly, BLG-NCA (3.01 g, 11.4 mmol) was dissolved in DMF/DCM (1/4, v/v, 100 mL) mixture under Ar. Then, 11-azido-3,6,9-trioxaundecan-1-amine (20.5 mg, 0.095 mmol) was added to the reaction solution to initiate the ring-opening polymerization. After two days of reaction at room temperature, the reaction mixture was poured into an excess amount of n-hexane/ethyl acetate (3/2, v/v), and the precipitate was collected by filtration and dried under vacuum to obtain a white powder (2.43 g, yield 90%, M_n = 14300, M_w/M_n = 1.20). The chemical structure of N_3-PBLG was analyzed by ^{1}H NMR using Bruker biospin AVANCE III 400 MHz (DMSO-*d6*, 25 °C). The reaction product was analyzed using SEC analysis equipped with an RI detector (RI 2075, JASCO, Tokyo, Japan) [column: superAW3000 (TOSOH, Tokyo, Japan), eluent: NMP with 50 mM LiBr].

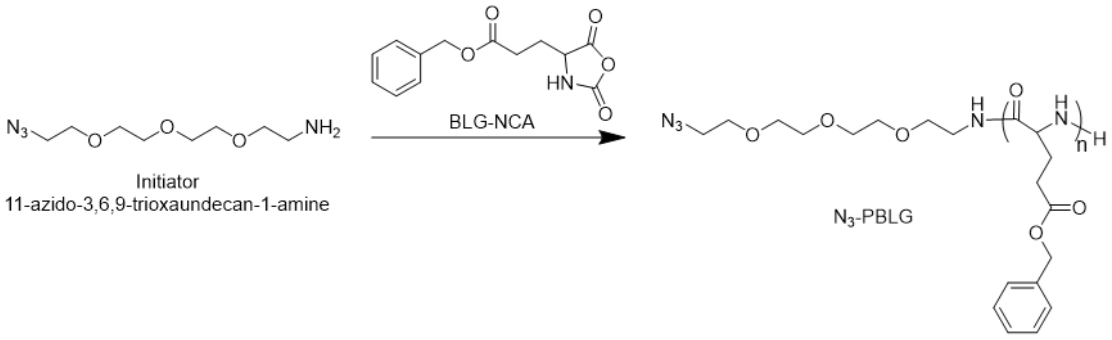

Scheme 2-1. Synthetic procedures of N_3-PBLG.

2.2.3 Synthesis of tert-butyl 3-{[(2-aminoethyl)-2-aminoethyl]-amino}-propanoate and tert-butyl 3-[(2-aminoethyl)-amino]-propanoate

Tert-Butyl acrylate (5.75 g, 45 mmol) was dropwisely added into DET (25 g, 242.5 mmol) and the reaction was stirred for 2 hours at room temperature (**Scheme 2-2**). After washing the reaction solution with sodium chloride solution three times to remove the

unreacted DET and drying by anhydrous sodium sulfate, the organic layer was evaporated and purified by column chromatography using MeOH/TEA (95/5, v/v) as an eluent to obtain tert-butyl 3-{[(2-aminoethyl)-2-aminoethyl]-amino}-propanoate as a colorless oil (3.1 g, 27%) and confirmed by ^{1}H NMR using Bruker biospin AVANCE III 400 MHz (D_2O/DCl (99.9/0.1(v/v), 25 °C)

Scheme 2-2. Synthetic procedures of tert-butyl 3-{[(2-aminoethyl)-2-aminoethyl]-amino}-propanoate.

2.2.4 Synthesis of poly(N-{N'-[N"-(2-carboxyethyl)-2-aminoethyl]-2-aminoethyl}glutamide) [N_3-PGlu(DET-Car)]

The synthesis followed **Scheme 2-3**. PBLG (50 mg, 2.31 μmol, 0.23 mmol of the benzyl group) was dissolved in THF (2 mL), followed by the addition of 2-hydroxypyridine (107 mg, 1.12 mmol) and tert-butyl 3-{[(2-aminoethyl)-2-aminoethyl]-amino}-propanoate (800 mg, 4.6 mmol). The reaction solution was stirred at room temperature overnight, and then acidified by 1 M HCl aq. for another two days. The obtained mixture was dialyzed against deionized water (molecular weight cut off: 8,000 Da) and lyophilized to obtain PGlu(DET-Car) as a white powder (51 mg, 79% yield). The structure of obtained PGlu(DET-Car) was confirmed *via* ^{1}H NMR (400 MHz NMR Spectrometer Bruker Biospin AG AVANCE III, Billerica, MA, USA) in D2O at 25 °C and SEC analysis was performed by Jasco HPLC system [RI-detector, column: Superdex 200 increase 10/300 GL (GE healthcare life science, Buckinghamshire, UK), eluent: 10 mM HEPES buffer with 500 mM of NaCl at pH 7.4]. In addition, the protonation behavior of PGlu(DET-Car) was measured by an automatic titrator (COM-1750, Hiranuma, Kyoto, Japan) according to the manufacturer's protocol.

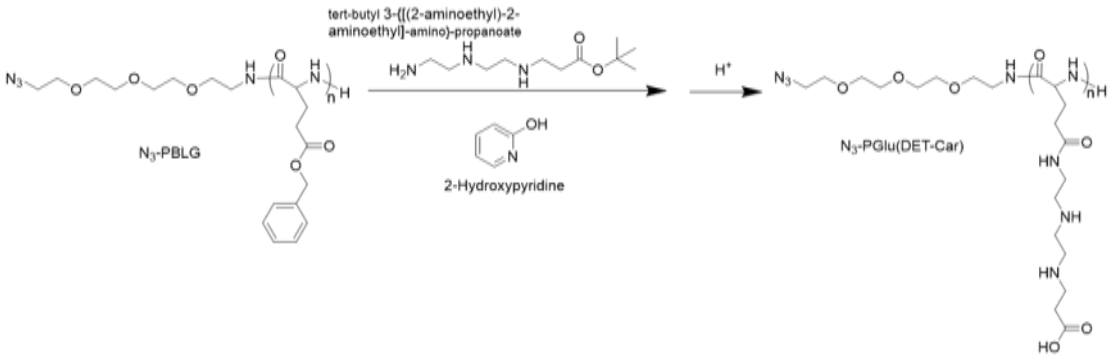

Scheme 2-3. Synthetic procedures of N_3-PGlu(DET-Car).

2.2.5 Synthesis of dibenzocyclooctyne modified polyethyleneimine (DBCO-bPEI)

DBCO-bPEI was synthesized by the reaction between the primary amine of PEI and DBCO-NHS (**Scheme. 2-4**). In brief, PEI (53 mg, 5.3 μmol, equivalent to 41.5 μmol of primary amine, M_w=25k, M_n=10k) was dissolved in dry DMSO followed by the addition of TEA (4.19 mg, 41.5 μmol) and stirred for 30 min at room temperature. Then, DBCO-NHS (16.7 mg, 4.15 μmol) dissolved in dry DMSO (1 mL) was added to the reaction mixture. After overnight, the mixture was dialyzed against MeOH for 1 day and then changed the system to water for another 2 days, followed by lyophilization to obtain the PEI-DBCO conjugates. The successful conjugation of DBCO was confirmed by comparing the peak area corresponding to DBCO (δ = 7-8 ppm) and PEI (δ = 2.75-3.75 ppm) in the 1H NMR spectrum. The modification degree of PEI-DBCO was further confirmed by UV spectroscopy (V-650, JASCO, Tokyo, Japan, λ = 294 nm).

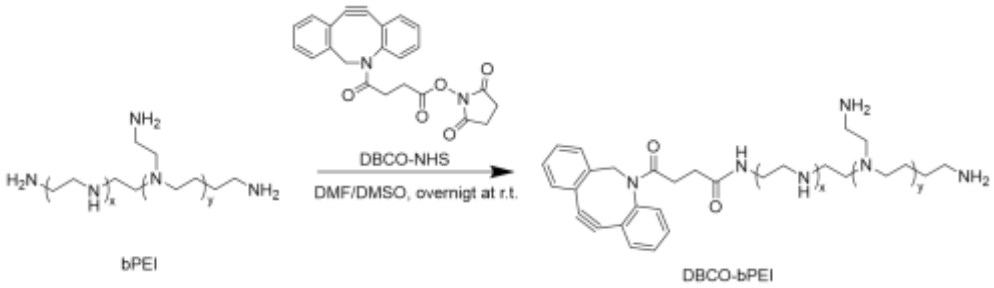

Scheme 2-4. Synthetic procedures of DBCO-bPEI.

2.2.6 Synthesis of PGlu(DET-Car)-bPEI

In **scheme 2-5**, the N_3-PGlu(DET-Car) (20 mg, 0.66 μmol) was dissolved in deionized water (1 mL) and mixed with PEI-DBCO (7.37 mg, 0.69 μmol, the DBCO group was 1.05 equiv. to azide group) dissolved in deionized water (0.5 mL). To promote the copper-free click-reaction, the frozen and thaw method was used in this study [8]. After three times of freeze-thawing circles, the obtained PGlu(DET-Car)-bPEI was purified by centrifuge filtration (MCWO = 30k) at room temperature. Then, the final product (21 mg, 77% yield) was obtained by lyophilization and characterized by ^{1}H NMR.

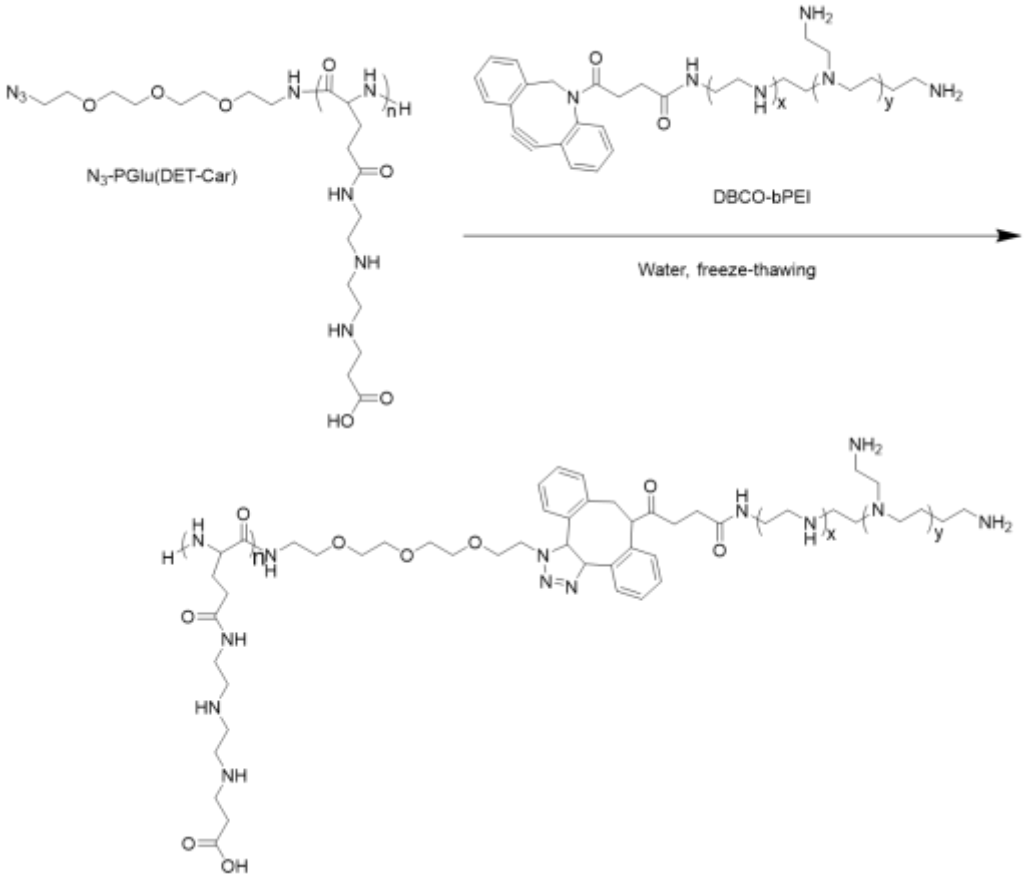

Scheme 2-5. Synthetic procedures of PGlu(DET-Car)-bPEI.

2.2.7 Synthesis of PEG-bPEI

In **scheme 2-6**, the N_3-PEG (15 mg, 0.75 μmol) was dissolved in deionized water (1 mL) and mixed with PEI-DBCO (8.38 mg, 0.78 μmol, the DBCO group was 1.05 equiv.

to azide group) dissolved in deionized water (0.5 mL). To promote the copper-free click-reaction, the frozen and thaw method was used in this study [8]. After three times of freeze-thawing circles, the obtained PEI-PEG was purified by centrifuge filtration (MCWO = 30k) at room temperature. Then, the final product (14 mg, 67% yield) was obtained by lyophilization and characterized by ^{1}H NMR.

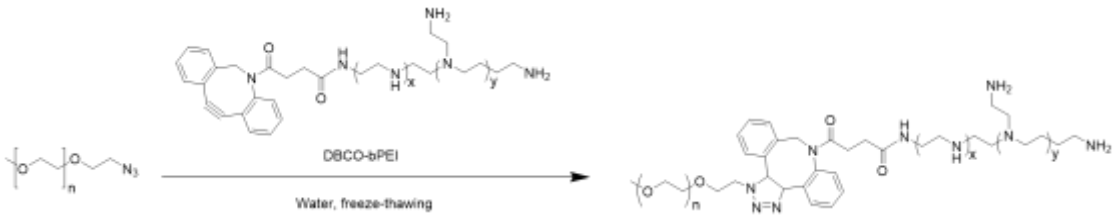

Scheme 2-6. Synthetic procedures of PEG-bPEI.

2.2.8 Cytotoxicity study of polymers

LDH assay and CCK assay were performed to study the *in vitro* cytotoxicity and viability of the polymers, respectively. Briefly, Huh-7 (5×10^3 cells/well) and Neuro-2A cells (5×10^3 cells/well) were seeded in 96-well plates. After overnight incubation, polymers were applied to the cells with different concentrations. After additional 48 h incubation, 100 μL of supernatant was transformed into another 96-well plates by adding 100 μL of LDH working solution and incubating in the dark for 30 minutes. 50 μL stop solution was added and measured the absorbance at 490 nm by Tecan microplate reader (SPARK TKS01, TECAN, Zürich, Switzerland). After removing the supernatant, cells were washed with D-PBS(−) twice. The fresh medium containing 10% CCK reagent was added to the plates and incubated for 2 h at 37 ℃. The absorbance at 450 nm was read by a Tecan microplate reader (SPARK TKS01, TECAN, Zürich, Switzerland). Cell cytotoxicity and viability were determined by the following equations:

$$\text{Cell cytotoxicity (\%)} = ([A]_{sample} - [A]_{low})/([A]_{high} - [A]_{low}) \times 100\%,$$

Where, $[A]_{sample}$, $[A]_{high}$, and $[A]_{low}$ represent the absorbance values of samples, high control groups, and low control groups, respectively.

$$\text{Cell viability (\%)} = ([A]_{sample} - [A]_{blank})/([A]_{control} - [A]_{blank}) \times 100\%,$$

whereas, $[A]_{sample}$, $[A]_{control}$, and $[A]_{blank}$ are the absorbance values of the wells belonging to treated cells, non-treated cells, and culture media, respectively.

2.3 Results and discussion

2.3.1 Synthesis of N_3-PBLG

Successfully synthesis of N_3-PBLG was confirmed by ^{1}H NMR analysis with the degree of polymerization of 100 based on the peak intensity ratio between phenyl protons (-$CH_2C_6H_5$, 7.1–7.3 ppm) in PBLG and oxyethylene protons (N_3-CH_2CH_2-$(OCH_2CH_2)_3$-NH, 3.5 ppm) in the initiator (**Figure 2-1**). The molecular weight distribution (M_w/M_n), calculated through SEC analysis, was found to be 1.21 (**Figure 2-2**).

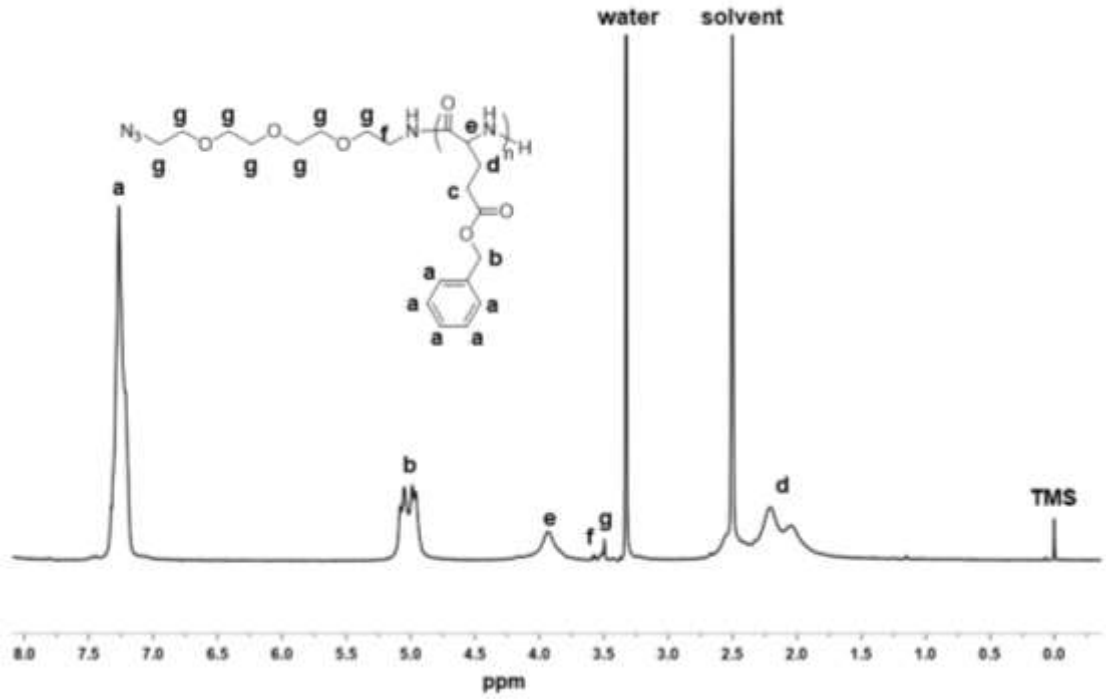

Figure 2-1. ^{1}H NMR spectrum of N_3-PBLG in DMSO-*d6* at 25℃.

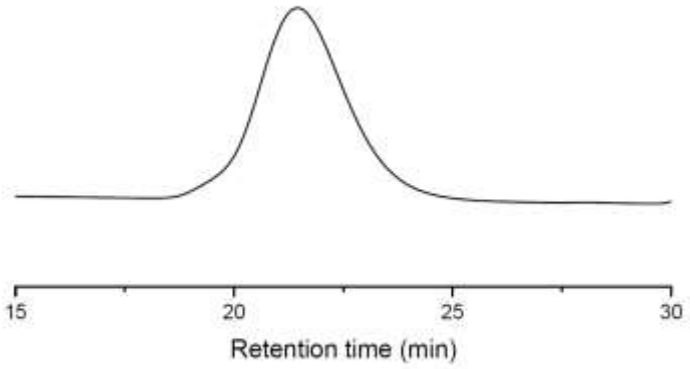

Figure 2-2. The GPC spectrum of retention time of N_3-PBLG.

2.3.2 Synthesis of N_3-PGlu(DET-Car)

The side chains of the N_3-PBLG (polymerization degree = 100) were modified with tert-butyl 3-{[(2-aminoethyl)-2-aminoethyl]-amino}-propanoate *via* aminolysis, followed by elimination of the tert-butyl groups to yield N_3-PGlu(DET-Car) as confirmed by ^{1}H NMR analysis (**Figure 2-3**). The molecular weight (M_w) of N_3-PGlu(DET-Car) was found to be approximately 18,000 g/mol utilizing SEC with PEG as a standard. Using potentiometric titration assay, the protonation behavior of PGlu(DET-Car) was studied on the pK_a and the degree of protonation (α) (**Table 2-1**), where the ethylenediamine-based carboxybetaine group demonstrated three unique pK_a values of 8.6, 6.2, and 4.5. As a result, the adoption of a gauche ring system by monoprotonated ethylenediamine and the subsequent substantial thermodynamic expenditure required to attain the preferred anti conformer of bi-protonated ethylenediamine in an acidic microenvironment [10, 11].

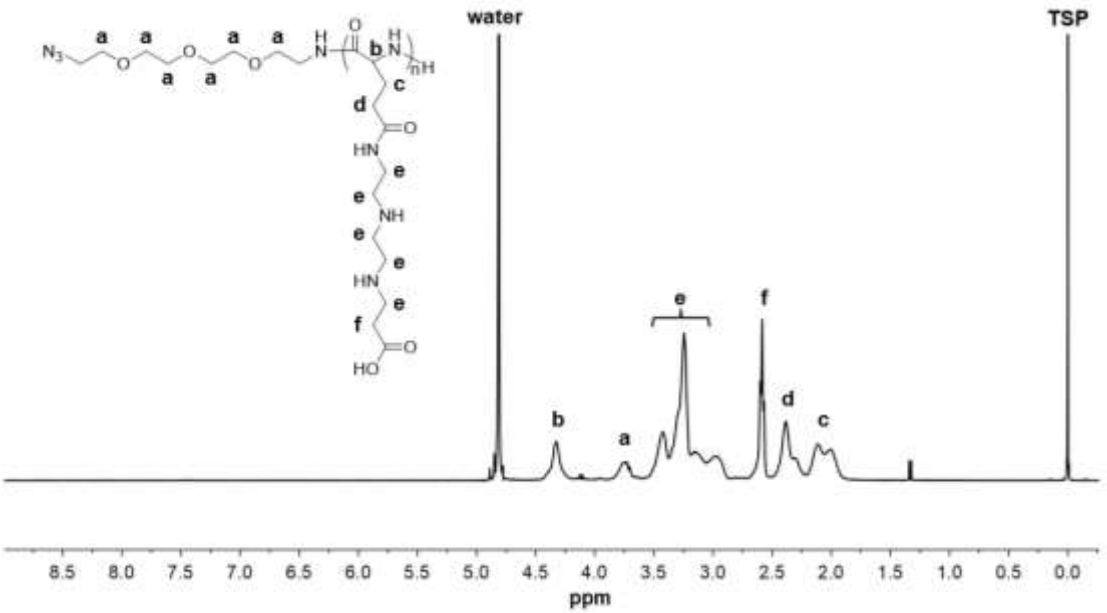

Figure 2-3. ^{1}H NMR spectrum of N_3-PGlu(DET-Car) in D_2O at 25℃.

Moreover, to comprehend the charge conversion behavior of N_3-PGlu(DET-Car), the ratio of cationic charges to anionic charges (C/A) was analyzed from the α/pH curves (**Table 2-1**). The C/A ratio of N_3-PGlu(DET-Car) was 1.09 at pH 7.4, showing a neutral net charge. Moreover, the C/A ratio of N_3-PGlu(DET-Car) increased to 1.39 at pH 6.5, suggesting that the net charge of N_3-PGlu(DET-Car) switched its neutral property to cationic at tumorous pH. N_3-PGlu(DET-Car) exhibited a C/A value of 1.84 when exposed to pH 5.5, implying substantial protonation of the ethylenediamine groups in PGlu(DET-Car).

Table 2-1. Chemical parameters of N_3-PGlu(DET-Car) at different pH milieu.

pK_{a1}[a]	pK_{a2}[a]	pK_{a3}[a]	Protonation degree (%) [b]			C/A ratio [c]		
			pH 7.4	pH 6.5	pH 5.5	pH 7.4	pH 6.5	pH 5.5
8.6	6.2	4.5	36.3	46.0	61.9	1.09	1.39	1.84

[a] The pK_a values of N_3-PGlu(DET-Car) were determined by an acid-base titration curve in an aqueous solution. [b] The degree of protonation (α) was determined from the titration curves measured by the potentiometric titration experiment. [c] C/A ratio is the ratio of cationic charges to anionic charges which was estimated from the α/pH curves.

2.3.2 Synthesis of DBCO-bPEI

PEI-DBCO was prepared by a condensation reaction of the primary amine groups on bPEI (M_w = 25 kDa) and the DBCO-NHS while maintaining the stoichiometry ratio (*i.e.*, 10/1 eq., primary amine basis). The successful introduction of DBCO into the PEI was confirmed by ^{1}H NMR analysis (**Figure 2-4**), from the peak intensity ratio of the phenyl protons in DBCO ($(C_4H_4)_2C_7H_2N$-, δ = 7.4-7.7 ppm). The introduction ratio of DBCO/PEI on a single bPEI was calculated as 1.9 by UV spectroscopy.

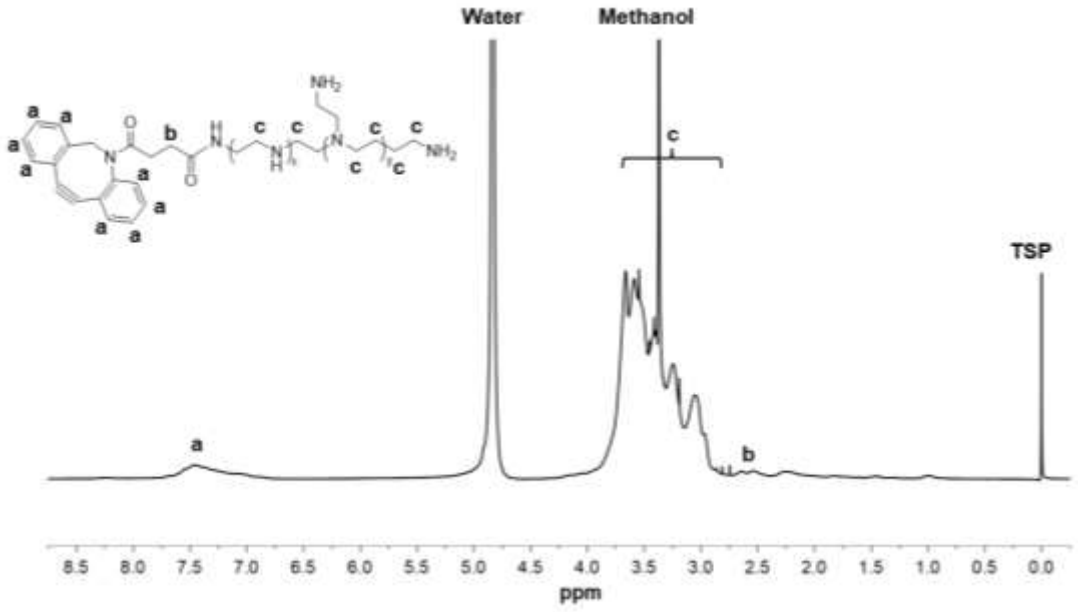

Figure 2-4. ^{1}H NMR spectrum of DBCO-bPEI in D_2O at 25°C.

2.3.4 Synthesis of PGlu(DET-Car)-bPEI

Subsequent click conjugation between N_3-PGlu(DET-Car) and DBCO-bPEI using the freeze−thaw technique led to an almost quantitative formation of PGlu(DET-Car)-bPEI with evidence provided by ^{1}H-NMR analysis (**Figure 2-5**). Likewise, PEG-bPEI (M_w of PEG is 20 kDa) was also synthesized as a control polymer and confirmed by ^{1}H-NMR analysis (**Figure 2-6**).

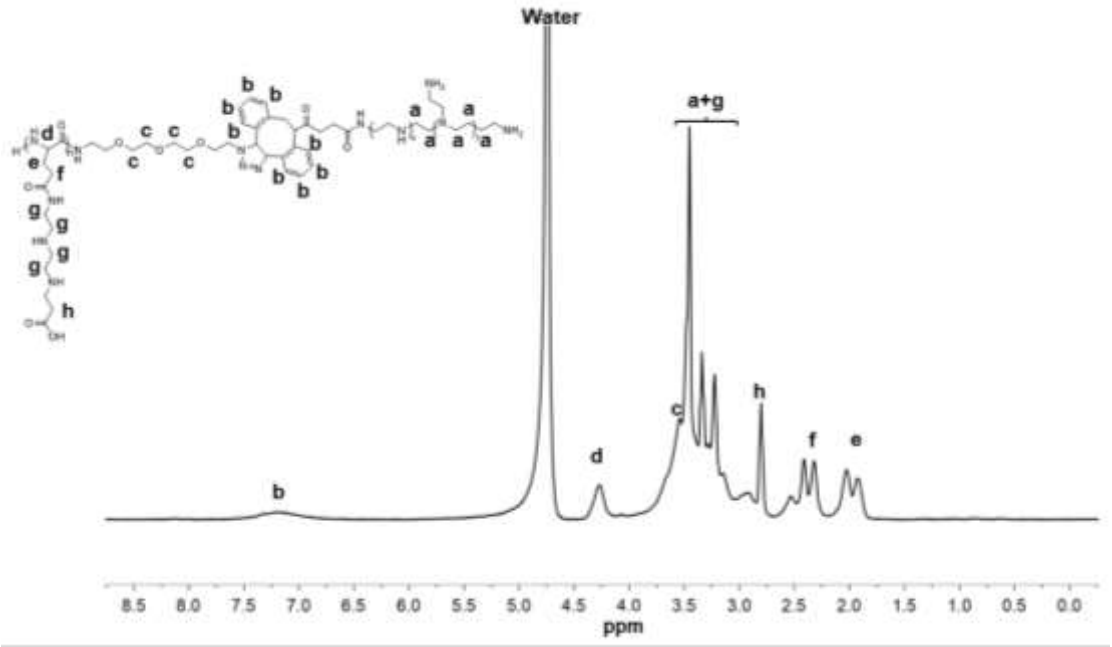

Figure 2-5. ^{1}H NMR spectrum of PGlu(DET-Car)-bPEI in D_2O at 25℃.

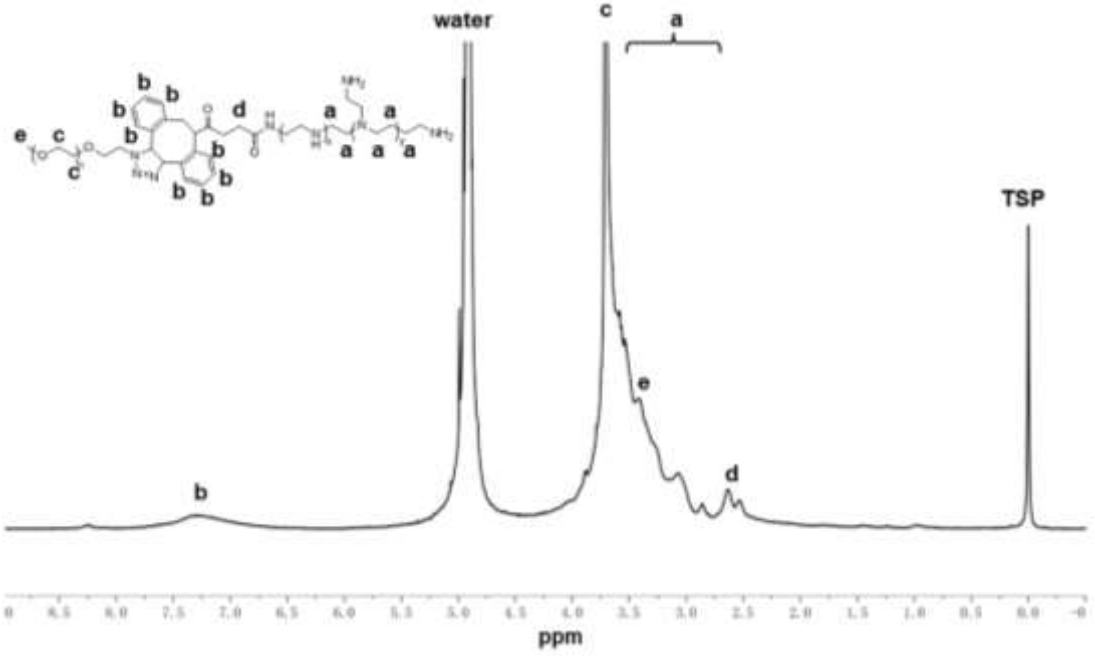

Figure 2-6. ^{1}H NMR spectrum of PEG-bPEI in D_2O at 25℃.

2.3.5 Biocompatibility study of polymers

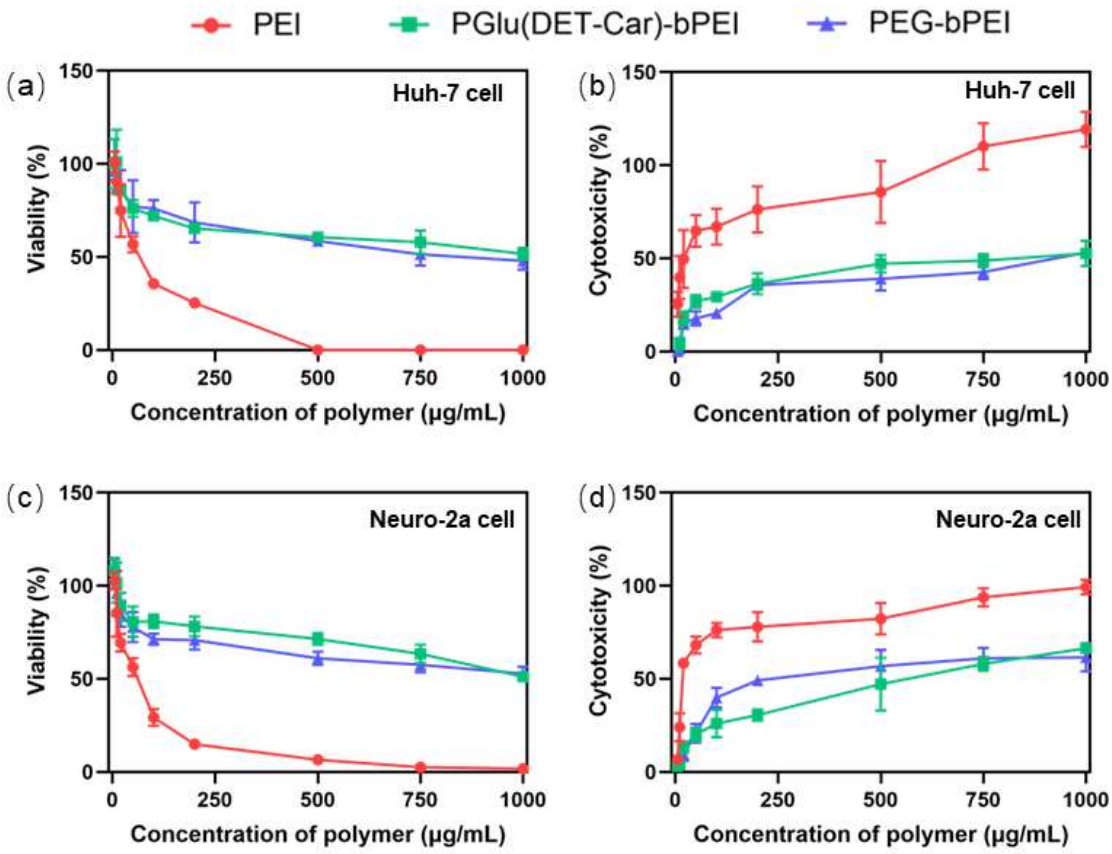

Figure 2-7. *In vitro* biocompatibility of the polymers. (a) Viability and (b) cytotoxicity of the different concentrations of polymers incubated for 48 h in Huh-7 cell line. (c) Viability and (d) cytotoxicity of the different concentrations of polymers for 48 h in Neuro-2a cell line. The results are expressed as mean ± SEM. (n = 6).

PEI is characterized by the presence of protonable amine groups at every third atom, which imparts high charge density and exceptional buffering capacity across a broad pH range [12]. Nevertheless, the high degree of protonation exhibited by PEI resulted in indiscriminate interactions and disruptions of lipid bilayers in cell membranes, leading to toxic effects [13]. Therefore, in this study, we modified PEI with polyzwitterion polymer PGlu(DET-Car) or PEG to reduce the cytotoxicity of the PEI. To assess the biocompatibility of the modified polymers, *in vitro* evaluations were performed using the Huh-7 and Neuro-2a cell lines, and the cell viability was determined *via* CCK and LDH assays. PEI has been included as a control group. As

shown in **Figure 2-7**, the viability of two cell lines was observed to be significantly enhanced while cytotoxicity was reduced upon modification of PEI with either PGlu(DET-Car) or PEG, in comparison to the use of PEI polymer alone. This indicated the potential of PEI modification with polyzwitterion such as PGlu(DET-Car) as a promising strategy for improving cell viability and reducing cytotoxicity. Moreover, IC_{50} values were calculated from cell viability curves and summarized in **Table 2-2**. The IC_{50} values of PGlu(DET-Car)-bPEI and PEG-bPEI were found to be 17-29 and 15-22 times higher than those of PEI in Huh-7 cells and Neuro-2a cells, respectively. These results suggest that PEI may have a stronger inhibitory effect on cell growth than the modified-PEI tested.

Table 2-2. IC_{50} values of polymers in different cell lines.

IC_{50} (μg/mL)	PEI	PGlu(DET-Car)-bPEI	PEG-bPEI
Huh-7 cell	6.09	106.9	90.2
Neuro-2a cell	5.11	151.4	113.1

2.4 Conclusion

In this chapter, based on the PBLG backbone, I prepared the N_3-PGlu(DET-Car) bearing ethylenediamine-based carboxybetaine moiety at the side chain. Through the investigation of the protonation behavior of N_3-PGlu(DET-Car), it has been observed that this compound displays a regulated ionization of cationic groups, exhibiting pH-responsive characteristics in a reversible manner. These findings hold potential for the advancement of the gene nanocarrier system as it is transported from the bloodstream to the tumor and finally into the intracellular endosomes, it undergoes a decrease in pH within the different physiological environments, dropping from 7.4 to 5.5. In parallel, N_3-PEG, possessing a comparable molecular weight, has been utilized as a non-ionic

control within the study.

Moreover, modified PEI with either N_3-PGlu(DET-Car) or N_3-PEG was synthesized, and studied their biocompatibility *in vitro*. PGlu(DET-Car)-bPEI and PEG-bPEI demonstrated a substantial ability to mitigate the cellular membrane damage induced by the positively charged PEI in both Huh-7 and Neuro-2A cell lines, consequently leading to a notable reduction in the toxicity associated with PEI. These results highlight that the modification of PEI represents a valuable avenue for optimizing its properties, enabling safer and more effective utilization in both *in vitro* and *in vivo* applications.

2.5 References

[1] R. Kircheis, L. Wightman, E. Wagner, Design and gene delivery activity of modified polyethylenimines, Adv. Drug Deliv. Rev. 53 (3) (2001) 341-358. https://doi.org/10.1016/s0169-409x(01)00202-2.

[2] M. Neu, D. Fischer, T. Kissel, Recent advances in rational gene transfer vector design based on poly(ethylene imine) and its derivatives, J. Gene Med. 7 (8) (2005) 992-1009. https://doi.org/10.1002/jgm.773.

[3] A. Akinc, M. Thomas, A.M. Klibanov, R. Langer, Exploring polyethylenimine-mediated DNA transfection and the proton sponge hypothesis, J. Gene Med. 7 (5) (2005) 657-663. https://doi.org/10.1002/jgm.696.

[4] A.H. Ranneh, H. Takemoto, S. Sakuma, A. Awaad, T. Nomoto, Y. Mochida, M. Matsui, K. Tomoda, M. Naito, N. Nishiyama, An ethylenediamine-based switch to render the polyzwitterion cationic at tumorous pH for effective tumor accumulation of coated nanomaterials, Angew. Chem. Int. Ed. 57 (18) (2018) 5057-5061. https://doi.org/10.1002/anie.201801641.

[5] A. Awaad, H. Takemoto, M. Iizuka, K. Ogi, Y. Mochida, A.H. Ranneh, M. Toyoda, M. Matsui, T. Nomoto, Y. Honda, K. Hayashi, K. Tomoda, T. Ohtake, Y. Miura,

N. Nishiyama, Changeable net charge on nanoparticles facilitates intratumor accumulation and penetration, J. Control Release 346 (2022) 392-404. https://doi.org/10.1016/j.jconrel.2022.04.025.

[6] Y.J. Sung, H. Guo, A. Ghasemizadeh, X. Shen, W. Chintrakulchai, M. Kobayashi, M. Toyoda, K. Ogi, J. Michinishi, T. Ohtake, M. Matsui, Y. Honda, T. Nomoto, H. Takemoto, Y. Miura, N. Nishiyama, Cancerous pH-responsive polycarboxybetaine-coated lipid nanoparticle for smart delivery of siRNA against subcutaneous tumor model in mice, Cancer Sci. 113 (12) (2022) 4339-4349. https://doi.org/10.1111/cas.15554.

[7] E. Kim, H. Koo, Biomedical applications of copper-free click chemistry: in vitro, in vivo, and ex vivo. Chem. Sci. 10 (34) (2019) 7835-7851. https://doi.org/10.1039/c9sc03368h.

[8] H. Takemoto, K. Miyata, T. Ishii, S. Hattori, S. Osawa, N. Nishiyama, K. Kataoka, Accelerated Polymer–Polymer Click Conjugation by Freeze–Thaw Treatment, Bioconjugate chem. 23 (8) (2012) 1503-1506. https://doi.org/10.1021/bc300182y.

[9] L. Cai, X. Qin, Z. Xu, Y. Song, H. Jiang, Y. Wu, H. Ruan, J. Chen, Comparison of cytotoxicity evaluation of anticancer drugs between real-time cell analysis and CCK-8 method. ACS Omega (2019) 4(7) (2019) 12036-12042. https://doi.org/10.1021/acsomega.9b01142.

[10] D. De Corte, C.-W. Schläpfer, C. Daul, A density functional theory study of the conformational properties of 1,2-ethanediamine: protonation and solvent effects, Theoretical Chemistry Accounts, 105 (2000) 39-45. https://doi.org/10.1007/s002140000177.

[11] K. Miyata, M. Oba, M. Nakanishi, S. Fukushima, Y. Yamasaki, H. Koyama, N. Nishiyama, K. Kataoka, Polyplexes from poly(aspartamide) bearing 1,2-diaminoethane side chains induce pH-selective, endosomal membrane destabilization with amplified transfection and negligible cytotoxicity, J. Am. Chem. Soc. 130 (48) (2008) 16287-16294. https://doi.org/10.1021/ja804561g.

[12] C. Brunot, L. Ponsonnet, C. Lagneau, P. Farge, C. Picart, B. Grosgogeat, Cytotoxicity of polyethyleneimine (PEI), precursor base layer of polyelectrolyte multilayer films, Biomaterials 28 (4) (2007) 632-640. https://doi.org/10.1016/j.biomaterials.2006.09.026.

[13] A. Hall, U. Lächelt, J. Bartek, E. Wagner, S.M. Moghimi, Polyplex evolution: understanding biology, optimizing performance, Mol. Ther. 25 (7) (2017) 1476-1490. https://doi.org/10.1016/j.ymthe.2017.01.024.

Chapter 3 Preparation and Characterization of PMs

3.1 Introduction

Upon confirmation of successful polymer synthesis *i.e.*, PGlu(DET-Car)-bPEI, PEG-bPEI, as detailed in Chapter 2, this chapter proceeded to investigate the formation and physicochemical characteristics of the produced PMs. This investigation aimed to shed light on the nature and behavior of the PMs under various conditions mimicking the different physiological environments in the body and to provide a better understanding of their potential applications and limitations.

The present study utilized a micelle formation method that draws upon prior literature [1, 2], which established that electrostatic interaction between positively charged polymers and negatively charged nucleic acids can lead to self-assembly and the formation of stable micelles under aqueous solutions. In this study, the formation of the PMs was under physiological conditions (pH 7.4). This choice of conditions was informed by the observation that at this pH level, the C/A value of PGlu(DET-Car) equates to 1.09, rendering it uncharged at pH 7.4. Therefore, only the positively charged PEI was involved in the micelle formation process, with PGlu(DET-Car) serving as a protective outer shell for the micelle. The utilization of this approach allowed for a more nuanced understanding of the formation and behavior of the resulting micelles, and their potential applications in various contexts. Meanwhile, PEI-polyplex was employed as the control to assess the shielding potential, estimation of specific characteristics of PMs, and the specific parameters that undergo alterations as a result of modifications.

In this chapter, the polyplex and PMs will be investigated to determine their hydrodynamic size, PDI, and stability under varying pH conditions. This inquiry was prompted by the significant role that nanoparticle size plays in blood circulation, as particle sizes less than 5 nm are rapidly eliminated through renal filtration and tend to extravasate into healthy tissues [3, 4]. Conversely, particles within the size range of approximately 15-200 nm have demonstrated the longest circulation times and the highest level of tumor permeability [5]. As such, understanding the size and stability of

the generated micelles will provide valuable insights into their potential efficacy and safety in various applications.

In addition, the surface charge of polyplex and PMs will be investigated in this section. As previously discussed, the PGlu (DET-car) can regulate the ratio of cationic to anionic groups in response to changes in environmental pH representing a distinctive feature which is absent in PEG. With this in mind, the current study has undertaken an examination of the surface charge of the micelles generated and conducted tests to evaluate their charge response under varying pH conditions (pH 7.4, 6.5, and 5.5). These investigations were undertaken with the aim of providing critical insights that can inform subsequent cellular experiments and further our understanding of the potential of PMs in biomedical applications.

3.2 Materials

4-(2-hydroxyethyl)-1-piperazineethanesulfonic acid (HEPES) and 2-(N-morpholino)ethanesulfonic acid (MES) were obtained from Wako Pure Chemical Industries, Ltd. (Osaka, Japan). Buffered saline (D-PBS(−)) and sodium acetate buffer (3 mM, pH 5.2) were acquired from Sigma Aldrich (St. Louis, MO, USA). Luciferase (pCAG-Luc2 DNA) encoding gene inserted pCAcc vector under control of CAG promoter was provided by RIKEN Gene Bank (Tsukuba, Japan) and amplified in *Escherichia coli* DH5α cells and endotoxin-free pDNAs were got using the NucleoBond® Xtra Maxi EF Kit (MachereyeNagel GmbH & Co., Germany).

3.3 Methods

3.3.1 Amplification of plasmid DNA

Stellar chemically competent *Escherichia coli* DH5α cells were thawed on ice. A 50 μL aliquot of cell suspension was subjected to transformation using 2 ng of pDNA solution,

immediately followed by transfer to an ice bath for a duration of 3 minutes. Subsequently, the cells were transferred to a 42°C heat block for 1 minute, then returned to the ice bath and allowed to incubate for an additional 1 minute. The transformed cells were then recovered by incubation in 900 µL of SOC medium at 37 °C for 30 minutes, with continuous shaking at 180 r/min. Following this, the cells were plated at various densities on LB-Agar plates supplemented with 50 µg/mL ampicillin and incubated overnight at 37 °C. Single, isolated colonies were carefully selected and transferred to culture tubes containing 5 mL of LB broth supplemented with 50 µg/mL ampicillin. These cultures were then incubated under shaking conditions at 180 r/min for a period of 6 hours. The resulting pre-cultures were utilized to inoculate larger overnight cultures for subsequent maxiprep (2 L). pDNA extraction from *E. coli* was carried out using the NucleoBond® Xtra Maxi EF Kit, following the manufacturer's instructions. The concentration of the final pDNA samples was determined using a NanoDrop spectrophotometer (Thermo Fisher Scientific, Waltham, MA, USA).

3.3.2 Preparation of polyplexes and polyplex micelle (PMs)

Polymers and Luc-pDNA were dissolved in HEPES buffer (pH 7.4, 10 mM) respectively. Polyplexes and PMs were prepared by adding a 1-unit volume of polymer solution to a 2-unit volume of pDNA solution under vortex mixing at different residual charge ratios ([N]/[P]), which is defined as [amino groups (N) in the bPEI]/[phosphate groups (P) in the pDNA]. The final pDNA concentration was adjusted to 33.3 µg/mL for *in vitro* experiments and 100 µg/mL for *in vivo* experiments. The obtained polyplexes and PMs were stored at 4 °C prior to use.

3.3.3 Characterization by Dynamic Light Scattering (DLS) measurement

Hydrodynamic diameter and polydispersity (PDI) of PMs and polyplexes were carried out by using Zetasizer Nano-ZS (Malvern Instruments Ltd., Worcestershire, UK) at

37 °C with a scattering angle of 173° at 25 °C. The stability of PMs in serum was evaluated with 10% FBS and incubating for 24 h or 48 h at 37 °C. In this study, the Z-averaged hydrodynamic diameter [*D*z] was calculated by the diffusion coefficient (DC) *via* the application of the Stokes-Einstein equation: $Dz = K_B T/3\pi\eta Dc$ (K_B: Boltzmann constant, T: temperature, and η: viscosity of polyplex solution). The PDI was determined by utilizing the second-order cumulant coefficient (μ_2) and the average line width of an electric field autocorrelation function (Γ).

3.3.4 DNA binding assay

PMs containing 100 ng of pDNA and loading buffer were loaded onto 1% agarose gel. After electrophoresis (100 V, 30 min), the migrations of pDNA were visualized by SYBR® Safe DNA gel stain (Invitrogen, Waltham, MA, US) and ChemiDoc XRS Plus (Bio-Rad Laboratories, Inc., CA).

3.3.5 Zeta-Potential measurement at different pH conditions

The stepwise pH-responsive behavior of PMs and polyplexes was examined at different pH, *i.e*., physiological (pH 7.4), intra-tumoral (pH 6.5), and endo/lysosomal (pH 5.5) conditions. PMs and polyplexes incorporating Luc-pDNA were incubated in 10 mM HEPES buffer (pH 7.4), 10 mM MES buffer (pH 6.5), and 10 mM acetic acid (pH 5.5) buffer for 1 h, and ζ-potential values were determined by laser-Doppler electrophoretic light scattering (LD-ELS) (Malvern Instruments Ltd., Worcestershire, UK). The Smoluchowski equation ($\zeta = 4\pi\eta\upsilon/\varepsilon$) was employed to calculate the ζ-potential, where η represents the viscosity of the solvent and ε refers to the dielectric constant of the solvent.

3.4 Results and discussion

3.4.1 The formation of the polyplexes and PMs

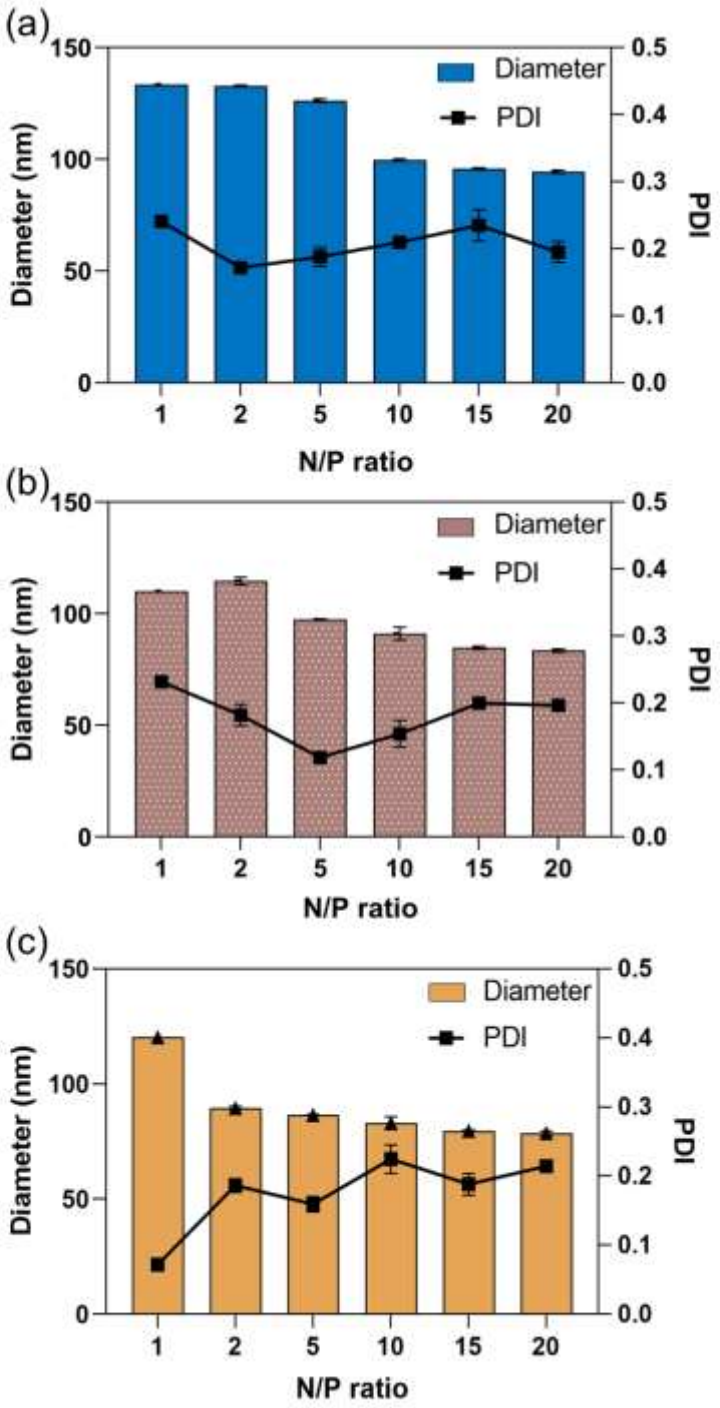

Figure 3-1. Physicochemical characteristics of PMs and polyplexes formulated at different N/P ratios. The intensity-weighted mean hydrodynamic diameters (Z-average, *Dz*) and PDI of (a)

PGDC PM, (b) PEG PMs**,** and (c) PEI-polyplexes at pH 7.4 (10 mM HEPES buffer). Data are expressed as mean ± SD. (n = 3).

Vortex mixing of either PGlu(DET-Car)-bPEI or PEG-bPEI with pDNA at pH 7.4 (10 mM HEPES buffer) at varying N/P ratios was used to create the PMs and were referred to as PGDC PMs and PEG PMs, respectively. While PEI-polyplexes were prepared as described above and employed as the control group. The formation of the PMs and polyplexes was confirmed by dynamic light scattering to assess the intensity-weighted mean hydrodynamic diameters (Z-average, *D*z) and polydispersity indices (PDI). The *D*z of PMs slowly declined with the increase in the N/P ratio from 1 to 5 and then became almost constant at N/P ratios from 10 to 20 with relatively narrow PDI values (**Figure 3-1**). The decreased size with increasing N/P ratios was due to the PMs being formulated through electrostatic interactions, thereby high N/P ratio increased cationic density resulting in the condensed structure of the PMs [7]. Moreover, with the same N/P ratio, the *D*z of PMs was larger than the PEI- polyplexes, probably due to the polymer modification, facilitating the formation of a hydrogen layer between the polyzwitterion as well as PEG and water molecules in aqueous solution [8]. Agarose gel electrophoresis further revealed the formation and condensation efficiency of pDNA-incorporated PMs at pH 7.4 (**Figure 3-2**). Uncomplexed pDNA was not detected at the N/P ratio of ≥ 5, suggesting that pDNA could be effectively encapsulated at these N/P ratios.

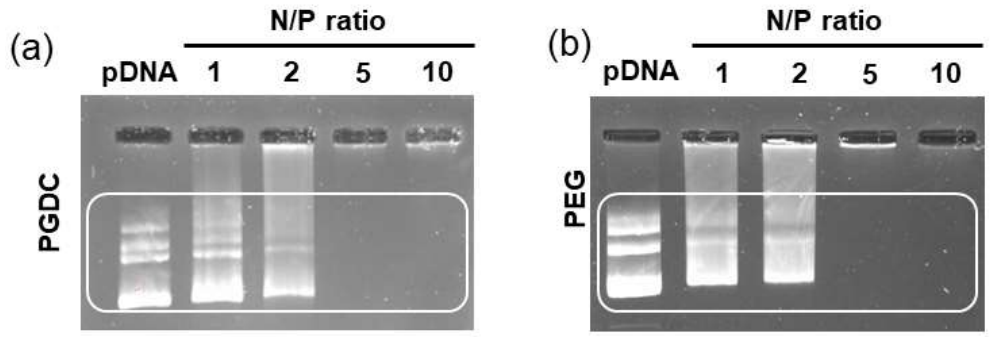

Figure 3-2. Agarose gel electrophoresis at pH 7.4 (10 mM HEPES buffer). (a) PGDC PM. (b) PEG PM. The bands corresponding to uncomplexed pDNA are visible in the area bounded by the rectangular solid line.

3.4.2 The stability of the PMs

PGDC PM and PEG showed minimal changes in the hydrodynamic size PM after exposure to 10% FBS for 48 h which could be attributed to the shielding effect of PGlu(DET-Car) or PEG imparted by surface modifications. These modifications served as a protective barrier, effectively reducing the interaction between the charged PEI core and the proteins present in the FBS. Therefore, PGDC PM and PEG PM prevented protein adsorption and subsequent aggregation or degradation, thereby maintaining their structural integrity and stability. Moreover, the size of PGDC PM and PEG PM remains remarkably consistent under different pH conditions, demonstrating their robust stability over a wide pH range.

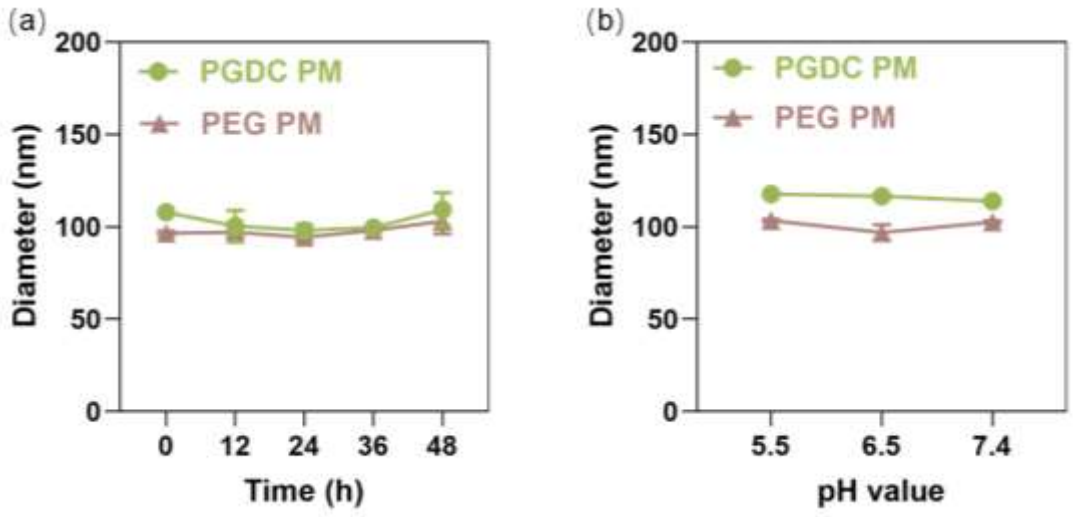

Figure 3-3. Stability of the PMs. (a) Serum stability as time changes. (b) Stability as pH changes. Data are expressed as mean ± SD. (n = 3).

3.4.3 The pH responsiveness of the PMs

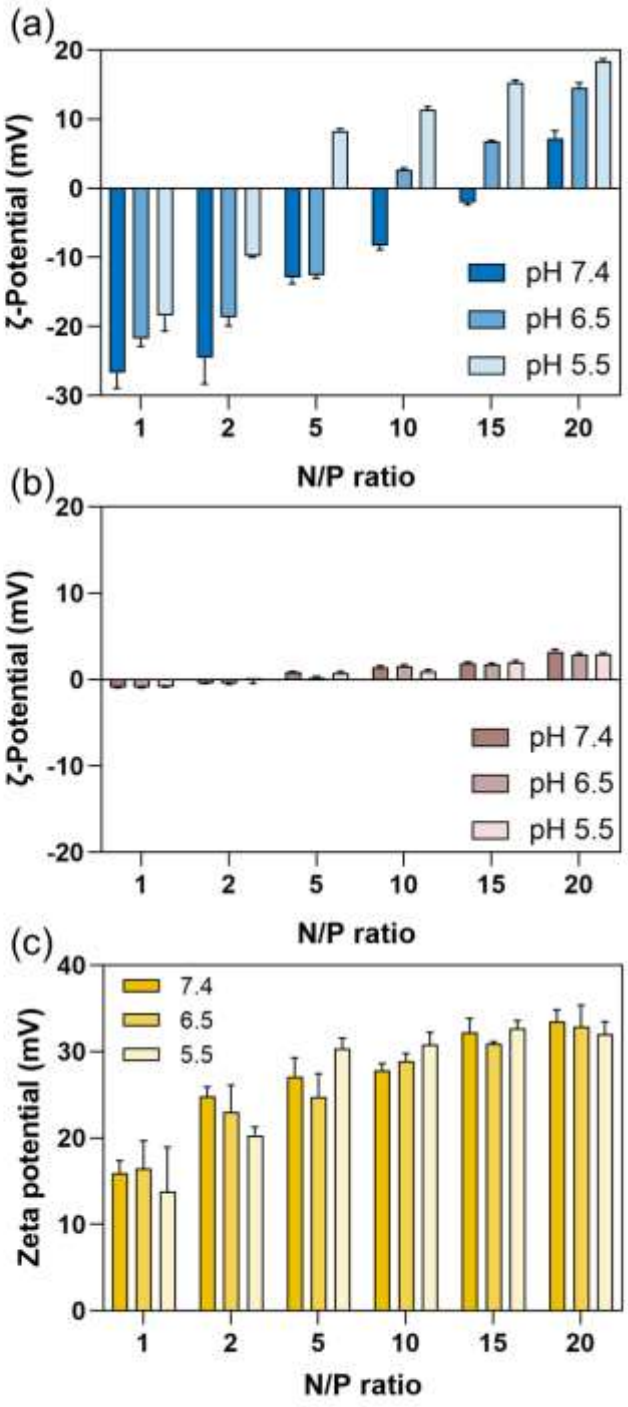

Figure 3-4. pH responsiveness of the PMs. Zeta-potential measurements of (a) PGDC PMs, (b) PEG PMs**,** and (c) PEI-polyplexes which were incubated in 10 mM HEPES buffer (pH 7.4), 10 mM MES buffer (pH 6.5), and 10 mM acetic acid (pH 5.5) buffer. Data are expressed as mean S.D. (n = 3).

Zeta (ζ)-potential values were evaluated in order to track the pH-triggered charge-conversion on the PMs and polyplexes surface. At pH 7.4, the ζ-potential of all PMs and polyplexes parallelly increased with altering the N/P ratio, possibly due to the high density of cationic charge binding to negatively charged pDNA (**Figure 3-4**). Over the N/P ratio 20, excess polymers in the formation of the PGDC PM displayed a positive charge. Meanwhile, PEG PMs also showed positive charges at pH 7.4 at the N/P ratios ranging from 5 to 20. Simultaneously, our observations revealed that despite PEI-polyplexes displaying higher surface charges (+ 15.90 ~ + 33.47 mV), either PGDC PMs or PEG PMs exhibited varied degrees of surface charge reduction with the same N/P ratio at pH 7.4. This decline in zeta-potential could be attributed to the shielding effect facilitated by the presence of PGDC or PEG shell, which effectively neutralized the surplus positive charges associated with PEI-polyplexes.

Then, the ζ-potential of PMs and polyplexes in acidic environments (pH 6.5 and pH 5.5) was evaluated. When exposed to pH 6.5, the ζ-potential of PGDC PMs at each N/P ratio was noticeably increased and then substantially enhanced upon pH 5.5 (**Figure 3-4, a**), suggesting the stepwise pH-switchable charge conversion property of PGDC PMs. Notably, PGDC PMs showed charge conversion from negative or neutrally charged at pH 7.4 to positive at pH 6.5 and 5.5 at N/P 10 and 15. On the contrary, the control PEG PMs and PEI-polyplexes did not show such charge-conversional property regardless of the pH change (**Figure 3-4, b and c**).

The pH-responsive charge conversion of PMs at the N/P ratio of 15 was systematically examined through time-dependent monitoring under varying pH conditions (**Figure 3-5**). Incubation of the PMs at different pH environments allowed for the investigation of charge dynamics. At pH 7.4, both PGDC PM and PEG PM exhibited a sustained negative ζ-potential over the entire 120-minute incubation period. This observation indicates the stability of the shielding to PEI within the physiological pH range. In contrast, at pH 6.5, the initially negative ζ-potential of PGDC PM rapidly transitioned to positive values, ultimately reaching approximately +6.8 mV. However,

PEG PM did not show such a change in surface potential during the incubation time.

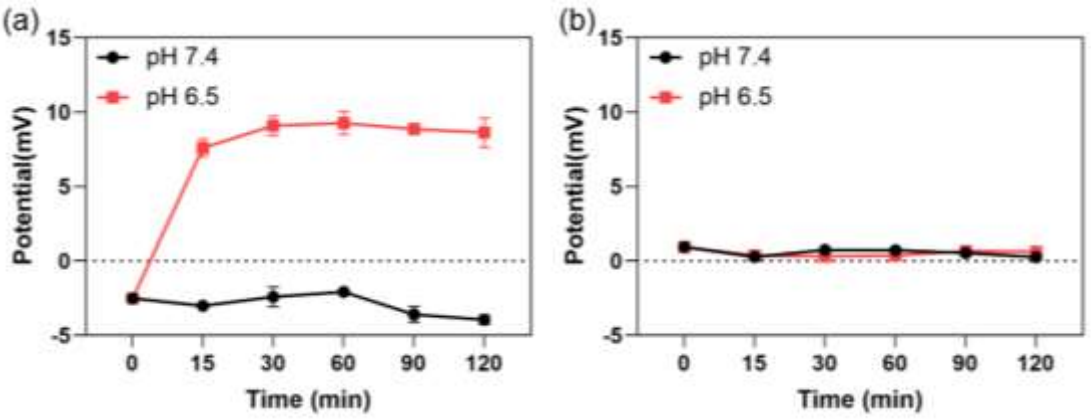

Figure 3-5. Time-dependent change in ζ-potential of PMs at N/P 15. (a) PGDC PM and (b) PEG PM at pH 7.4 (circle) and 6.5 (square). Data are expressed as mean ± S.D. (n = 3).

3.5 Conclusion

In this chapter, the PMs were formulated by mixing the pDNA and polymer solution at varying N/P ratios, which effectively condensed pDNA over N/P ratio 5. DLS measurements revealed all PMs exhibited uniformed hydrodynamic sizes ranging from 82~135 nm with relatively narrow PDI. I found that PGDC PMs prepared with high N/P values from 10 to 20 exhibited the efficient PM formation and condensation of pDNA at pH 7.4. Importantly, PGDC PM which processed a controlled ionization of cationic moieties exhibited pH-responsive performance in a reversible manner. This stepwise protonation behavior of PGlu(DET-Car) might supply the potential of the charge-switchable property to PMs, but the appropriate tuning of parameters such as N/P ratio and ζ-potential is critical to realize the high *in vitro* and *in vivo* performances. The C/A ratio of PGlu(DET-Car) was 1.09 at pH 7.4 which then increased to 1.39 at pH 6.5, suggesting that PGlu(DET-Car) switches its neutral property to cationic at tumorous pH. When exposed to pH 5.5, PGlu(DET-Car) exhibited a C/A value of 1.84, suggesting substantial protonation of the ethylenediamine groups in PGlu(DET-Car). This stepwise increase in the ζ-potential of PGDC PMs with varying N/P rations was

attributed to the progressive protonation of the ethylenediamine-based carboxybetaine group with regard to the decrease in pH. r, PGDC PM prepared at the N/P ratio of 15 represented a desirable characteristic that the ζ-potential values switched from negative at pH 7.4 to positive at pH 6.5. The value of ζ-potential was further amplified at pH 5.5. This charge-conversion behavior of PGDC PM should be applied for recognizing the narrow pH window in the route of gene delivery, *i.e.*, tumor microenvironment (pH 6.5) and endosomes (pH 5.5).

The PGDC and PEG PMs together displayed nearly constant Dz values and desirable pH-triggered charge-conversion behavior when they were produced at the N/P ratio above 5 (**Figures 3-1 and 3-4**). Therefore, in the subsequent *in vitro* investigation, we utilized these PMs of N/P ratios of 10, 15, and 20.

3.6 Reference

[1] A. Harada, K. Kataoka, Polyion complex micelle formation from double-hydrophilic block copolymers composed of charged and non-charged segments in aqueous media. Polym. J. 50 (1) (2018) 95-100. https://doi.org/10.1038/pj.2017.67.

[2] S. Uchida, K. Kataoka, Design concepts of polyplex micelles for in vivo therapeutic delivery of plasmid DNA and messenger RNA. J Biomed Mater Res A. 107 (5) (2019) 978-990. https://doi.org/10.1002/jbm.a.36614.

[3] M.J. Ernsting, M. Murakami, A. Roy, S.D. Li, Factors controlling the pharmacokinetics, biodistribution and intratumoral penetration of nanoparticles. J. Control Release. 172 (3) (2013) 782-794. https://doi.org/10.1016/j.jconrel.2013.09.013.

[4] N. Hoshyar, S. Gray, H. Han, G. Bao, The effect of nanoparticle size on in vivo pharmacokinetics and cellular interaction. Nanomedicine (Lond) 11 (6) (2016) 673-692. https://doi.org/10.2217/nnm.16.5.

[6] J. Wu, The enhanced permeability and retention (EPR) effect: the significance of

the concept and methods to enhance its application. J. Pers. Med. 11 (8) (2021) 771. https://doi.org/10.3390/jpm11080771.

[7] D.J. Gary, J. Min, Y. Kim, K. Park, Y.Y. Won, The effect of N/P ratio on the in vitro and in vivo interaction properties of PEGylated poly[2-(dimethylamino)ethyl methacrylate]-based siRNA complexes. Macromol. Biosci. 13 (8) (2013) 1059-1071. https://doi.org/10.1002/mabi.201300046.

[8] L.Y. Zhou, Y.H. Zhu, X.Y. Wang, C. Shen, X.W. Wei, T. Xu, Z.Y. He, Novel zwitterionic vectors: multi-functional delivery systems for therapeutic genes and drugs. Comput. Struct. Biotechnol. J. 18 (2020) 1980-1999. https://doi.org/10.1016/j.csbj.2020.07.015.

`

Chapter 4 *In vitro A*ssessment

4.1 Introduction

In the previous chapter, the PGDC PMs displayed nearly constant *D*z values and desirable pH-triggered charge-conversion behavior when they were produced at the N/P ratio above 5 (**Figures 3-1** and **3-4**). Therefore, in this chapter's *in vitro* investigations, we utilized these N/P ratios of 10, 15, and 20.

The *in vitro* gene transfection of PMs *via* luciferase assay was first evaluated at pH 7.4 and pH 6.5 culture medium, mimicking physiological and tumorous pH conditions. Here, PEI-polyplexes were also examined as the positive control. The cell lines used in this experiment were Huh-7 (human hepatoma cell line) and Neuro-2A (murine neuroblastoma cell line), while the Neuro-2A made subcutaneous tumor model mice in the subsequent *in vivo* experiments. The transfection-mediated cytotoxicity was also performed to confirm the biocompatibility of all PMs and PEI-polyplexes by using CCK assay.

The degree of transfection efficiency is significantly impacted by the intracellular trafficking profile [1, 2]. Thus, to understand how a pH drop from 7.4 to 6.5 contributed to the transfection activity, we assessed the cellular uptake of PMs prepared at the optimized N/P ratio of 15. Cellular uptake efficiency was quantified in Neuro-2A cells and Huh-7 cultured at pH 7.4 and 6.5 by calculating the fluorescence intensity of whole-cell lysate by using a microplate reader as well as observation of the intracellular fluorescence signals by utilizing CLSM.

The PMs that were trapped in the endosome were eventually subjected to enzymatic degradation [3, 4]. Therefore, PM with sufficient endosomal escape activity is beneficial for efficient intracellular delivery. We evaluated the endosomal escape capability of PMs by using CLSM at pH 6.5 after 24 and 48 h incubation of Cy5-labeled pDNA (red) packaged PMs, followed by staining endo/lysosomes with LysoTracker (green), which visualized pDNA entrapped within the endo/lysosomal compartments as colocalization (yellow). We also quantified the percentage of cells that exhibited

endosomal escape in response to charge conversion of PGDC PM in the endosomal pH 5.5 using a calcein assay.

4.2 Materials

Dulbecco's phosphate-buffered saline (D-PBS(−)), LysoTracker Red DND-99, Hoechst 33342, Dulbecco's modified Eagle's medium (DMEM), Eagle's Minimum Essential Medium (EMEM), trypsin-EDTA, sodium acetate buffer (3 mM, pH 5.2) and Micro BCA^{TM} Protein Assay Reagent Kit solution were acquired from Sigma Aldrich (St. Louis, MO, USA). Fetal Bovine Serum (FBS) was procured from Biosera Co., Ltd. (Caille, France). Cell Counting Kit-8 (CCK) was purchased from Dojindo Molecular Technologies Inc. (Kumamoto, Japan). Cell culture lysis buffer and Luciferase Assay System Kit were obtained from Promega Co. (Madison, WI). Luciferase (pCAG-Luc2 DNA) and soluble fms-like tyrosine kinase-1 (pCAG-sFlt-1) encoding gene inserted pCAcc vector under control of CAG promoter were provided by RIKEN Gene Bank (Tsukuba, Japan) and amplified in Escherichia coli DH5α cells and endotoxin-free pDNAs were got using the NucleoBond® Xtra Maxi EF Kit (MachereyeNagel GmbH & Co., Germany). pDNA was labeled with Cy5 using the Label IT Tracker® Intracellular Nucleic Acid Localization Kit obtained from Mirus Bio Corp. (Madison, WI) following the manufacturer's instructions.

4.3 Cell lines

Murine neuroblastoma (Neuro-2A) cells and human hepatocarcinoma (Huh-7) cells were obtained from the American Type Culture Collection (ATCC, Manassas, VA) and cultured in EMEM medium and DMEM medium respectively. All media were supplemented with 10% FBS and 100 U/mL penicillin. The cultured cells were grown at 37 °C in a 5% CO_2 humidified atmosphere.

4.4 Methods

4.4.1 Label the pDNA with Cy5

Luc2-pDNA was labeled with Cy5 following the manufacturer's protocol with minor modifications. Luc2-pDNA (1 mg/mL) was reacted with the label reagents and incubated in the dark at 37°C for 1 hour. Then, 5 M NaCl and ice-cold 100% ethanol were added to the reaction mixture for another 30 minutes of incubation at -20°C. After that, the reaction solution was centrifuged at full speed (15,000 rpm) for 20 minutes to remove the supernatant. The blue color precipitate was washed with 70% ethanol and centrifuged at full speed for an additional 15 minutes. After removing all traces of ethanol, the sediment was resuspended with 100 μL sterile water, and quantified the concentration of Cy5-labeled DNA was with Nanodrop and fluorescence intensity by Nanodrop ND-3300 Fluorospectrometer.

4.4.2 *In vitro* evaluation of sFlt-1 expression by delivering Flt-1 pDNA

To study the expression of sFlt-1 proteins *in vitro*, Neuro-2A cells (2×10^4 cells/well) were seeded into each well of the 24-well plates and incubated overnight. Thereafter, the medium was replaced with fresh medium containing free pDNA, PEG PM, and PGDC PM at an N/P ratio of 15 containing 1 μg sFlt-1 pDNA. After 48 h incubation, the cell culture medium was collected and centrifuged at 3500 rpm for 10 min to collect the expressed sFlt-1 proteins. The sFlt-1 protein expression was measured by ELISA kit.

4.4.3 *In vitro* gene transfection of PMs *via* luciferase assay

Neuro-2A cells (2×10^4 cells/well) and Huh-7 (1×10^4 cells) were seeded on 24-well plates in a medium containing 10% FBS. After 24 h incubation, the medium was replaced with the fresh one, and PM solution containing 1 μg of Luc-pDNA was added

to each well. The cells were cultured for 48 h with replacing the culture medium at 24 h time point. Then the cells were washed with D-PBS(−) twice and lysed by the cell culture lysis buffer for 30 min. After this, the luciferase activity of the cell lysate was determined by Luciferase Assay Kit and Luminometer Glomax 96 (Promega Co., Madison, WI). The results were expressed in terms of relative light units per mg protein. CCK and LDH assay was used to assess transfection-mediated cytotoxicity according to the manufacturer's instructions.

4.4.4 Cellular uptake

For quantitative analysis of cellular uptakes, the cells (5×10^3 cells/well) were seeded in a 96-well plate. The culture medium was replaced by a fresh medium (pH 7.4 and 6.5) with PM solutions containing 250 ng of Cy5-labeled pDNA. After 24 h incubation, the cells were lysed with cell culture lysis buffer (100 μL). After additional 30 minutes of incubation, the fluorescence intensity of each lysate was measured using a microplate reader (SPARK TKS01, TECAN, Zürich, Switzerland, *E*x/*E*m: 640/680 nm) to calculate the amount of Cy5-labeled pDNA in the cells.

To examine the intracellular uptake efficiency, Neuro-2A cells (5×10^4 cells) and Huh-7 cells (2×10^4 cells) were seeded on a 35-mm glass-based dish (Iwaki, Japan) and treated with a fresh medium (pH 7.4 and 6.5) containing PM solution with 4 μg of Cy5-labeled pDNA. After 24 h incubation, the cells were washed with D-PBS(−) twice and the nuclei were stained with Hoechst 33342. Confocal laser scanning microscopy (CLSM: LSM710, Carl Zeiss AG, Oberkochen, Germany) was used to observe the intracellular uptake of Cy5-labeled pDNA. CLSM images were used to quantify intracellular fluorescence intensity (n = 30 cells).

4.4.5 Endosomal escape *via* co-colocalization

Neuro-2A cells (5×10^4 cells) and Huh-7 cells (2×10^4 cells) were seeded on a 35-mm glass-based dish (Iwaki, Japan). The cells were treated with a fresh medium containing

PM solution with 4 μg of Cy5-labeled pDNA. After 24 h or 48 h incubation, the cells were washed twice with D-PBS(−), and the distribution of Cy5-labeled pDNA was examined using CLSM with co-staining of endo/lysosomes by LysoTracker Red DND-99 (50 nM). Hoechst 33342 was also used to stain the cell nuclei. ZEN software was used to calculate the colocalization ratio of Cy5-labeled pDNA and late-end lysosomes. The following equation was used to analyze 30 individual cells:

Colocalization ratio = Number of yellow pixels/All the number of yellow and red pixels

4.4.6 Endosomal escape *via* calcein assay

Neuro-2A cells (1×10^4 cells) and Huh-7 (5×10^3 cells) were seeded on Lab-Tak® chambered #1.0 Borosilicate Coverglass System (NUNC, Rochester, NY, US). After overnight incubation, the medium was replaced with 200 μL fresh medium containing 250 μM calcein (Dojindo, Kumamoto, Japan) and 30 μL PMs containing 1 μg of Cy5-labeled pDNA. After 2 h incubation, the medium was washed with D-PBS(−) twice, and stained the nuclei using Hoechst 33342. The endosome escape was evaluated by confocal laser scanning microscopy (CLSM: LSM710, Carl Zeiss AG, Oberkochen, Germany) at the excitation wavelengths of 405 nm for Hoechst33342 and 488 nm for calcein (Ar laser).

4.5 Results and discussion

4.5.1 *In vitro* gene transfection of PMs

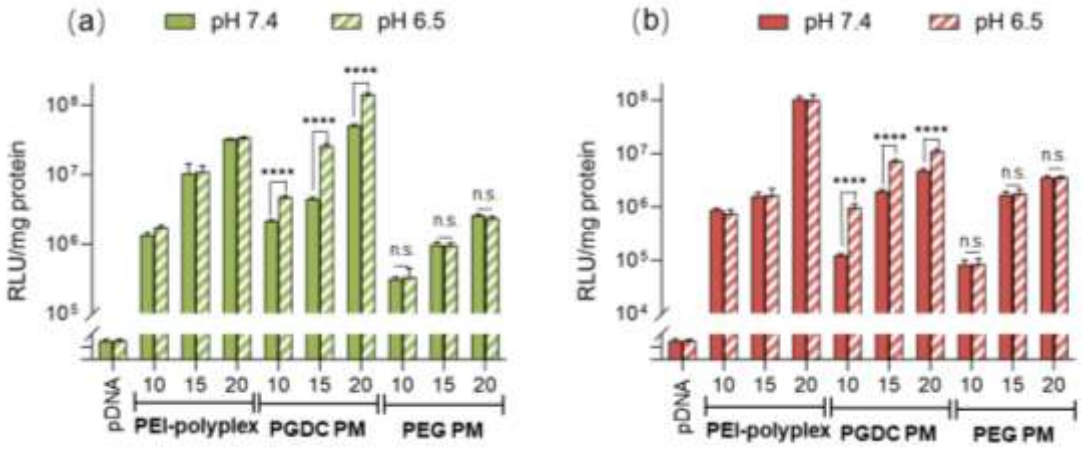

Figure 4-1. Transfection performance of PMs. Gene expression effectiveness of PGDC PMs, PEG PMs, and PEI-polyplexes formulated at varying N/P ratios against (a) Neuro-2A cells and (b) Huh-7 cells cultured at pH 7.4 and 6.5 (n = 6). pDNA encoding luciferase (pCAG-Luc2) was used in these experiments. (1 μg of pDNA/well). Data are expressed as mean ± SD, ****p < 0.0001 (Two-way ANOVA with Tukey's multiple comparisons test).

In vitro gene transfection efficiency of PMs loaded with pDNA encoding a luciferase (Luc) reporter protein in Neuro-2A and Huh-7 cell lines was evaluated under the different pH conditions (pH 7.4 and pH 6.5) (**Figure 4-1**). Here, PEI-polyplex was also examined as a positive control. The Luc expression was gradually increased with the increment of the N/P ratios in all the formulations at pH 7.4 and pH 6.5. Notably, regardless of the N/P ratios, PGDC PM exhibited drastic enhancement (2.3−5.7 fold) in Luc expression efficiency at pH 6.5 compared to that observed at pH 7.4. Such pH-responsiveness in Luc expression was not observed for PEI-polyplex and PEG PM. These results suggested that the PGDC shell might contribute to the pH-responsive gene expression of PGDC PM. Regarding the gene expression level, PEG PM showed significantly lower Luc expression compared with other formulations, suggesting PEG

shell might attenuate the gene expression. On the other hand, PGDC PM showed appreciably higher gene expression even compared with PEI-polyplex at 7.4. These results suggested that the charge-conversional property of PGDC in response to pH 6.5 can enhance the expression ability of PMs.

Transfection-mediated cytotoxicity was also examined by measuring dehydrogenase activity, which is directly related to the quantity of living cells with an equivalent pDNA dose (1 μg/well) used in the transfection assay. Both PGDC and PEG PMs of all examined N/P ratios exhibited a negligible decrease in cell viability compared to PEI-polyplexes (**Figure 4-2**). PEI-polyplex demonstrated the N/P ratio-dependent reduction in cell viability. Thus, the enhanced transfection efficiencies of cationic polyplexes with increasing the N/P ratios were accompanied by an increment in the cytotoxicity. In contrast, both PEG and PGDC PMs showed no obvious cytotoxicity up to the N/P ratio of 15 regardless of the N/P ratio-dependent enhancement in the gene transfection (**Figure 4-1**). Hence, in the subsequent *in vitro* analyses and *in vivo* systemic gene delivery investigations, we fixed the N/P ratio at 15 for the preparation of PMs.

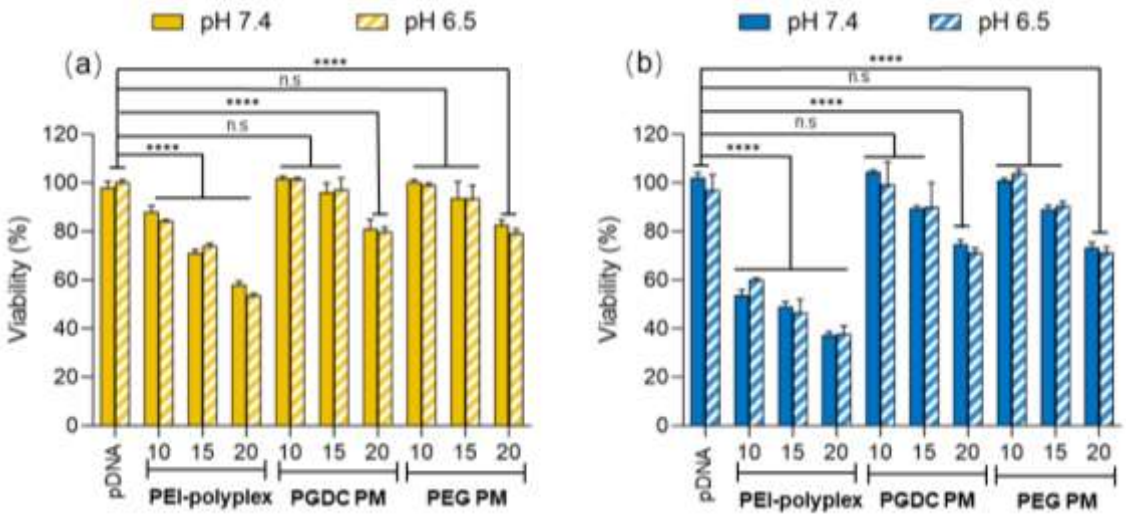

Figure 4-2. Transfection-mediated cytotoxicity. Cell viability of PGDC PMs, PEG PMs, and PEI-polyplexes formulated at varying N/P ratios against (a) Neuro-2A cells and (b) Huh-7 cells

cultured at pH 7.4 and 6.5 (n = 6). pDNA encoding luciferase (pCAG-Luc2) was used in these experiments. (1 μg of pDNA/well). Data are expressed as mean ± SD, ****p < 0.0001 (Two-way ANOVA with Tukey's multiple comparisons test).

Furthermore, the results obtained from the *in vitro* experiment of sFlt-1 introduction provide support for the promotion of the expression capability of PMs by PGDC in response to tumorous pH, as determined by the previously optimized N/P ratio discussed earlier (**Figure 4-3**).

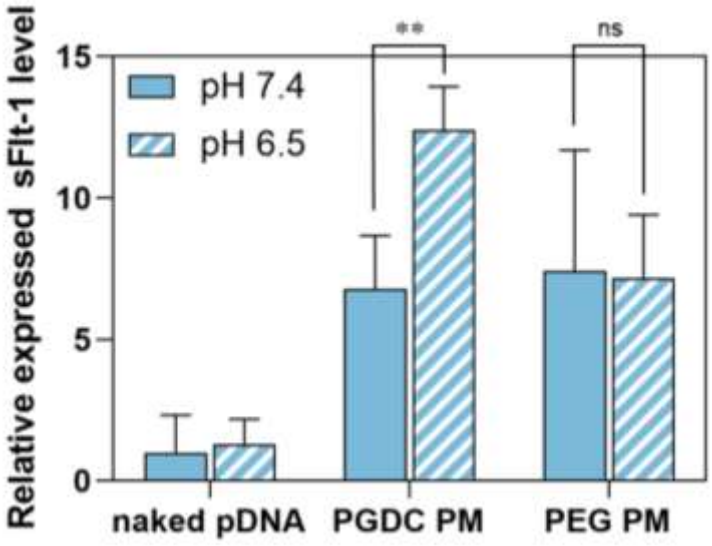

Figure 4-3. Effect of culture medium pH on sFlt-1 expression by ELISA. Samples were incubated in Neuro-2A cells for 48 h at pH 7.4 and 6.5 while the sFlt-1 level in naked pDNA at pH 7.4 was defined as 1. Data are expressed as mean ± SEM. (n = 6). **p < 0.01 (two-tailed Student's t-test). Using ELISA buffer, the cultured medium's total protein concentration was increased to 2.5 mg/mL.

4.5.2 Cellular uptake

The cellular absorption and uptake are prerequisites for gene transfection, we assessed

the cellular uptake of PMs prepared at an N/P ratio of 15 at pH 7.4 and 6.5 in Neuro-2A and Huh-7 cell lines. The cellular uptake efficiency was quantified by measuring the fluorescence intensity of Cy5-labeled pDNA in the whole-cell lysate by using a microplate reader. As depicted in **Figure 4-4**, PGDC PM demonstrated higher cellular uptake at pH 6.5 compared to pH 7.4, while PEG PM displayed similar cellular uptake efficiency despite pH values in both cell lines.

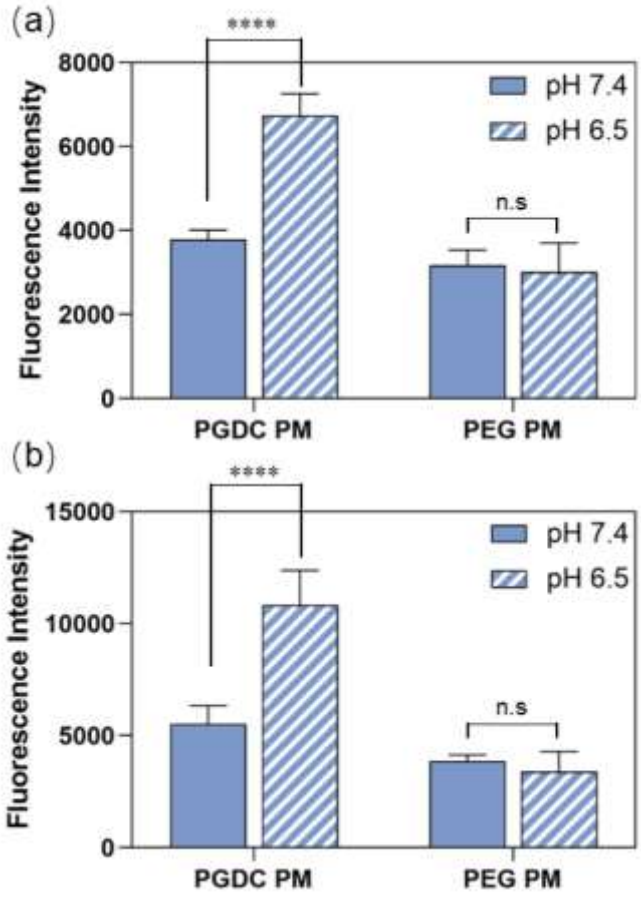

Figure 4-4. Cellular uptake efficiency. PGDC and PEG PMs loading Cy5-labeled pDNA in (a) Neuro-2A cells and (b) Huh-7 cells cultured at pH 7.4 and 6.5 at a dose of 0.25 μg Cy5-pDNA after 24 h incubation. Data are expressed as mean ± SD (n = 6). ****$p < 0.0001$ (two-tailed Student's t-test).

Of note, the fluorescence in this experiment includes both internalized PM and cellular membrane-bound PM. Taking this into account, we also quantified the

intracellular fluorescence signals by utilizing CLSM. In PGDC PM snap shots, the cells cultured at pH 6.5 displayed high-intensity red pixels (Cy5-pDNA) in the cytoplasm, while the cells cultured at pH 7.4 displayed low-intensity red pixels. In contrast, PEG PM-treated cells cultured at pH 7.4 and 6.5 displayed similar red pixels (**Figure 4-5, a and c**). It was revealed by corresponding fluorescence quantification from the CLSM images that the cells treated with PGDC PM exhibited higher Cy5 fluorescence intensity than that of PEG PM when pH decreased from 7.4 to 6.5, suggesting that the increased positive charge of the PGDC shell at acidic pH 6.5 could enhance internalization of PGDC PM (**Figure 4-5, b and d**). Thus, the cationic charge-conversion ability of the PGDC shell can facilitate cellular uptake and concomitant internalization of PGDC PM selectively in the acidic tumor microenvironment (pH 6.5).

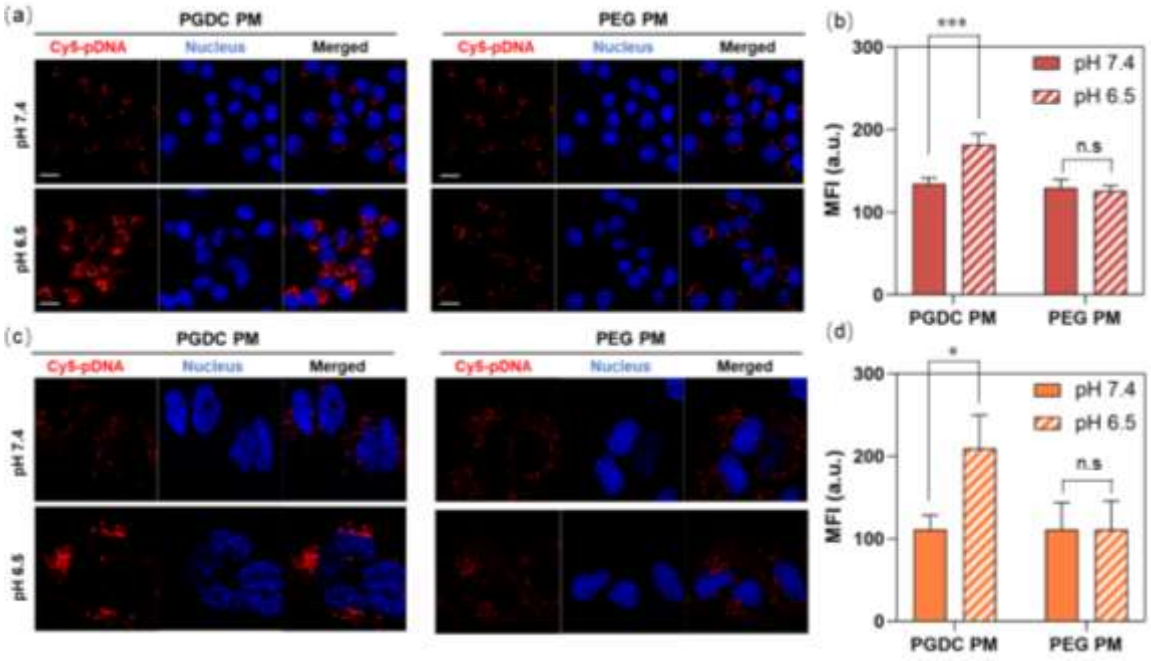

Figure 4-5. Internalization of PGDC and PEG PMs. CLSM images showing the intracellular pDNA delivery in (a) Neuro-2A and (c) Huh-7 cell lines. Scale bar = 10 μm. Quantification of intracellular fluorescence intensity of Cy5-pDNA in the CLSM images in (b) Neuro-2A and (d) Huh-7 cell lines (n = 30 cells). Data are expressed as mean ± SD, *p < 0.05, ***p < 0.001 (Two-way ANOVA with Tukey's multiple

comparisons test).

4.5.3 Endosomal escape

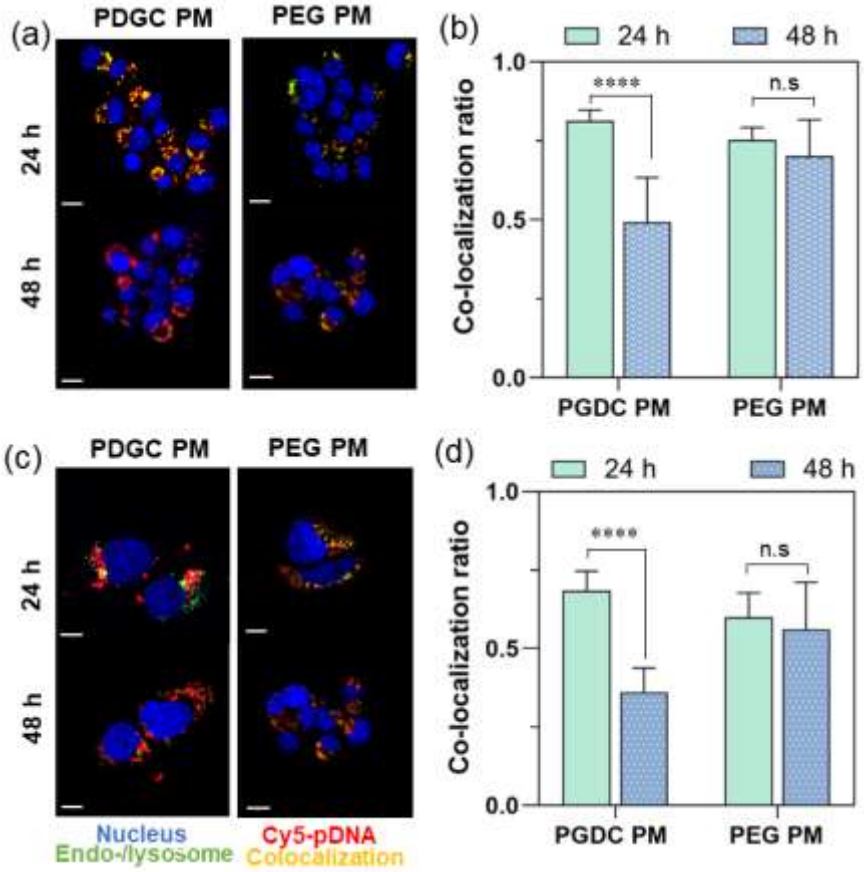

Figure 4-6. Assessment of endosomal escape of PMs cultured at pH 6.5. (c) (d) CLSM pictures showing the intracellular distribution of PMs loading Cy5-labeled pDNA after 24 and 48 hr incubation in (a) Neuro-2A and (c) Huh-7 cell lines, Scale bar = 10 μm. Red: Cy5-labeled pDNA; Green: late endo/lysosomes (LysoTracker Green); Yellow: colocalization between Cy5-labeled pDNA and DNA endo/lysosomes; Blue: nuclei (Hoechst 33342). Colocalization ratio of Cy5-labeled pDNA with late endo/lysosome after 24 and 48 h of PM incubation in (b) Neuro-2A and (d) Huh-7 cell lines (n = 30 cells). A decrease in the colocalization ratio indicates an endosomal escape. Data are expressed as mean ± SD, ****$p < 0.0001$ (Two-way ANOVA with Tukey's multiple comparisons test).

We evaluated the endosomal escape capability of PMs by using CLSM. Both cell lines were incubated with Cy5-labeled pDNA (red) packaged PMs at pH 6.5 for 24 and 48 h, followed by staining endo/lysosomes with LysoTracker (green) to visualize pDNA entrapped within the endo/lysosomal compartments as colocalization (yellow). Also, the colocalization ratio of Cy5-labeled pDNA with endo/lysosomes in the CLSM images was quantified to estimate the endosome escape potential of PMs (**Figure 4-6, b and d**). PEG PM showed comparable yellow pixels at both 24 and 48 h-post incubation (**Figure 4-6, a and c**), indicating that many portions of PEG PM were stuck in the endo/lysosomes. On the contrary, PGDC PM showed more red pixels after 48 h when compared to 24h (**Figure 4-6, a and c**). Consistently, the colocalization ratio of PGDC PM significantly decreased after 48 h (**Figure 4-6, b and d**). These results suggest that a substantial portion of Cy5-labeled pDNA might be delivered to the cytoplasm by PGDC PM.

Calcein is a well-known “cell membrane impermeable dye” and is internalized into the cells through co-endocytosis with PM [5]. When calcein is released into the cytosol accompanied by the endosomal membrane rupture, diffused fluorescence can be observed throughout the cell. On the other hand, endosomal entrapment is indicated by punctate fluorescence because calcein is trapped inside the endosome for an extended period of time [6]. As shown in **Figure 4-7, a and c**, PGDC PM displayed diffused fluorescence in the cytosol, suggesting that the PGDC PM could be escaped from the endosome. In contrast, PEG PM failed to show punctate fluorescence indicating ineffective endosomal escape, therefore, exhibited punctate fluorescence due to the lack of pH-responsive characteristics in the PEG shell (**Figure 4-7, b and d**).

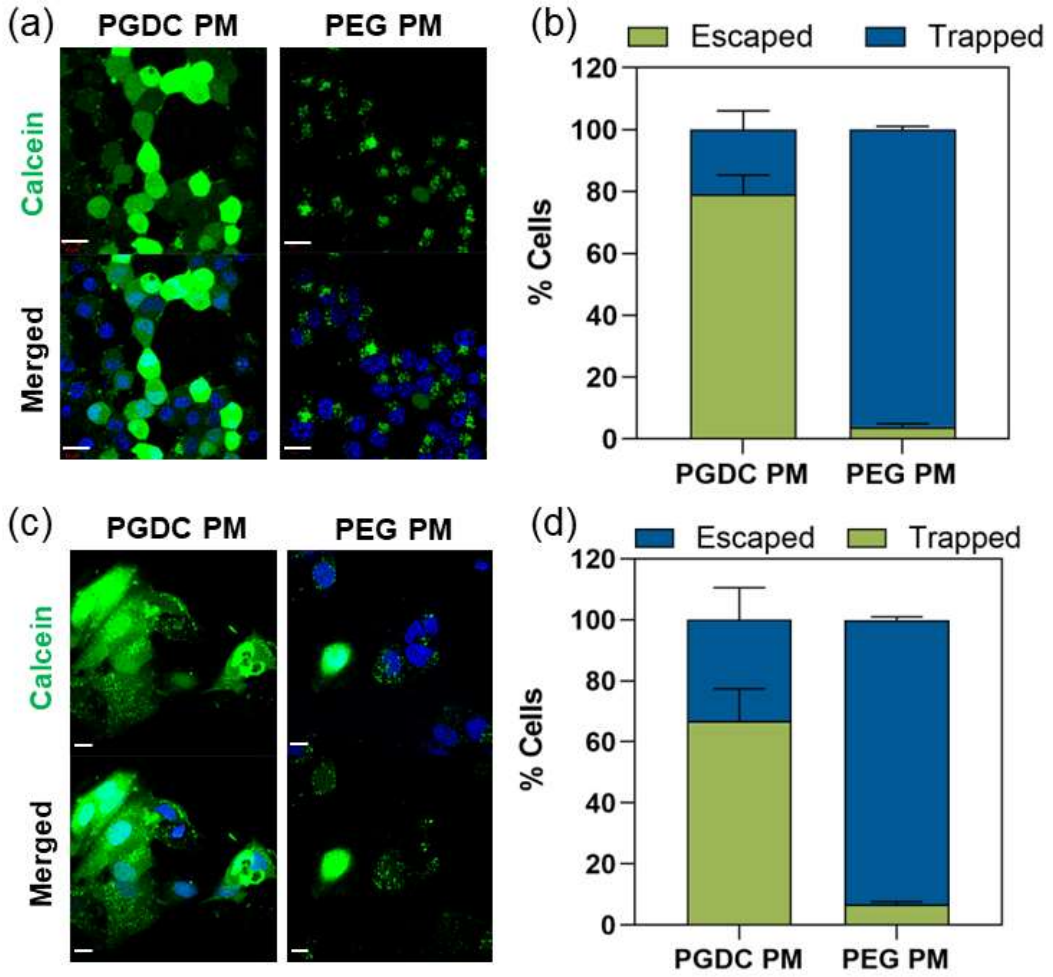

Figure 4-7. Calcein leakage assay for quantification of the percentage of cells showing endosomal escape. Cytosolic distribution of calcein at 2 h coincubation of calcein and PM in (a) Neuro-2A and (c) Huh-7 cell lines. Green: calcein; Blue: nuclei (Hoechst 33342). Endosomal escape is indicated by diffuse fluorescence throughout the cell, whereas punctate fluorescence represents endosomal trapping. Percentage of cells showing endosomal escape (diffused fluorescence) and endosomal trapping (punctate fluorescence) of (b) Neuro-2A and (d) Huh-7 cell lines as quantified from CLSM images (n = 114 cells). Scale bar = 10 μm. Data are expressed as mean ± SD.

4.6 Conclusion

With the above-optimized formulation (N/P = 15), positively charged PGDC PM (+ 6.8

mV) at pH 6.5 promoted electrostatic interactions with the negatively charged cell membrane, resulting in the enhanced uptake and concomitant internalization of PGDC PM in the acidic tumor microenvironment (**Figures 4-4** and **4-5**). Interestingly, PGDC PMs at the N/P ratios up to 15 did not cause transfection-related cell damage even at pH 6.5 (**Figure 4-2**), although the PGDC shell is assumed to act as a cationic polymer. This phenomenon may be attributed to its low cation density (C/A value: 1.39) and inherent lower cytotoxicity compared with PEI. Additionally, PGDC PM was shown to enhance the endosomal escape, as observed by the consistent results in the colocalization study of Cy5-labeled pDNA with endo-/lysosomes (**Figure 4-6**) and the calcein assay (**Figure 4-7**). This was due to the increment in the cationic charge density of the PGDC shell (value shifts from 1.39 to 1.84), which provides + 15 mV of ζ-potential for PGDC PM at pH 5.5 in the endo-/lysosomal compartment-mimicking conditions. Namely, the electrostatic interactions between PGDC PM and the negatively charged endo-/lysosomal membrane might contribute to the endosomal membrane destabilization in addition to the proton sponge effect. Contrarily, the PEG shell prevented the interactions with the negatively charged membranes, leading to low cellular uptake and endosomal escape of PEG PM. Moreover, the Luc expression is known to be closely interrelated with the intracellular trafficking profile of the PMs [1, 2]. Our PGDC PMs showed enhanced transfection efficiency at pH 6.5 compared to pH 7.4, while other control groups showed no difference, as evidenced by delivering Luc-pDNA into Neuro-2A cells (**Figure 4-1**). Overall, we revealed the stepwise charge-switchable property of PGDC PM, thereby facilitating the cellular uptake and endosomal escape, leading to the enhanced gene transfection *in vitro*.

4.7 References

[1] L.K. Medina-Kauwe, J. Xie, S. Hamm-Alvarez, Intracellular trafficking of nonviral vectors. Gene Ther. 12 (2005) 1734-1751. https://doi.org/10.1038/sj.gt.3302592.

[2] S, Kommareddy, S.B. Tiwari, M M. Amiji, Long-circulating polymeric nanovectors for tumor-selective gene delivery. Technol. Cancer Res. Treat. 4 (6): (2005) 615-625. https://doi.org/10.1177/153303460500400605.

[3] E. Xu, W.M. Saltzman, A.S. Piotrowski-Daspit, Escaping the endosome: assessing cellular trafficking mechanisms of non-viral vehicles. J. Control Release 335 (2021) 465-480. https://doi.org/10.1016/j.jconrel.2021.05.038.

[4] A.K. Varkouhi, M. Scholte, G. Storm, H.J. Haisma, Endosomal escape pathways for delivery of biologicals. J. Control Release 151 (3) (2011) 220-228. https://doi.org/10.1016/j.jconrel.2010.11.004.

[5] F. Hausig-Punke, F. Richter, M. Hoernke, J.C. Brendel, A. Traeger, Tracking the Endosomal Escape: A Closer Look at Calcein and Related Reporters. Macromol. Biosci. 22 (10) (2022) e2200167. https://doi.org/10.1002/mabi.202200167.

[6] R.A. Day, E.M. Sletten, Experimental Perspectives on Direct Visualization of Endosomal Rupture. Chembiochem. (22) 2021 3277-3282. https://doi.org/10.1002/cbic.202100379.

Chapter 5 *In vivo* Assessment

5.1 Introduction

The prior chapter conducted that PGDC PMs featuring pH-responsive characteristics exhibited superior cellular uptake and enhanced endosomal escape, resulting in improved gene transfection outcomes. Building upon this foundation, the current study investigated the potential of these micelles *in vivo* using A/J mice bearing Neuro-2A tumors. Given the known high toxicity of PEI, the chapter eschewed the use of this compound as a control group. The findings of this inquiry will provide valuable insights into the potential applications of PGDC-based micelles in biomedical research and practice.

In this chapter, we initially examine the biodistribution profile and gene expression of the PMs *in vivo*. Moreover, the enhanced tumor accumulation and tumor-specific gene expression by PGDC PM motivated us to examine the therapeutic ability of PGDC PM. The adopted method in this study is the antiangiogenic gene therapy using pDNA encoding soluble fms-like tyrosine kinase-1 (sFlt-1) [also known as soluble vascular endothelial growth factor receptor-1 (sVEGFR-1)], which traps vascular endothelial growth factor (VEGF) to prevent the formation of tumor vessels [1-4]. Finally, assessments of the biocompatibility of the PMs were conducted to facilitate the optimal utilization in future biological contexts.

5.2 Materials

4-(2-hydroxyethyl)-1-piperazineethanesulfonic acid (HEPES) were obtained from Wako Pure Chemical Industries, Ltd. (Osaka, Japan). Dulbecco's phosphate-buffered saline (D-PBS(−)) and Micro BCA^{TM} Protein Assay Reagent Kit solution were acquired from Sigma Aldrich (St. Louis, MO, USA). Cell culture lysis buffer and Luciferase Assay System Kit were obtained from Promega Co. (Madison, WI). Soluble fms-like tyrosine kinase-1 (pCAG-sFlt-1) encoding gene inserted pCAcc vector under control of

CAG promoter was provided by RIKEN Gene Bank (Tsukuba, Japan) and amplified in *Escherichia coli* DH5α cells and endotoxin-free pDNAs were got using the NucleoBond® Xtra Maxi EF Kit (MachereyeNagel GmbH & Co., Germany). A mouse vascular endothelial growth factor (VEGF) enzyme-linked immunosorbent assay (ELISA) Kit was obtained from Proteintech Group, Inc. (Chicago, IL). The anti-platelet endothelial cell adhesion molecule-1 (PECAM-1, CD31) rabbit monoclonal antibody (ab182981) and goat anti-rabbit IgG H&L (Alexa Fluor® 488) (ab150077) were purchased from Abcam (Cambridge, UK).

5.3 Animals

A/JJmsSlc (A/J) mice were obtained from Japan SLC, Inc. (Shizuoka, Japan). The Animal Care and Use Committee of the Tokyo Institute of Technology (Yokohama, Japan) and the Animal Committee of the Innovation Center of NanoMedicine (iCONM, Kawasaki, Japan) approved all animal experiments and performed following the Guidelines for the Care and Use of Laboratory Animals as stated by Tokyo Institute of Technology and iCONM.

5.4 Methods

5.4.1 Establishment of subcutaneous tumor model

Neuro-2A cells (1 X 10^5 cell in 100 μL D-PBS(−)) were subcutaneously implanted into the right flank of female A/J mice, aged 6 ~ 8 weeks. The subsequent measurement of tumor volume was conducted by applying the equation “a X $b^2/2$”, wherein “a” represents the largest diameter observed and “b” denotes the smallest diameter.

5.4.2 *In vivo* biodistribution

Subcutaneous Neuro-2A tumor models in A/J mice (female, 6 weeks, 18–20 g, n = 3)

were treated with a single intravenous injection with Cy5-labeled pCAG-Luc2 (20 μg in 200 ml of 10 mM HEPES containing 150 mM NaCl) by tail vein to assess the biodistribution profile. The mice were sacrificed 1, 6, and 24 h after administration. The tumors and other organs were excised, washed with D-PBS(−), and weighed after extracting excess fluid. The entire sample was homogenized in a passive lysis buffer, followed by centrifugation. Blood was drawn from the inferior vena cava, heparinized, and centrifuged to obtain the plasma. The supernatants were poured into black 96-well plates, and the fluorescence of Cy5 was measured with the fluorophotometer (Ex/Em: 640/680 nm, Spark TKS01, TECAN, Zürich, Switzerland). The data on blood circulation and organ accumulation as % dose/ mL blood or % dose/g tissue which was calculated by the following equations:

$$\%\ \text{dose/mL blood} = \{\text{sample count}/[\text{sample volume (mL)} \times \text{injected count}]\} \times 100\%$$

$$\%\ \text{dose/g of tissue} = \{\text{sample count}/[\text{sample weight (g)} \times \text{injected count}]\} \times 100\%$$

5.4.3 *In vivo* gene transfection assay *via* luciferase activity

To examine *in vivo* gene transfection, A/J mice bearing Neuro-2A tumor (200 mm^3 of tumor size) were intravenously injected with Luc2-pDNA loaded PMs (20 μg in 200 ml of 10 mM HEPES containing 150 mM NaCl) or the buffer or the buffer (10 mM HEPES buffer containing 150 mM NaCl). Tumors were harvested and homogenized with passive lysis buffer after 48 hours. The analysis was conducted using the Luciferase Assay System. The Micro BCA Protein Assay Reagent Kit's measurement of the total amount of protein in the homogenates was used to standardize the luminescence intensity values.

5.4.4 Tumor growth suppression experiment

A/J mice bearing Neuro-2A tumor (n = 5, 30 mm^3 of tumor size) were treated with PMs loading sFlt-1 pDNA (20 μg in 200 ml of 10 mM HEPES containing 150 mM NaCl) were intravenously injected into the tail vein three times at a 3-day interval (days 1, 4,

and 7). Likewise, the HEPES buffer (10 mM, pH 7.4) treated group was employed as a control. Anti-tumor efficacy was assessed by measuring the tumor size (*V*), which was estimated using the following equation:

$$V = a \times b^2/2$$

where *a* and *b* are the major and minor axes of the tumor measured using a microcaliper every two days.

5.4.5 *In vivo* evaluation of sFlt-1 expression

The *in vivo* expression of the Flt-1 protein was investigated in the A/J mice bearing Neuro-2A tumor (n = 5, 200 mm^3 of tumor size). After being intravenously injected with PMs loading sFlt-1 pDNA at a dose of 20 μg pDNA/mouse or HEPES buffer (10 mM, pH 7.4) for 48 h, the mice were sacrificed and the plasma, tumors, and other main organs were collected to observe the Flt-1 level by employing the ELISA kit.

5.4.6 Histological analysis

The tumors and organs were fixed with 4% paraformaldehyde, embedded with paraffin, and sliced into 5 μm by using a cryostat microtome (Leica Biosystems RM2245, Germany). For immunofluorescence staining, the vasculature or the tumor sections were stained with rabbit monoclonal antibody against mouse PECAM-1 (1/2000 dilution), followed by incubation with Alexa Fluor 488-conjugated goat anti-rabbit IgG secondary antibody (1/500 dilution). The nuclei were stained with DAPI. Finally, the slides were mounted with an antifade mounting medium (Vector Laboratories, Inc., U.S.) and analyzed using CLSM (LSM710, Carl Zeiss AG, Oberkochen, Germany). The vascular density was quantified by measuring the percentage area of PECAM-1-positive green pixels per image with 15 snap-shots for each sample from CLSM images by using Image J software. In addition, the sections of normal organs were stained with hematoxylin and eosin (H&E) and observed using an optical microscope. Additionally, the sections of normal organs were stained with hematoxylin and eosin (H&E) and

observed using an optical microscope (Leica DMI6000 B) for Histomorphological analysis.

5.4.7 *Ex vivo* Hemolysis assay

Mouse blood was collected and washed with D-PBS(−) twice. Red blood cell (RBCs) suspension was prepared by adding 500 μL blood into 9.5 mL D-PBS(−) buffer. One volume of positive control (TritonX-100), negative control (HEPES buffer, pH 7.4), and PMs samples were added to 10 volumes of RBC suspension and incubated at 37℃ for 2 h. After centrifugation, UV absorption was measured at 541 nm. The final concentration of pDNA was adjusted to 10 μg/mL, which is the same as the calculated concentration of pDNA in the blood when the dose of 20 μg pDNA was evenly distributed in 2 mL of mouse blood.

5.4.8 Blood test

A/J mice (female, 6 weeks, 18-20 g) were intravenously injected with PMs (20 μg in 200 μL of 10 mM HEPES containing 150 mM NaCl) following the schedule of tumor therapeutic regimen with three times injections. Blood was collected 48 h after the final injection, and blood parameters including blood urea nitrogen (BUN), blood urea dehydrogenase (LDH), aspartate aminotransferase (AST), alanine aminotransferase (ALT), and creatinine (Cre) in the acquired plasma were evaluated using a DRI-CHEM 7000i system (Fujifilm, Tokyo, Japan).

5.5 Results and discussion

5.5.1 *In vivo* biodistribution

One of the important characteristics of systemically injectable gene carriers is prolonged blood retention which allows effective tumor accumulation through leaky vasculature [5, 6]. To assess the clearance of PMs from the blood compartment, Cy5-

pDNA loaded PMs were intravenously injected into mice subcutaneously inoculated with Neuro-2A murine neuroblastoma (150 mm^3 of tumor size). By measuring the Cy5-fluorescence intensity, the blood retention was expressed as a percentage of injected dose (% dose/mL Blood). PGDC PM showed more prolonged blood circulation compared to PEG PM (**Figure 5-1, a**). With regard to the accumulation in major organs (**Figure 5-1, c**), PGDC PM showed significantly less accumulation in the liver after 1 h and then in the spleen after 6 h in comparison with PEG PM. These results might be attributed to an excellent antifouling property of the PGDC shell at pH 7.4, avoiding interactions with biological molecules and subsequent recognition by the reticuloendothelial system (RES). Regarding the tumor accumulation of PMs, PGDC PM exhibited an approximately 4-fold higher accumulation (6% dose/g tumor) compared to PEG PM (1.6% dose/g tumor) at 6 h post-injection, maintaining significantly superior tumor accumulation until 24 h (**Figure 5-1, b**).

The superior blood retention, reduced liver and spleen accumulation, and enhanced tumor accumulation of PGDC PM over PEG PM were consistent with our previous results for PGDC-coated quantum dots, gold nanoparticles (AuNPs), and lipid nanoparticles [7-9]. The stealth property of the PGDC shell was assumed to be due to the superhydrophilic nature of carboxy betaine-based PGlu(DET-Car) shell-forming hydration sheaths as previously reported [10, 11]. This stealthiness in the circulation should contribute to escape from the adsorption against biological substances including low-density lipoprotein receptors (LDLRs) and scavenger receptors (SRs) on organs [12, 13], which accounts for the reduced accumulation in the liver and kidney (**Figure 5-1, c**). It is known that PEG-modified carriers showed relatively higher uptake by hepatocytes (highly expressed LDLRs) as well as SR-enriched macrophages in splenic red pulp [14]. On the other hand, the tumor-selective cationic charge derivatization of our PGDC shell in response to external tumoral pH (~ 6.5) should play a pivotal role in the enhanced tumor accumulation of PGDC PM. It is assumed that both PEG and PGDC PMs might accumulate in the tumor in a passive manner *via* permeable tumor

vasculature; nevertheless, PGDC PM showed remarkably higher tumor accumulation compared with PEG PM. We hypothesize that PEG PM could not be retained in the tumor tissue due to its weak interaction with tumorous tissues, so some portions of PM might go back to the bloodstream or be cleared from the tumor to the lymphatic system. In contrast, the PGDC shell could become cationic specifically under acidic tumor microenvironment, leading to improved tumor retention and promoted cellular internalization. It is worth mentioning that we previously demonstrated the deep tumor tissue penetration of PGDC-coated AuNPs reaching the hypoxia in contrast with PEG-coated AuNPs localized at perivascular regions in the tumor [8]. Owing to these unique properties of the PGDC shell, PGDC PM may have achieved better cancer accumulation than PEG PM.

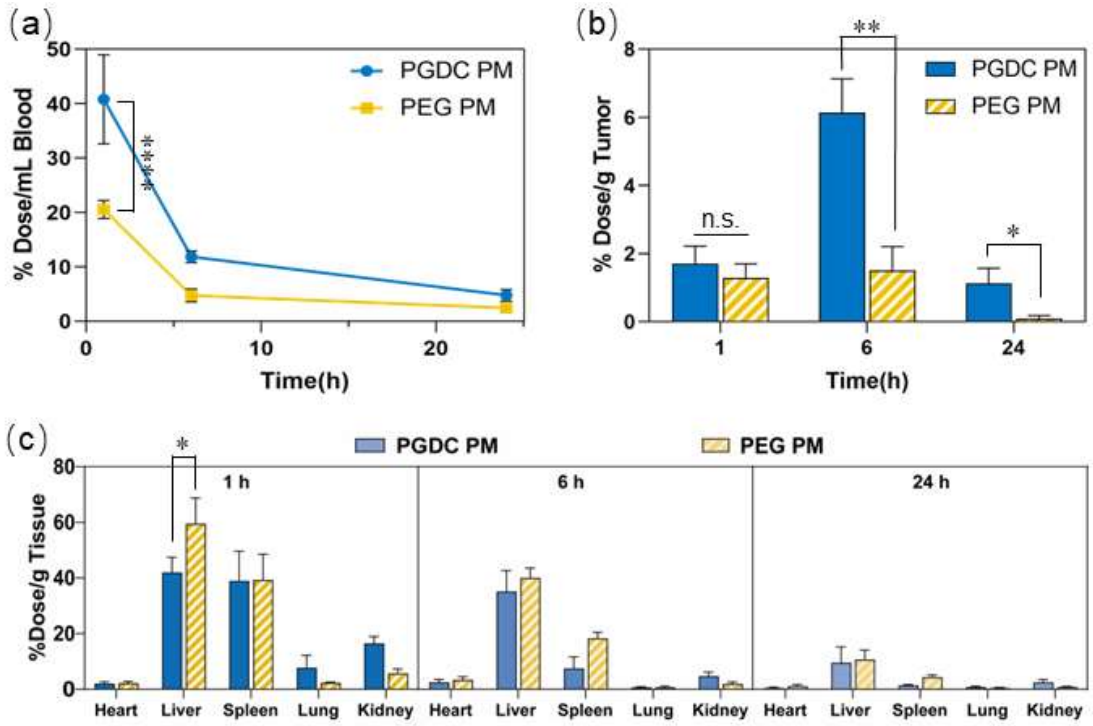

Figure 5-1. *In vivo* biodistribution and gene transfection efficiency of PMs in mice bearing subcutaneously inoculated Neuro-2A tumor after intravenous injection (tumor volume ~150 mm3). (a) Blood circulation profile. (b) Tumor accumulation level. (c) Accumulation of PGDC PM and PEG PM in major organs. Data are expressed as mean ± SD. (n = 3). *p < 0.1, **p <

0.01, and ****p < 0.0001 (Two-way ANOVA with Sidak's multiple comparisons test). PMs loading Cy5-labeled pDNA were injected (20 μg/mouse).

5.5.2 *In vivo* gene transfection assay *via* luciferase activity

We assessed the *in vivo* transfection performance of PGDC PM loading pCAG-Luc2 DNA in the tumor (~ 150 mm^3 of tumor size) and major organs in comparison to the PEG PM and buffer injected group (10 mM HEPES buffer containing 150 mM NaCl) at 48 h post-injection by measuring the luciferase activity. Mice injected with PGDC PM revealed significantly higher Luc expression selectively in the tumor tissue compared to mice injected with PEG PM and buffer (**Figure 5-2**). Such enhanced tumor-specific gene expression by PGDC PM was explained by the enhanced tumor accumulation as well as endosomal escape brought about by acidic pH-promoted cationization of the PGDC shell as described in Chapter 4. Additionally, despite the appreciable accumulation of PGDC and PEG PMs in the liver and spleen (**Figure 5-1, c**), both PMs did not display gene transfer activity in those organs (**Figure 5-2**). Presumably, the active deoxyribonuclease activity in the liver and spleen is likely the cause of the low hepatic and splenic Luc expression [15].

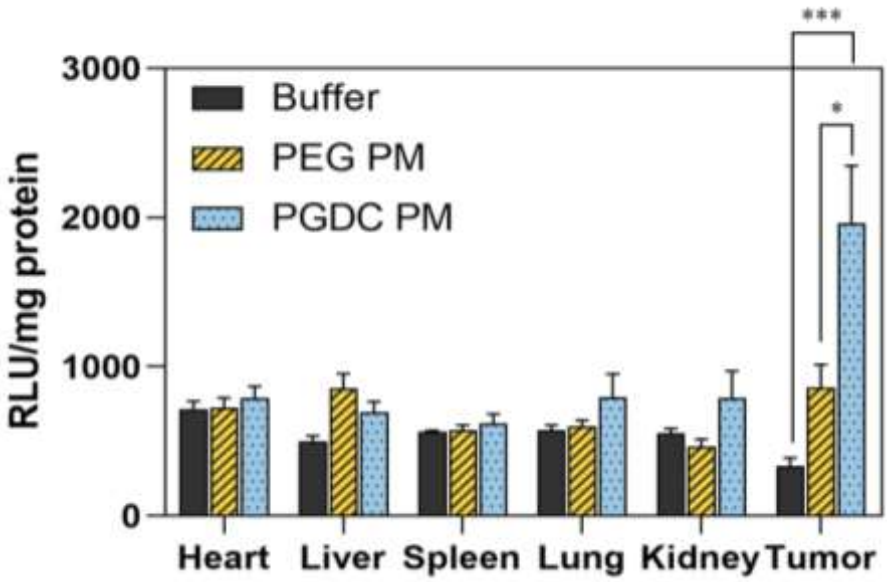

Figure 5-2. *In vivo* Luc expression. PMs loading pCAG-Luc2 DNA were injected (20 μg/mouse) and the Luc expression was quantified at 48 h-post; injection. Data are expressed as mean ± standard error of the mean (SEM) (n = 7). **p < 0.01 and ***p < 0.001 (One-way ANOVA with Tukey's multiple comparisons test).

5.5.3. Anti-tumor effect

We prepared PGDC and PEG PMs loading the pDNA encoding sFlt-1 (pCAG-sFlt-1) and studied their antiangiogenic performance against mice bearing subcutaneously inoculated murine neuroblastoma Neuro-2A cells (**Figure 5-3, a**). PGDC PM significantly suppressed the tumor growth progression compared to the PEG PM, naked pCAG-sFlt-1, and buffer-treated groups (**Figure 5-3, b**), indicating the potential of PGDC PM as a promising gene delivery platform for systemic gene therapy. Meanwhile, no apparent body weight loss was detected in all groups (**Figure 5-3, c**).

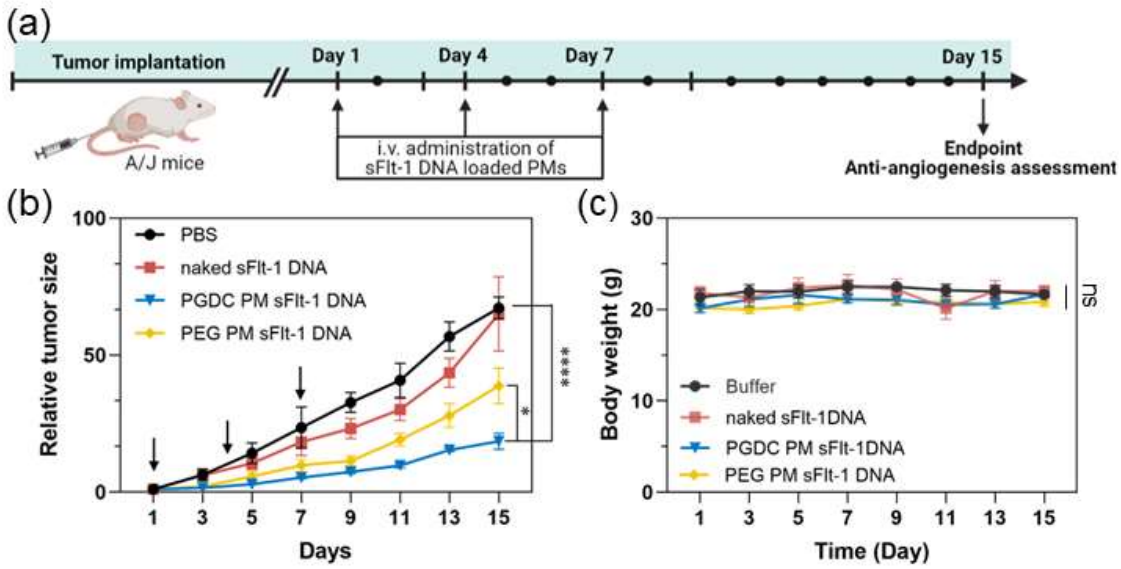

Figure 5-3. *In vivo* therapeutic performance of PMs loading pCAG-sFlt1 and naked pCAG-sFlt1 (20 μg/mouse) against subcutaneous Neuro-2A tumor after tail vein injection (tumor size ~50 mm3 on day 1). In all the tests, tumor-bearing mice treated with 10 mM HEPES buffer (pH 7.4) with 150 mM NaCl were used as a control group. (a) Timeline showing the establishment of the tumor and therapeutic regimen. (b) Profiles for preventing tumor growth showing the relative size of subcutaneous Neuro-2A tumors. On days 1, 4, and 7, mice were received injections of PMs by tail vein (marked by black arrows). (c) Body weight change during the tumor growth suppression study. Data are expressed as mean ± SD (n = 5). *p < 0.01, and ****p < 0.0001 (Two-way ANOVA with Tukey's multiple comparisons test).

5.5.4 *In vivo* evaluation of sFlt-1 expression

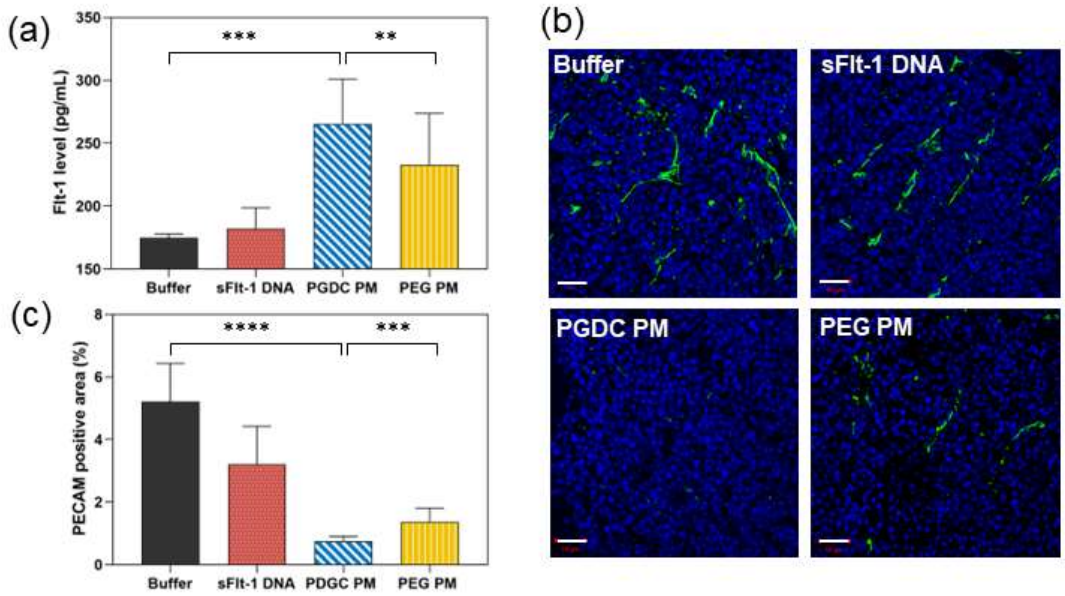

Figure 5-4. Antiangiogenesis assessment of tumor growth suppression experiment. (a) Quantification of the Flt-1 expression level (expressed sFlt-1 plus naturally existing Flt-1) in tumor tissue lysates at 48 h-post *i.v.* injection of the samples using the ELISA test. The total protein concentration of the tissue lysates was adjusted using ELISA buffer to 5 mg/mL. ***p < 0.001, ****p < 0.0001 (One-way ANOVA with Tukey's multiple comparisons test). (b) CLSM images representing PECAM-1 positive vasculature (green) in the tumor tissue cryosections (blue: nuclei). Scale bar = 50 µm. (c) Percentage area of tumor vasculature by quantifying PECAM-1 positive signals from CLSM images (n = 15). Data are expressed as mean ± SD. **p < 0.01, ***p < 0.001 (One-way ANOVA with Tukey's multiple comparisons test).

To verify the effectiveness of antiangiogenesis [2-4], we then quantified the Flt-1 level (expressed sFlt-1 plus inherently existing Flt-1) in the tumor and other major organs by using ELISA. PGDC PM-administered groups exhibited a significantly higher level of Flt-1 in the tumor compared to the other treated groups (**Figure 5-4, a**), whereas no noticeable difference was observed in the other major organs (**Figure 5-5**). The

enhanced expression of sFlt-1 by PGDC PM is consistent with the above-mentioned Luc expression (**Figure 5-2**). Additionally, substantially decreased tumor microvessel density following treatment, as measured by immunofluorescent labeling of vascular endothelial cells using an anti-PECAM-1 antibody (**Figure 5-4, b and c**), provided further evidence of the antiangiogenic action of expressed sFlt-1. Notably, PGDC PM-administered mice group showed a significantly lowered PECAM-1 positive area compared to the PEG PM-injected mice group. These investigations confirmed that the obtained tumor growth inhibition was unquestionably due to the expressed sFlt-1 suppressing tumor microvessel formation. These results validate the universality of our strategy that pH-triggered behavior of PGDC PM promotes tumor accumulation and retention, subsequently facilitating internalization, endosomal escape, and gene transfection in the tumor cells toward cancer gene therapy.

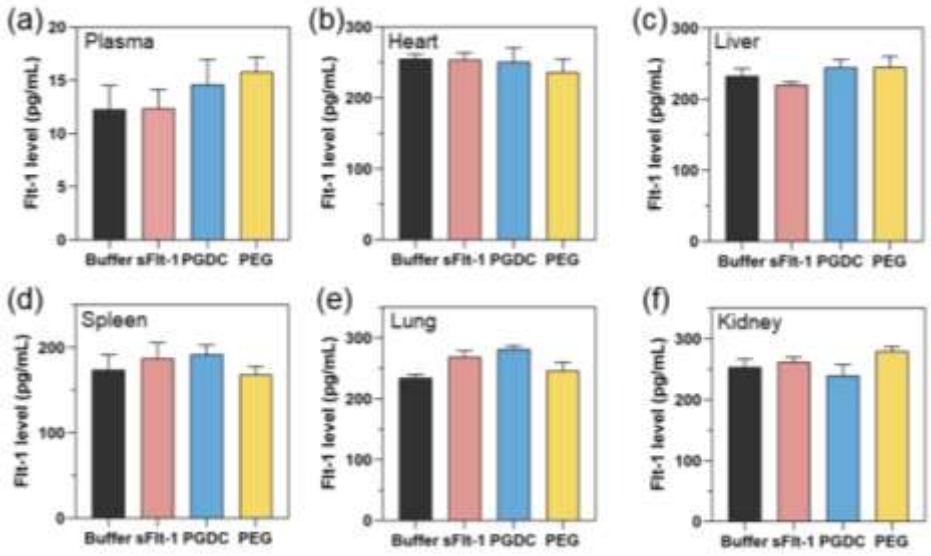

Figure 5-5. Quantification of the Flt-1 expression level in the plasma and lysates of major organs. Flt-1 expression of (a) plasma, (b) heart, (c)liver, (d)spleen (e) lung, and (f) kidney from the mice bearing subcutaneous Neuro-2A tumor measured by using ELISA assay after 48 h of tail vein injection of the samples. The expression of sFlt-1 and endogenous Flt-1 levels together make up the Flt-1 level. Using ELISA buffer, the protein content in the tissue and plasma lysates was increased to 5 mg/mL. Data are expressed as mean ± SEM. (n = 5).

5.5.5. Safety assessment of PMs

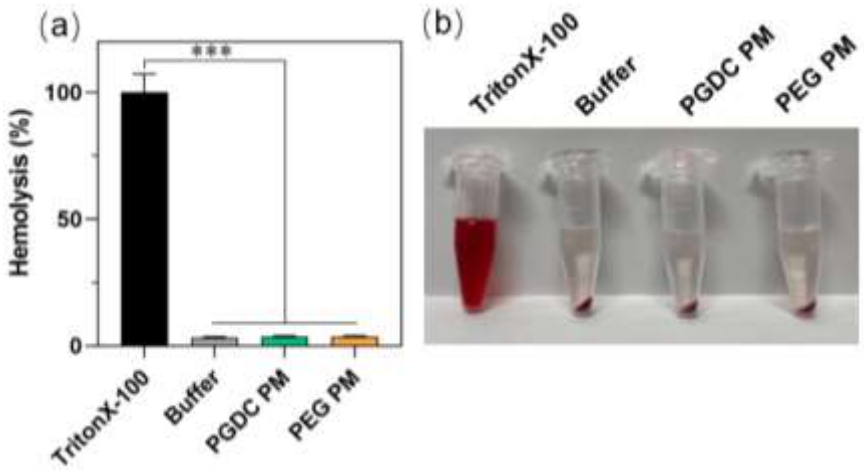

Figure 5-6. Hemolytic activity of PMs using ex vivo hemolysis assay. Mouse red blood cells were incubated with Triton X-100 (a positive control), 10 mM HEPES buffer (pH 7.4) containing 150 mM NaCl (a negative control), PGDC PM (N/P = 15), and PEG PM (N/P = 15) for 2 h at 37°C. (a) The hemolysis percentage. The release of hemoglobin was spectroscopically quantified. Data are expressed as mean ± SD. (n = 4). ****p < 0.0001 (ANOVA followed by Tukey's test). (b) Photographs of incubated samples after centrifugation at 2000× g for 5 min. Red supernatants in tubes suggest hemoglobin release as a result of red blood cell destruction.

Minimal toxicity, besides maximized therapeutic efficacy, is important in developing clinically applicable gene delivery systems [16]. Considering the assumption that the PGDC PM might meet the blood cells in the tumor area or might leak into the bloodstream after cationic derivatization in the acidic milieu of the tumor, we evaluated the hemolytic activity, toxicity bioindicators, and tissue toxicity in major organs for PGDC and PEG PMs. No *ex vivo* hemolysis activity was observed in both PGDC or PEG PMs after incubating with red blood cell suspension at 37°C for 2 hours (**Figure 5-6**). Twenty-four hours after systemic administration of PGDC and PEG PMs, blood parameters such as lactate dehydrogenase (LDH), liver damage makers [aspartate aminotransaminase (AST), and alanine aminotransferase (ALT)], and kidney function

markers [blood urea nitrogen (BUN), and creatinine (Cre)], were maintained the same level as those of the control group (**Figure 5-7**). Furthermore, H&E staining showed that there are no pathological changes in major organs treated by both PGDC and PEG PMs (**Figure 5-8**), indicating the good biocompatibility of PGDC PM formulations for gene delivery applications regardless of their unique pH-responsive behavior.

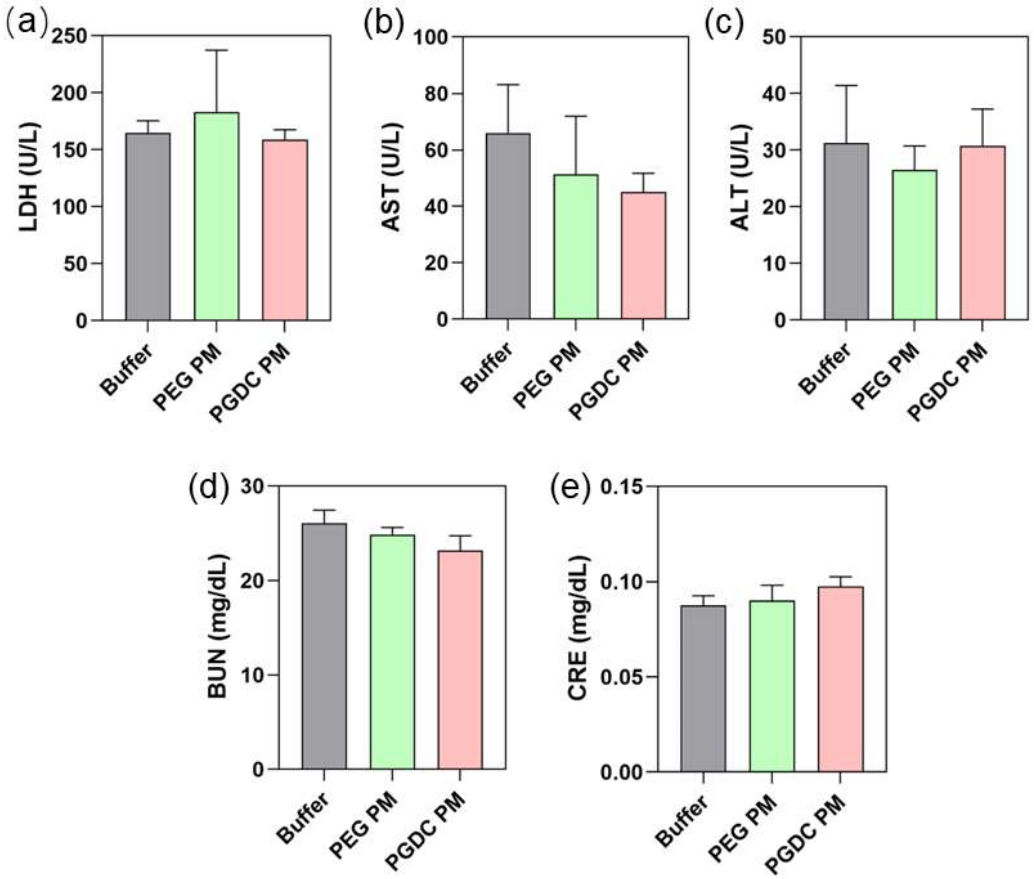

Figure 5-7. Changes in toxicity markers of the plasma after intravenous injection of PMs. (a) Lactate dehydrogenase (LDH), (b) Aspartate transaminase (AST), (c) Alanine transaminase (ALT), (d) Blood urea nitrogen (BUN), and (e) Creatinine (CRE). Blood was obtained 24 h after the injection and centrifuged at 2000× g for 5 min to obtain the plasma. Data are expressed as mean ± SD. (n = 4).

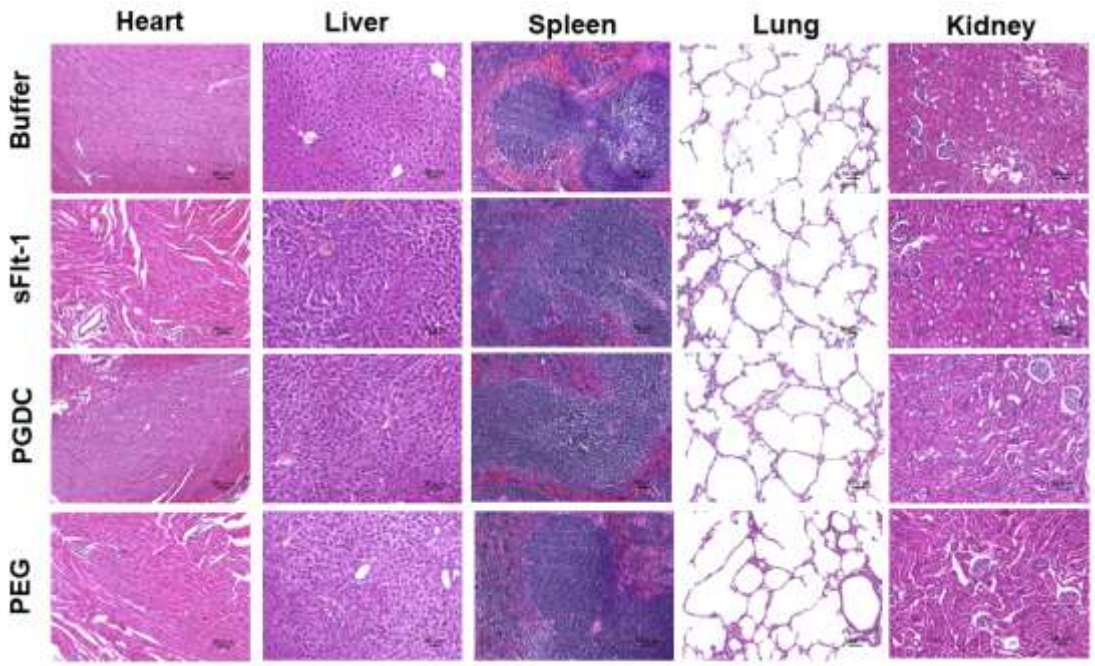

Figure 5-8. Hematoxylin and eosin (H&E) staining of major organs. The organs were from Neuro-2A tumor-bearing mice after the treatment for 14 days as illustrated in the timeline of Figure 6. Scale bar = 50 μm.

5.6 Conclusion

This chapter demonstrated the potential of PGDC-based micelles as promising carriers for gene delivery by investigating the *in vivo* potential of PGDC PM using A/J mice bearing Neuro-2A tumors. First, we focused on the biodistribution profile and gene expression of the PGDC micelles *in vivo*. These results revealed enhanced tumor accumulation and tumor-specific gene expression, further highlighting the potential of PGDC micelles as effective carriers for targeted gene delivery.

The therapeutic capabilities of PGDC PM by using sFlt-1 DNA shed light on the potential of PGDC PM as a vehicle for delivering therapeutic genes and exerting antiangiogenic effects. By trapping vascular endothelial growth factor (VEGF), this gene therapy approach aimed to prevent the formation of tumor vessels. Finally, we conducted comprehensive assessments of the biocompatibility of the PGDC PM to ensure its optimal utilization in future biological contexts. These evaluations are crucial

for considering the clinical translation and practical applications of PGDC-based micelles in gene therapy and other biomedical fields.

Overall, the *in vivo* performance of PGDC PM has provided valuable insights into the potential applications of PGDC-based micelles in gene delivery and therapy. The findings contribute to the growing body of knowledge in the field of nanomedicine, emphasizing the importance of pH-responsive carriers in improving gene transfection efficiency and targeting specific tissues or diseases. The outcomes of this research open up new avenues for further investigations and potential advancements in the development of safe and effective gene delivery systems.

5.7 References

[1] L. Persano, M. Crescenzi, S. Indraccolo, Anti-angiogenic gene therapy of cancer: current status and future prospects, Mol. Aspects Med. 28 (1) (2007) 87-114. https://doi.org/10.1016/j.mam.2006.12.005.

[2] S. Yamaguchi, K. Iwata, M. Shibuya, Soluble Flt-1 (soluble VEGFR-1), a potent natural antiangiogenic molecule in mammals, is phylogenetically conserved in avians, Biochem. Biophys. Res. Commun. 291 (3) (2002) 554-559. https://doi.org/10.1006/bbrc.2002.6478.

[3] M. Shibuya, Vascular endothelial growth factor and its receptor system: physiological functions in angiogenesis and pathological roles in various diseases, J. Biochem. 153 (1) (2013) 13-19. https://doi.org/10.1093/jb/mvs136.

[4] H. Zhang, J. Liu, Q. Chen, P. Mi, Ligand-installed anti-VEGF genomic nanocarriers for effective gene therapy of primary and metastatic tumors. J. Control Release 10 (320) (2020) 314-327. https://doi.org/10.1016/j.jconrel.2020.01.026.

[5] J. Wu, The enhanced permeability and retention (EPR) effect: the significance of the concept and methods to enhance its application, J. Pers. Med. 11 (8) (2021) 771. https://doi.org/10.3390/jpm11080771.

[6] J. Bourquin, A. Milosevic, D. Hauser, R. Lehner, F. Blank, A. Petri-Fink, B. Rothen-Rutishauser, Biodistribution, clearance, and long-term fate of clinically relevant nanomaterials, Adv. Mater. 30 (19) (2018) 1704307. https://doi.org/10.1002/adma.201704307.

[7] A.H. Ranneh, H. Takemoto, S. Sakuma, A. Awaad, T. Nomoto, Y. Mochida, M. Matsui, K. Tomoda, M. Naito, N. Nishiyama, An ethylenediamine-based switch to render the polyzwitterion cationic at tumorous pH for effective tumor accumulation of coated nanomaterials, Angew. Chem. Int. Ed. 57 (18) (2018) 5057-5061. https://doi.org/10.1002/anie.201801641.

[8] A. Awaad, H. Takemoto, M. Iizuka, K. Ogi, Y. Mochida, A.H. Ranneh, M. Toyoda, M. Matsui, T. Nomoto, Y. Honda, K. Hayashi, K. Tomoda, T. Ohtake, Y. Miura, N. Nishiyama, Changeable net charge on nanoparticles facilitates intratumor accumulation and penetration, J. Control Release 346 (2022) 392-404. https://doi.org/10.1016/j.jconrel.2022.04.025.

[9] Y.J. Sung, H. Guo, A. Ghasemizadeh, X. Shen, W. Chintrakulchai, M. Kobayashi, M. Toyoda, K. Ogi, J. Michinishi, T. Ohtake, M. Matsui, Y. Honda, T. Nomoto, H. Takemoto, Y. Miura, N. Nishiyama, Cancerous pH-responsive polycarboxybetaine-coated lipid nanoparticle for smart delivery of siRNA against subcutaneous tumor model in mice, Cancer Sci. 113 (12) (2022) 4339-4349. https://doi.org/10.1111/cas.15554.

[10] J. Ladd, Z. Zhang, S. Chen, J.C. Hower, S. Jiang, Zwitterionic polymers exhibiting high resistance to nonspecific protein adsorption from human serum and plasma, Biomacromolecules 9 (5) (2008) 1357-1361. https://doi.org/10.1021/bm701301s.

[11] L.Y. Zhou, Y.H. Zhu, X.Y. Wang, C. Shen, X.W. Wei, T. Xu, Z.Y. He, Novel zwitterionic vectors: multi-functional delivery systems for therapeutic genes and drugs, Comput. Struct. Biotechnol. J. 18 (2020) 1980-1999. https://doi.org/10.1016/j.csbj.2020.07.015.

[12] N. Bertrand, P. Grenier, M. Mahmoudi, E.M. Lima, E.A. Appel, F. Dormont, J.M.

Lim, R. Karnik, R. Langer, O.C. Farokhzad, Mechanistic understanding of in vivo protein corona formation on polymeric nanoparticles and impact on pharmacokinetics, Nat. Commun. 8 (1) (2017) 777. https://doi.org/10.1038/s41467-017-00600-w.

[13] E. Chnari, J.S. Nikitczuk, J. Wang, K.E. Uhrich, P.V. Moghe, Engineered polymeric nanoparticles for receptor-targeted blockage of oxidized low density lipoprotein uptake and atherogenesis in macrophages, Biomacromolecules 7 (6) (2006) 1796-1805. https://doi.org/10.1021/bm0600872.

[14] S. Bultel-Brienne, S. Lestavel, A. Pilon, I. Laffont, A. Tailleux, J.C. Fruchart, G. Siest, V. Clavey, Lipid free apolipoprotein E binds to the class B Type I scavenger receptor I (SR-BI) and enhances cholesteryl ester uptake from lipoproteins, J. Biol. Chem. 277 (39) (2002) 36092-36099. https://doi.org/10.1074/jbc.M201943200.

[15] R. Kircheis, L. Wightman, A. Schreiber, B. Robitza, V. Rössler, M. Kursa, E.Wagner, Polyethylenimine/DNA complexes shielded by transferrin target gene expression to tumors after systemic application. Gene Ther. 8 (1) (2001) 28-40. https://doi.org/10.1038/sj.gt.3301351.

[16] R. Kircheis, L. Wightman, A. Schreiber, B. Robitza, V. Rössler, M. Kursa, E. Wagner, Polyethylenimine/DNA complexes shielded by transferrin target gene expression to tumors after systemic application, Gene Ther. 8 (1) (2001) 28-40. https://doi.org/10.1038/sj.gt.3301351.

Chapter 6 Summary and Future Perspective

6.1. Summary of the present study

Gene therapy poses significant obstacles, primarily centered around the effective delivery of therapeutic genes to the cytosol within tumor cells [1, 2]. A commonly employed approach involves surface modification of nanocarriers using polyethylene glycol (PEG), which facilitates tumor targeting via the leaky tumor vasculature and imparts stealth functionality [3, 4]. However, PEGylation has been observed to hinder the internalization of gene carriers into cancer cells, resulting in reduced cellular uptake and compromised gene transfection efficiency [5]. In order to circumvent these unfavorable influences associated with PEGylation, this study aimed to develop a pH-responsive polyzwitterion-coated micelle, incorporating PGlu(DET-Car)-bPEI (PGDC PM) to address the contradictory requirements of biocompatibility during blood circulation and enhanced cellular interactions at the tumor site. This system overcomes the limitations of conventional PEG-coated systems, commonly associated with the "PEG dilemma".

The developed pH-responsive core-shell gene delivery system, referred to as PGDC PM, exhibits the remarkable capability to sense the specific pH range within diverse physiological conditions within the body. Consequently, this system is anticipated to demonstrate distinct and unique biological functionalities, including:

(1) The PGDC shell exhibits a neutral charge (– 2.08 mV) at pH 7.4, leading to prolonged blood circulation (pH 7.4);

(2) Following tumor accumulation *via* leaky vasculature, the PGDC shell becomes slightly cationic (+ 6.80 mV) at pH 6.5, promoting the interaction with the anionic cell membrane, resulting in improved tumor retention and cellular internalization;

(3) In the endo-/lysosomal compartment (pH 5.5), the cationic charge of the PGDC shell is augmented (+ 15.3 mV), facilitating endosomal escape. Indeed, after systemic administration, PGDC PM accomplished prolonged blood circulation, higher tumor accumulation, and enhanced gene transfer activity than PEG PM in subcutaneous tumor

models.

The utility of PGDC PM loading the sFlt-1 DNA was also demonstrated by successful tumor antiangiogenesis therapy.

6.2 Future perspective

Our novel design of pH-responsive polyzwitterion covered polyplex micelle exhibits a remarkable potency as a replacement for PEG-based delivery systems, and can be effectively employed for delivering various nucleic acid medicines, including mRNA, siRNA, to treat intractable diseases. Moreover, further investigation is warranted to achieve precise control over the pH responsiveness of delivery systems. This can involve understanding the factors influencing the protonation behavior of amine groups, such as molecular structure, pK_a values, and local environment. By tailoring these parameters, it becomes possible to optimize the pH-triggered release kinetics and ensure efficient drug delivery at specific target sites. Advanced characterization techniques and computational modeling can aid in elucidating the underlying mechanisms and guiding the design of more sophisticated pH-responsive systems.

Furthermore, in order to deepen our comprehension of the behavior exhibited by pH-responsive polymers within diverse acidic environments, there is a need for more intricate and nuanced insights. Acquiring such invaluable knowledge will empower us to devise similar drug delivery systems that can effectively tackle the challenges associated with diseases manifesting in acidic environments, extending beyond the realm of tumors. Notably, the presence of acidity can be discerned in the cutaneous epidermis as well as at sites of inflammation [6, 7]. For example, in the context of rheumatoid arthritis, characterized by joint inflammation and heightened acidity levels, the utilization of a pH-responsive nanoparticle holds the potential for targeted drug delivery directly to the affected joint tissue [8, 9]. Similarly, in cases of ischemic stroke, where cerebral tissue sustains damage due to oxygen and nutrient deprivation, resulting

in the formation of an acidic microenvironment, an acidity-responsive nanoparticle has the potential to facilitate the delivery of therapeutic agents or drugs precisely to the affected brain tissue [10].

6.3 References

[1] C.E. Dunbar, K.A. High, J.K. Joung, D.B. Kohn, K. Ozawa, M. Sadelain, Gene therapy comes of age, Science 359 (6372) (2018) eaan4672. https://doi.org/10.1126/science.aan4672.

[2] J.A. Kulkarni, D. Witzigmann, S.B. Thomson, S. Chen, B.R. Leavitt, P.R. Cullis, R. van der Meel, The current landscape of nucleic acid therapeutics, Nat. Nanotechnol. 16 (6) (2021) 630-643. https://doi.org/10.1038/s41565-021-00898-0.

[3] J.S. Suk, Q. Xu, N. Kim, J. Hanes, L.M. Ensign, PEGylation as a strategy for improving nanoparticle-based drug and gene delivery, Adv. Drug Deliv. Rev. 99 (2016) 28-51. https://doi.org/10.1016/j.addr.2015.09.012.

[4] T. Nomoto, Y. Matsumoto, K. Miyata, M. Oba, S. Fukushima, N. Nishiyama, T. Yamasoba, K. Kataoka, In situ quantitative monitoring of polyplexes and polyplex micelles in the blood circulation using intravital real-time confocal laser scanning microscopy, J Control Release 151(2) (2011) 104-109. https://doi.org/10.1016/j.jconrel.2011.02.011.

[5] S. Mishra, P. Webster, M.E. Davis, PEGylation significantly affects cellular uptake and intracellular trafficking of non-viral gene delivery particles, Eur. J. Cell Biol. 83 (3) (2004) 97-111. https://doi.org/10.1078/0171-9335-00363.

[6] V. Pucino, M. Bombardieri, C. Pitzalis, C. Mauro, Lactate at the crossroads of metabolism, inflammation, and autoimmunity. Eur. J. Immunol. 47 (1) (2017) 14-21. https://doi.org/10.1002/eji.201646477.

[7] Y. Dou, C. Li, L. Li, J. Guo, J. Zhang, Bioresponsive drug delivery systems for the treatment of inflammatory diseases. J. Control Release. 10 (327) (2020) 641-666.

https://doi.org/10.1016/j.jconrel.2020.09.008.

[8] M. Zhang, W. Hu, C. Cai, Y. Wu, J. Li, S. Dong, Advanced application of stimuli-responsive drug delivery system for inflammatory arthritis treatment. Mater Today Bio. 21 (14) (2022) 100223. https://doi.org/10.1016/j.mtbio.2022.100223.

[9] C. Li, H. Li, Q. Wang, M. Zhou, M. Li, T. Gong, Z. Zhang, X. Sun, pH-sensitive polymeric micelles for targeted delivery to inflamed joints. J. Control Release 28 (246) (2017) 133-141. https://doi.org/10.1016/j.jconrel.2016.12.027.

[10] O. M Tóth, Á. Menyhárt, R. Frank, D. Hantosi, E. Farkas, F. Bari, Tissue acidosis associated with ischemic stroke to guide neuroprotective drug delivery. Biology (Basel) 11;9 (12) (2020) 460. https://doi.org/10.3390/biology9120460.

Achievements

Publications

X. Shen, et al. “Facilitated DNA delivery and therapeutic efficiency through stepwise pH-responsiveness induced by polyzwitterion- covered nanocarriers,” Journal of Controlled Release. (Under review, 2023)

Conferences

Oral presentation: Xin Shen, Dirisala Anjaneyulu, Toyoda, Masahiro, Yuto Honda, Takahiro Nomoto, Hiroyasu Takemoto, Yutaka Miura, and Nobuhiro Nishiyama. ‘プラスミド DNA デリバリーを指向した pH 変換型ポリ双性イオン導入ナノシステムの開発’, 71st Symposium on Macromolecules (2022).

Poster presentation: Xin Shen, Dirisala Anjaneyulu, Toyoda, Masahiro, Yuto Honda, Takahiro Nomoto, Hiroyasu Takemoto, Yutaka Miura, and Nobuhiro Nishiyama. ‘pH-changeable polyzwitterion-introduced nanosystem for plasmid DNA delivery’, 第 38 回日本 DDS 学会学術集会 (2022).

Acknowledgment

I would like to express my deepest gratitude to several individuals who have played instrumental roles in the completion of this doctoral thesis.

First and foremost, I would like to extend my heartfelt appreciation to Prof. Nishiyama for his invaluable guidance, unwavering support, and extensive expertise in the field. His mentorship has been instrumental in shaping the direction of my research and fostering my academic growth.

I would also like to extend my sincere thanks to Prof. Miura for his insightful feedback, constructive criticism, and valuable suggestions throughout the course of this research. His expertise and mentorship have significantly contributed to the quality and depth of this thesis.

Additionally, I would like to acknowledge the indispensable support of Anjel, whose dedication, assistance, and collaboration have been instrumental in various aspects of this research project. Their contributions have been invaluable, and I am deeply grateful for their involvement.

I am incredibly fortunate to have a loving and supportive family and my boyfriend who has been with me every step of the way. Their unconditional love, belief in my dreams, and unwavering encouragement have been the pillars of my success. I am indebted to them for their sacrifices, guidance, and the unwavering support they have provided me throughout my journey.

Last but certainly not least, I would also like to extend my appreciation to all the members of my lab. Their camaraderie, collaboration, and shared enthusiasm for research have made my time in the lab truly enjoyable and fulfilling. I am grateful for their support, guidance, and the valuable insights they have provided me.